Feasible operation region of an electricity distribution network with SOPs

Xun Jiang

School of Engineering

Cardiff University

A thesis submitted for the degree of

Doctor of Philosophy

March, 2024

Acknowledgement

First and foremost, I would like to express my deepest appreciation to my supervisor, Prof. Jianzhong Wu, for his remarkable and continuous guidance and engagement in my PhD research. He guides me towards conducting research that is valuable but sometimes challenging, as opposed to work that is easy but lacks applicability. Furthermore, he underscores the significance of presentations and communication within the realm of academic research. His patience and continuous guidance in mastering clear, logical and concise English writing hold great value to me and my future academic endeavours. Words cannot express my gratitude to my supervisor, Dr. Yue Zhou, for his great effort in the supervision of my PhD study. He always stays open to new ideas and willing to offer suggestions. The discussions with him throughout my PhD studies are a cherished memory for me. I must also thank my supervisor, Dr. Wenlong Ming, for his generous support and valuable suggestions throughout the research study, particularly in the field of power electronics. I am also deeply thankful for the invaluable encouragement and feedback provided by my supervisors during the early stages of my research, which were crucial for the successful completion of my study.

I would like to extend my sincere gratefulness to Prof. Nick Jenkins, Prof. Carlos E. Ugalde-Loo and Dr. Sheng Wang, for their invaluable comments and suggestions in the Smart Grid group meetings, which greatly help in my research study. Thanks should also go to the CIREGS team where I gained a lot of new insights from a group of brilliant individuals. It was a genuine pleasure to work in such an interdisciplinary and inspiring team.

I am extremely grateful to all my friends, colleagues and visiting scholars for their moral support and help during these years. Special mention to Dr. Gen Li, Dr. Wei Gan, Dr. Jinlei Chen, Dr. Chuanyue Li, Dr. Peng Yang, Dr. Shuai Yao, Dr. Jia Liu, Dr. Chuanshen Wu, Pengfei Su, Kaiqing Qiu, Shuang Kang and Wangbiao Zhou for the weekend gatherings and sharing meals. Thanks should also go to my roommates during the hardest time of Covid-19 for many life support from them.

I would like to thank Cardiff University for providing me the opportunity of study. I would also like to thank the China Scholarship Council, the projects of UK-China MC2 and Supergen Energy Networks Hub, and my supervisors who financed my research and life in Cardiff.

Finally, my deepest appreciation goes to my family for their unwavering support, encouragement, and companionship throughout my years in the UK. Their understanding and faith in me have consistently provided warmth, courage, and the willpower to persevere through this journey.

Abstract

Soft open points (SOPs), which are advanced power electronic devices placed at normally open points of electricity distribution networks, have proved to be an alternative to enhance the hosting capacity of the distribution network. To conduct effective hosting capacity assessment and active management of distribution networks with SOPs, this thesis develops a novel feasible operation region (FOR) methodology. The FOR is denoted as the range of nodal power injections of a distribution network, within which no network constraints are violated. The FOR boundaries represent the maximum power injections that can be hosted by a distribution network, offering insights into the network hosting capacity. It can also be a useful tool for active management and efficient expansion of distribution networks.

In this thesis, quadratic analytical expressions of the FOR boundaries are first developed. An effective high-dimensional error analysis approach is subsequently provided for validating the analytical FOR boundaries. Simulation results show that the quadratic analytical boundaries well approximate the real FOR boundaries. Compared to the existing linear approximation (termed as hyperplane expressions) of FOR boundaries, the proposed quadratic expressions are proved to have higher accuracy.

Based on the developed expressions of FOR boundaries, this thesis further models the FOR of a distribution network with SOPs (denoted as FOR^{SOP}) as the Minkowski Sum of the FOR of the distribution network and the range of power transfer of SOPs. A practical Minkowski Sum algorithm is further developed to derive the analytical expressions of the boundaries of FOR^{SOP}. The proposed method is validated to be effective to formulate the analytical expressions of FOR^{SOP} boundaries.

A novel FOR-based method for constraint management of distribution networks with SOPs is also developed, which can adapt to various measurement conditions. Simulation results under case studies show that the FOR-based method can achieve near-global optimum results as the optimal power flow (OPF)-based method, but with fewer measurement units and within milliseconds.

Contents

List of Figures

List of Tables

Nomenclature

List of abbreviations

AC	alternating current
BSC	boundary supply capability
DC	direct current
DG	distributed generation
DNO	distribution network operator
DSR	dynamic security region
FLB	feeder load balancing
FOR	feasible operation region
FOR^{DN}	the FOR of the distribution network without SOPs
FOR^{SOP}	the FOR of a distribution network with SOPs
GHG	greenhouse gas
GM	global measurement
HV	high voltage
LM	local measurement
MB	multi-constraint boundary
MM	moderate measurement
MMC	modular multilevel converter
MV	medium voltage
MVDC	medium voltage direct current
NOP	normally open point
Ofgem	office of gas and electricity markets
OLCT	on-load tap changer

OPF	optimal power flow
PLR	power losses reduction
PV	photovoltaics
SOP	soft open point
SOP^{OR}	operating range of SOPs
SR	security region
SR_{N-1}	security region under N-1 criteria
SSSC	static series synchronous compensator
SSSR	steady-state security region
STATCOM	static synchronous compensator
STB	single-constraint thermal boundary;
SVB	single-constraint voltage boundary
SVC	static var compensator
SVSR	static voltage stability region
UKGDS	United Kingdom generic distribution system
UPFC	unified power flow controller
VPI	voltage profile improvement
VSC	voltage source converter
VSSR	voltage stability security region

List of mathematical symbols

$\boldsymbol{A}$	the coefficient matrix for linear inequations
$\boldsymbol{A_{eq}}$	the coefficient matrix for linear equations
A_i^{SOP}	the losses coefficient of the SOP
$\boldsymbol{A_j}$	the set of the adjoining downstream nodes of node j
$\boldsymbol{B}$	the set of power lines in the distribution network

$\boldsymbol{b}$	the constant column vector for linear inequations
$\boldsymbol{b_{eq}}$	the constant column vector for linear equations
$\boldsymbol{C_T}$	the sets of thermal constraints
$\boldsymbol{C_V}$	the sets of voltage constraints
c	the constant term in a polynomial
D_j	the set of the downstream nodes of node j (including node j)
$\boldsymbol{d^{(k)}}$	the kth power-increasing direction within the high-dimensional power injection space
$\boldsymbol{f}$	the constant column vector of coefficients for the linear terms in a polynomial
$\boldsymbol{G}$	the set of DG units
$\boldsymbol{H}$	the matrix of coefficients for the quadratic terms in a polynomial
$\boldsymbol{I}$	the column vector for line currents
$I_{\varphi,0}$	the complex current on phase φ (φ=a, b, c) of the substation outlet
$\left\|I_{ij}\right\|$	the magnitude of the current through the power line ij
I_{ij}^{M}	the limit to the magnitude of the line current through line ij
$\boldsymbol{l_b}$	the lower bound for variables
N	the set of nodes in the distribution network
N_T	the number of the terminals of the SOP
n	the number of nodes in the distribution network
n_b	the number of power lines in the distribution network
$\boldsymbol{n_k^{FOR}}$	the projection of the normal vector of the kth FOR^{DN} boundary onto the subspace defined by the power injections at the nodes connected by SOPs

$\boldsymbol{P}$	the column vector for nodal active power injections in the distribution network
$\boldsymbol{P}^{ext}$	the extended active power injection vector along the kth power-increasing direction
$\boldsymbol{P}^{SOP}$	the column vector of active power injections from terminals of SOPs
P_i^{SOP}	the active power injection from the ith terminal of the SOP
$P_i^{SOP,\mathrm{L}}$	the power losses of the ith converter of the SOP
P_i^{L}	the active power load at node i
$P_{ij,t}$	the active power flow on line ij at time t
$P_{j,eq}$	the equivalent active power loading at the receiving end node of line ij in the distribution network
P_k	the active power injection at node k
$P_{k,t}^{SOP}$	the active power output from the SOP at node k at time t
$\Delta P_{k,t+\Delta t}^{SOP}$	the adjustment in the active power set point of the SOP after a total elapsed time Δt since time t
$P_{\text{max-load}}$	the maximum loading in the distribution network
$P_{g,i}$	the active power injection from the DG unit at node i
$\boldsymbol{Q}$	the column vector for nodal reactive power injections in the distribution network
$\boldsymbol{Q}^{ext}$	the extended reactive power injection vector along the kth power-increasing direction
$\boldsymbol{Q}^{SOP}$	the column vector of reactive power injections from terminals of SOPs

Q_i^{SOP}	the reactive power injection from the *i*th terminal of the SOP
$Q_{ij,t}$	the reactive power flow on line *ij* at time *t*
$Q_{j,eq}$	the equivalent reactive power loading at the receiving end node of line *ij* in the distribution network
Q_k	the reactive power injection at node *k*
$Q_{k,t}^{SOP}$	the reactive power output from the SOP at node *k* at time *t*
$\Delta Q_{k,t+\Delta t}^{SOP}$	the adjustment in the reactive power set point of the SOP after a total elapsed time Δt since time *t*
R_j	the resistance of the line *ij*
$R_{0,x}$	the total resistance of the lines from the slack node to node *x*
S_i^{DG}	the capacity of DG at node *i*
S_i^{SOP}	the capacity of the *i*th converter of the SOP
$S_{ij,rate}$	the rated capacity of the line *ij*
S_k	the apparent power flow through the power line *k*
$S_{k,\mathrm{rated}}$	the rated capacity of the power line *k*
s_k	the distance between the origin and the *k*th real boundary point
$\boldsymbol{u_b}$	the upper bound for variables
$\boldsymbol{V}$	the column vector for node voltages
V_i	the real voltage magnitude at node *i*
$V_{i,ref}$	the nominal voltage magnitude at node *i*
V_i^{SOP}	the voltage of the network at the *i*th terminal of SOP
ΔV_{ij}	the horizontal element of the voltage difference between node *i* and node *j*
δV_{ij}	the vertical element of the voltage difference between node *i* and *j*

$V_{i,t}$	the voltage magnitude at node *i* and time *t*
$\Delta V_{i,t+\Delta t}$	the voltage change at node *i* and time $t+\Delta t$
$V_{\varphi,i}$	the complex voltage on phase φ (φ=a, b, c) at node *i*
$V_i^{\min}$	the minimum allowed network voltage at node *i*
$V_i^{\max}$	the maximum allowed network voltage at node *i*
$\boldsymbol{v_k}$	the vector of the point inside SOP^{OR}, which starts at the origin of SOP^{OR} and ends at the point
X_j	the reactance of the line *ij*
$X_{0,x}$	the total reactance of the lines from the slack node to node *x*
$z_{\alpha/2}$	the *z*-value to the predefined confidence level
$\gamma^{(k)}$	the positive coefficient to extend $\boldsymbol{d}^{(k)}$
ε	the acceptable error to the predefined confidence level
$\boldsymbol{\theta}$	the column vector for voltage phase angles
θ_{ij}	the difference of the phase angles at the two endpoints of line *ij*
λ_i	the coefficient associated with the recovery level of load at node *i,* where $\lambda_i \in [0,1]$
π_i	the weighting factor of the load at node *i*
$\sigma(\cdot)$	the standard deviation of a set
$\Omega \in R^{2n}$	the FOR in the 2*n*-dimensional complex power injection space, where *n* is the number of nodes (excluding the slack bus) in the distribution network
Ω_{SOP}	the set of nodes connected by the SOP

Mathematical operators

$\oplus$	Minkowski Sum operation
$\cup$	the set union operation
$D(\cdot,\cdot)$	the distance between two points, two point sets or one point and one point set, which can be measured under different distance functions
$[\cdot]^T$	the transpose operation of a vector or matrix

Chapter 1. Introduction

1.1. Background

Greenhouse gas (GHG) emissions predominantly caused by human activities, have caused global temperatures to rise. This further results in long-term changes to the climate, leading to observable impact on our planet, such as rising ocean levels, ocean acidification and more intense extreme weather events [1].

To stop the trend of climate change, almost every country in the world signed the Paris Agreement in 2015, aiming to reduce GHG emissions and hold "the increase in the global average temperature to well below 2°C above pre-industrial levels" and pursue efforts "to limit the temperature increase to 1.5°C above pre-industrial levels" [1]. Following the UK's Nationally Determined Contribution agreed in Paris, the UK commits to reducing economy-wide GHG emissions by at least 68% by 2030 compared to 1990 levels and to achieving net zero emissions before 2050 [2].

Electricity sectors in advanced economies are expected to reach net zero emissions by 2035 and globally by 2040, which enable other sectors such as industry, transport and buildings sectors to cut emissions through electrification [3]. In this context, increasing low-carbon technologies for electricity generation and supply are developed in electricity networks. The focus of this thesis is on electricity distribution networks. With the development of distributed renewable generation and new electrified demand, electricity distribution networks are undergoing unprecedented changes.

1.1.1. Changes in electricity distribution networks

- **Renewable generation development**

According to the report from International Energy Agency in 2022, the share of renewables in electricity generation is expected to increase from 28% in 2021 to over 60% in 2030 and nearly 90% in 2050 [3]. Fig. 1.1 provides the total installed capacity

and electricity generation in the world since 2010. Solar photovoltaics (PV) and wind are deemed as the leading renewables of cutting electricity sector emissions. Their global share of electricity generation is expected to increase from 10% in 2021 to 40% by 2030, and 70% by 2050.

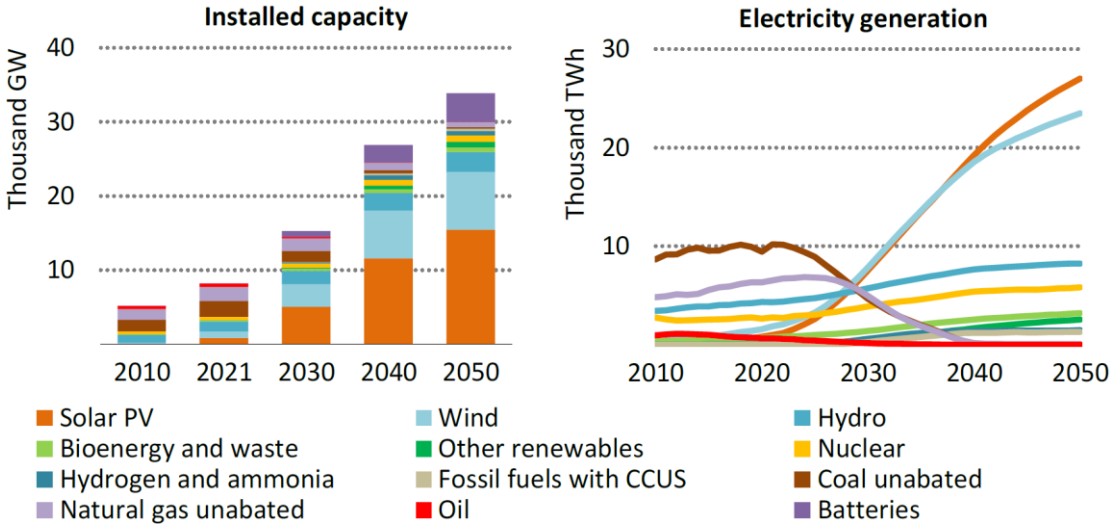

Fig. 1.1. Total installed capacity and electricity generation by source between 2010 and 2050 [3].

The integration of the renewable generation in distribution networks can reduce electricity losses caused by long-distance electricity transmission from centralised power plants located far from load centres [4]. In addition, it has been observed that instability in fossil fuel supply and fluctuations in electricity prices have encouraged small residential and commercial consumers to generate their own power from distributed renewable generation and feed extra power to the power grid [5], [6]. These benefits facilitate a significant increase in distributed renewable generation in distribution networks. For instance, the global deployment of solar PV systems has seen a consistent rise from 2019 to 2022, with the installed capacity of distributed PV systems adding up to 226 GW according to the estimation from the International Energy Agency [6]. In 2023, distributed PV systems accounted for even half of this year's overall deployment of solar PV [7]. This trend is anticipated to continue in the future,

supported by growing incentives for customers and escalating concerns over the energy crisis.

- **Electricity demand growth**

Electricity is one of the most rapidly expanding sectors in final energy consumption. Its proportion in final energy use will escalate from 20% in 2021 to an anticipated 30% by 2030, and it is projected to exceed 50% by 2050 [3].

Fig. 1.2 shows the change of the global electricity demand in different sectors between 2010 and 2050. As a consequence of the electrification in different sectors, the total electricity demand will double by 2050 in comparison to the 2020 level. Regarding the industry and building sectors, the electricity consumption will increase by 47% and 12% respectively by 2030 and nearly 130% and 33% respectively by 2050. Notably, the electrified traffic demand will experience an almost eightfold increase by 2030 and a staggering 37-fold augmentation by 2050 relative to 2020.

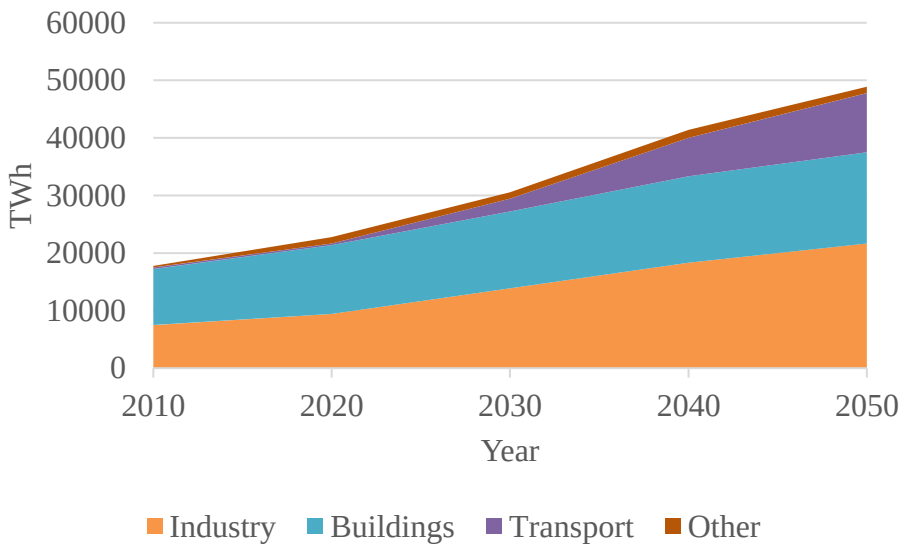

Fig. 1.2. World electricity consumption by sector [3].

In the UK, driven by accelerated residential appliance and lighting efficiency improvements, there can be a short-term fall in electricity demand before 2050 [8]. However, the increasing levels of electrification, particularly through the adoption of

electric vehicles on a large scale and the transition to electric-based domestic heating systems (e.g., heat pumps), are expected to significantly increase the electricity demand from the late 2020s into the 2030s. As a result, electricity demand could more than double by 2050 [9].

- **Challenges to hosting capacity of distribution networks**

The large-scale integration of low carbon distributed renewable generation and new electrified demand will greatly increase the total/peak power generation/load in distribution networks, which bring great challenges to electricity distribution networks, including overloading problems, voltage violation problems (especially overvoltage problems due to high penetration of renewables).

To host the increasing power generation and power demand in distribution networks, additional network capacity is needed. If all aspirational targets announced by governments are met on time, more than 45 million km of distribution lines (compared to 4 million km of transmission lines) worldwide will be added along with primary equipment, transformers and associated control and protection equipment [3].

In developing countries, new electricity lines will be built, while in advanced economies where electricity networks are well developed and generally older, there is more focus on replacement and less on new lines.

Three direct consequences are anticipated:

1) High investment cost.

As stated by the International Energy Agency, global grid investment is expected to rise to USD 630 billion (over £ 500 billion) by 2030 and USD 830 billion (nearly £ 680 billion), with distribution networks accounting for the largest share [3]. This investment could be paid eventually by customers.

2) Impact on the society and environment.

Construction or reinforcement of distribution networks typically necessitates significant excavation and can lead to disruptions. Residents in proximity to proposed line routes might experience adverse impacts from these initiatives and may consequently oppose the projects.

3) Long permitting and construction time.

Depending on the length of the line and geographic and weather factors, it often takes 4-7 years for the permitting and construction of a single distribution line [3]. Additionally, conditions and specifications have to be assessed, and stakeholders must be engaged before being permitted.

In this context, innovative solutions are imperative to either defer the conventional reinforcement or reduce the investment costs. SOPs provide an alternative promising solution.

1.1.2. SOPs solution

Distribution networks are usually operated in radial configurations, where normally open points (NOPs) are built, connecting adjacent feeders to provide alternative routes of electricity supply in case of planned or unplanned power outages. Such configuration has the benefits of inherent simplicity of operation and protection. However, it may constrain further integrations of demand and generation due to potential voltage and thermal violations, uncontrolled power flows and short-circuits problems [10]. Moreover, due to the uncertainties in the potential locations, capacity and power output/consumption of distributed generation (DG) and demand in the future, distribution networks may be stressed somewhere yet underutilised elsewhere. Rebalancing and rerouting of power flows are therefore needed.

A solution is to close NOPs and form a meshed network, which eases feeder stress by transferring the power through less heavily loaded routes [11]. However, this can

result in excessive fault current and requires more complicated and expensive protection schemes [12].

A hybrid solution that combines the advantages of both radial and meshed configurations while effectively removing their disadvantages is to utilise SOPs, which are power electronic devices usually placed at NOPs of electricity distribution networks [12], [13]. Compared to NOPs, an SOP can not only transfer active power loading between the connected feeders, but also provide/absorb reactive power at each terminal of the SOP independently [10]. Moreover, it can isolate the fault between the connected feeders immediately and provide supply restoration during post-fault period [14], [15]. With great real-time power controllability, they have been verified promising in dealing with the aforementioned challenges of distribution networks .

These distribution-level power electronics were invented and named as Siemens multifunctional power link (SIPLINK) by Siemens AG in Germany in 2001 [16]. The name of SOPs was used in [17] in 2010, emphasizing on the replacement of normally open points in distribution networks. Since its inception, different names were also used to describe such type of devices although they may have different focuses, such as direct current (DC)-link [18], DC interlink [19], medium voltage direct current (MVDC)-link [20], [21], soft multi-state open point [22], loop balance controller [23], [24], back-to-back active power controller [25], back-to-back system [26], [27], flexible interconnection device [28] and partition flexible interconnection converter station [29]. Among these names, SOPs have been widely accepted by researchers and will be used in the thesis.

1.1.3. Development of feasible operation regions

SOPs can reinforce electricity distribution networks, thus increasing the capability of distribution networks to accommodate increasing generation and/or demand (i.e.,

hosting capacity of distribution networks). Distribution network operators (DNOs) need effective tools to assess the hosting capacity of distribution networks and to conduct active management of networks with SOPs.

The conventional methods for assessing the hosting capacity of distribution networks rely largely on the selected scenarios, which lead to conservative or limited results. The most commonly used methods by the power utilities are "worst-case" analysis [30], [31]. For example, the capability of distribution networks to accommodate increasing DG is assessed under the minimum loading conditions. This makes the results very conservative and leads to the network headroom not efficiently used. Moreover, the uncertainties in the potential locations, capacity and power output/consumption of future DG and demand significantly obstruct the identification of the "worst cases". An alternative way is to consider the maximum total hosting capacity among all candidate locations [31], [32], [33], [34]. Monte Carlo simulation can be used for such assessment [35], [36], [37], but the result is still not accurate because of the curse of dimensionality.

To overcome the deficiency of the scenario-based methods, another stream of methods with different philosophy, termed as security region-based methods, describe the overall picture of the network capability to integrate generation and demand. The security region is denoted as the range of operating states of a distribution network, within which no security constraints are violated. The methodology was first developed for assessing the security of electricity transmission networks [38], [39] in 1975, but has started to be applied to electricity distribution networks [40], [41], [42] and integrated energy systems [43], [44], [45], [46], [47] in recent ten years. The milestones of security region methodology are summarised in Fig. 1.3.

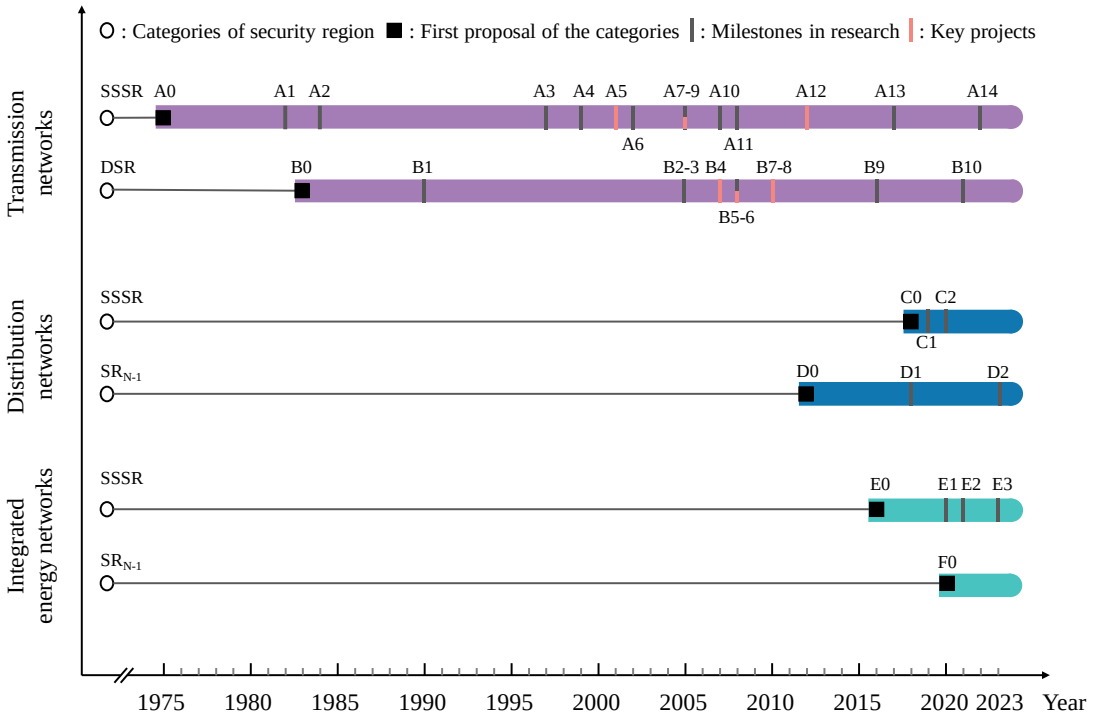

Transmission networks
Steady-state security region (SSSR)
A0. SSSR is firstly proposed-1975, [48]
A1. SSSR is approximated by a hyperbox-1982, [38]
A2. Small-disturbance stability region is firstly developed-1984, [49]
A3. SSSR is obtained by artificial neural network-1997, [50]
A4. Static voltage stability region (SVSR) is firstly developed-1999, [51]
A5. Project in Henan (China)-2001, [52]
A6. SVSR boundaries are approximated by hyperplanes in cut-set complex power space-2002, [52]
A7. Project in Liaoning (China)-2005, [53]
A8. SVSR constraints are used in optimal power flow model-2005, [54]
A9. SSRR is used in probabilistic security assessment-2005, [55]
A10. SVSR boundaries are approximated by tangent hyperplane around voltage collapse points -2007, [56]
A11. SVSR boundaries are approximated by quadratic hypersurface around voltage collapse points -2008, [57]
A12. Project in China Southern Power Grid (China)-2012, [58][59]
A13. SVSR boundaries are approximated by polynomials -2017, [60]
A14: SSSR boundaries are simulated by the optimisation method -2022, [47]
Dynamic security region (DSR)
B0. DSR is firstly proposed-1983, [39]
B1. DSR boundaries are approximated by pairs of hyperplanes for practical application-1990, [61]
B2. Voltage stability security region (VSSR) is firstly developed-2005, [62]
B3. DSR is used in probabilistic security assessment-2005, [55]
B4. Project by Electric Power Research Institute (the US)-2007, [63]
B5. DSR is used in OPF model for unit commitmnet-2008, [64]
B6. Project by East Kentucky Power Cooperative (the US)-2008, [65]
B7. Project by Pacific Northwest National Laboratory (the US)-2010, [66]
B8. Project in Saudi electricity system (Saudi Arabia)-2010, [67]
B9. DSR is used in DC-OPF model for market clearing and power dispatch-2016, [68]
B10. DSR is obtained by sparse oblique decision tree-2021, [69]
Distribution networks
Steady-state security region (SSSR)
C0. Static voltage security region is approximated by using hyperplane boundaries-2018, [41]
C1. Thermal security region is approximated by using hyperplane boundaries-2019, [42]
C2. Impact of SOPs on SSSR is firstly analysed by the simulation method-2020 (see the last publication in Section 1.5 List of publications)
Security region under N-1 (SR_{N-1})
D0. SR_{N-1} is firstly proposed based on DC power flow-2012, [70]

D1. SR_{N-1} is used in power supply capability assessment-2018, [71]
D2. Concave SR_{N-1} is firstly observed-2023, [72]
Integrated energy networks
Steady-state security region (SSSR)
E0. SSSR is firstly used in electricity-gas integrated energy networks-2016, [73]
E1. SSSR is firstly used in electricity-heat integrated energy networks-2020, [74]
E2. SSSR is firstly used in electricity-gas-heat integrated energy networks -2021, [75]
E3. Sequential SSSR is developed considering dynamics of combined heat and power plants-2023, [76]
Security region under N-1 (SR_{N-1})
F0. SR_{N-1} is firstly used in electricity-gas-heat integrated energy networks-2020, [77]

Fig. 1.3. Timeline of security region methodology. The milestones are identified considering the emerging of the subcategories of security region and different methods for obtaining security region, and significant applications.

Inspired by security region methods, this thesis proposes the "feasible operation regions (FORs)" for the assessment of the steady-state operation of distribution networks. It is noteworthy that security regions of energy networks encompass concerns about network stability following faults, in addition to steady-state security. In contrast, this thesis focuses on electricity distribution networks, where the violations of node voltages or line currents are of primary concern during operation and also having direct implications for the investment on network reinforcement. Accordingly, the formulation of FORs is specifically aimed at tackling the constraints associated with node voltages and line currents within distribution networks.

Limited by the node voltage and line flow constraints, one operating state of a distribution network can be either feasible or infeasible. With all possible operating states marked as feasible or infeasible, the region that encloses all the feasible operation states is the FOR of the distribution network. In this regard, the boundaries of FOR provide the limitations to operating the network and contain the whole information of the capability of the network to integrate generation and demand. With the mathematical expressions of the FOR boundaries, FORs can also be used to conduct active management of networks by replacing the power flow equations and network constraints with FOR boundaries in optimal power flow models [41], [42]. Furthermore, the safety margin of a feasible operating state or the degree of unsafety of an infeasible

operating state can be obtained through analysing the distance between the operating state and the FOR boundaries [78].

1.2. Research motivation

Since FORs can provide accurate description of the hosting capacity and effective active management and safety analysis of a distribution network, this thesis is motivated to develop and exploit the FOR methodology in distribution networks considering the impact of SOPs. The research motivation is as below.

1.2.1. Feasible operation region methodology

Modelling of the FOR of the distribution network needs to be first investigated before being used for efficient network capability assessment and active management of distribution networks with SOPs. There have been many studies (which are discussed in detail in Section 2.2.3) on developing analytical expressions of operation region boundaries for transmission networks, but they cannot be directly applied to distribution networks because distribution networks are with high R/X ratio (i.e., the ratio of network resistance to network reactance) and the power flow equations cannot be simplified as decoupled active/reactive power flow equations. For distribution networks, linear approximation (termed as hyperplane expressions) for voltage and thermal boundaries of FORs were derived in [41] and [42], respectively. However, the hyperplane expressions might not be accurate especially for thermal boundaries of FOR. Analytical expressions of FOR boundaries need to be further investigated before being used in the analysis of distribution networks with SOPs.

1.2.2. Characterisation of feasible operation regions with SOPs

With the development of FORs of distribution networks, the impact of power electronic devices on FORs needs to be investigated. It has been demonstrated that SOPs can improve line flow and node voltage profiles effectively in distribution

networks (see detailed discussion in Section 2.1.1). These improvements can boost the network capability [21], [79], [80] to accommodate increasing generation and/or demand, thereby expanding the FOR of an electricity distribution networks. In our previous study (see the last publication), the expansion of the FOR by SOPs is first observed by simulating the boundary points of the FOR in two-dimensional or three-dimensional space. However, the FOR of the distribution network with SOPs has not been modelled, hindering the application of FORs in analysing distribution networks with SOPs. Therefore, the modelling of the impact of SOPs on the FOR of the distribution network needs to be investigated.

1.2.3. Constraint management of distribution networks with SOPs

In studies on SOP control targeting diverse objectives like feeder load balancing, voltage profile improvement, and power losses reduction (the detailed discussion is in Section 2.1.2), OPF-based methods are normally employed for optimal SOP control. However, they require global information regarding power load and generation, which makes the OPF-based methods impractical given that the measurements across most distribution networks are not universally available [81]. Moreover, the complex global optimisation might hinder the fast response of SOPs against the frequent power/voltage fluctuations in the networks [79], [82]. The FOR methodology has been proved to be effective in the OPF-based model [54], [64], [68] (as discussed in Section 2.2.3) in the cases that the concerned security constraints are not available or/ and the computational efficiency is required. Moreover, due to the one-to-one correspondence between FOR boundaries and the network constraints, the FOR constraints of the components equipped with real-time measurements are simply needed to be included into the constraints of the optimisation model. This makes the FOR-based constraint management method promising in adapting to various measurement conditions.

1.3. Objectives of the thesis

The objectives of the thesis are to:

- Develop analytical expressions of the FOR of an electricity distribution network. The FOR can describe the overall picture of the network capability to integrate generation and demand, which can be a useful tool for active management and efficient expansion of distribution networks.
- Model the impact of SOPs on the FOR of the distribution network and develop the analytical expressions of the FOR of a distribution network with SOPs.
- Exploit the FOR of the distribution network for optimal constraint management of the distribution network using SOPs.

1.4. Main contributions of the thesis

The main contributions of the thesis are described below.

- Quadratic expressions are proposed for describing both voltage and thermal boundaries of FORs, considering both active and reactive power injection at each node. Compared with the existing hyperplane expressions, the proposed quadratic expressions are more accurate especially for thermal boundaries. An effective high-dimensional error analysis approach is also provided for validating the analytical boundaries of FORs, in contrast to the existing methods mainly applicable to low-dimensional cross-sections of the FOR.
- A novel geometry model of the FOR with SOPs (FOR^{SOP}) has been established. The model interprets the FOR^{SOP} as the Minkowski Sum of the FOR of the distribution network (FOR^{DN}) and the operating range of SOPs (SOP^{OR}). Additionally, a practical Minkowski Sum algorithm is developed to derive the analytical expressions of FOR^{SOP} boundaries, which exploits the

translation and fitting methods within the algorithm. The Minkowski Sum method is not commonly used in electrical engineering but is prevalent in some other domains like robot motion planning. Notably, this thesis introduces this interdisciplinary geometric method to the field of electrical engineering, where it holds great potential for formulating the FOR of distribution networks with various types of power electronic devices and for aggregating different types of flexible power sources.

- A novel FOR-based method for optimal SOP control is developed. The FOR can be used to replace the power flow equations and network constraints in conventional optimal power flow-based model. Due to the one-to-one correspondence between FOR boundaries and thermal/voltage constraints, FOR-based constraint management method can adapt to various measurement conditions. Moreover, the FOR constraints can be converted into a format based on line flows and node voltages, allowing for the use of real-time measurements of these operating parameters rather than the measurements of nodal power load/generation that are normally not accessible online. The method can rapidly generate SOP set points, with the cost of time being solely dependent on the number of SOP terminals and measurement units, rather than the scale of the distribution network.

1.5. List of publications

- **First-authored journal papers**

[1] **X. Jiang**, Y. Zhou, J. Wu, W. Ming, "Feasible operation region-based constraint management of distribution networks with soft open points," ***IEEE Trans. Power Systems***. (Under review)

[2] **X. Jiang**, Y. Zhou, J. Wu, W. Ming, "Feasible operation region of a

distribution network with soft open points," ***IEEE Trans. Smart Grid***. (Under review)

[3] **X. Jiang**, Y. Zhou, W. Ming, and J. Wu, "Feasible operation region of an electricity distribution network," ***Appl. Energy***, vol. 331, pp. 120419, 2023. (https://doi.org/10.1016/j.apenergy.2022.120419)

[4] **X. Jiang**, Y. Zhou, W. Ming, P. Yang, and J. Wu, "An Overview of Soft Open Points in Electricity Distribution Networks," ***IEEE Trans. Smart Grid***, vol. 13, no. 3, pp. 1899–1910, 2022. (http://dx.doi.org/10.1109/TSG.2022.3148599)

- **First-authored conference papers**

[1] **X. Jiang**, J. Wu, Y. Zhou and W. Ming. "Feasible operation region of a distribution network considering thermal constraints", *Proceeding of the 13th international conference on applied energy (**ICAE2021**)*, 2021. (https://orca.cardiff.ac.uk/id/eprint/149081/1)

[2] **X. Jiang**, W. Ming, Y. Zhou and J. Wu. "Optimal operation of soft open points to minimize energy curtailment of distributed generation in electricity distribution networks", *Proceedings of applied energy symposium 2020: Low carbon cities and urban energy systems (**CUE2020**)*, 2020. (https://doi.org/10.46855/energy-proceedings-7459)

- **Other publications**

[1] G. Zu, Y. Wang, **X. Jiang**, Z. Hao, X. Zhang, "Total supply capability of electricity distribution networks considering flexible interconnection of low‐voltage service transformers," ***IET Smart Grid***, 2024. (https://doi.org/10.1049/stg2.12157)

[2] J. Xiao, Y. Fan, and **X. Jiang**, "Decoupling and dimension reduction method

for distribution system security region," ***IET Energy Syst. Integr.***, vol. 5, no. 3, pp. 338–354, 2023. (https://doi.org/10.1049/esi2.12105)

[3] J. Xiao, G. Zu, Y. Wang, X. Zhang, and **X. Jiang**, "Model and observation of dispatchable region for flexible distribution network," ***Appl. Energy***, vol. 261, pp. 114425, 2020. (http://dx.doi.org/10.1016/j.apenergy.2019.114425)

1.6. Thesis outline

Fig. 1.4 presents the structure of the thesis.

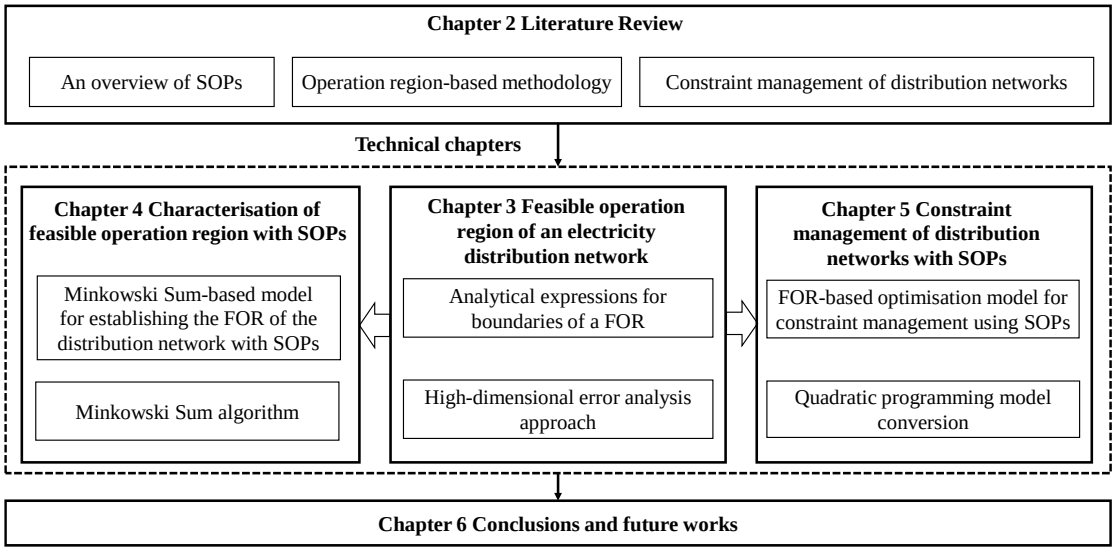

Fig. 1.4. Thesis structure.

The thesis is organised as follows:

Chapter 2 provides a review on SOPs in distribution networks. The methodology used in the thesis, which is referred to security region-based methodology, is reviewed subsequently. Emerging technologies and their control methods for constraint management of distribution networks are also investigated.

Chapter 3 proposes quadratic expressions of the boundaries of the FOR of a distribution network to accurately express the network capability and efficiently exploit the network headroom for integration of more DG/demand. This chapter also provides a high-dimensional error analysis approach. Case studies were conducted to validate

the effectiveness of the proposed expressions of FOR boundaries. The results were compared with the existing linear approximation (termed as hyperplane expressions) of FOR boundaries.

Chapter 4 develops a Minkowski Sum-based model and its associated practical solving algorithm to analytically express the FOR of a distribution network with SOPs. The effectiveness of the proposed method was validated through case studies.

Chapter 5 develops a novel FOR-based optimisation model for constraint management using SOPs in distribution networks. The model can be transformed into a quadratic programming formulation to enhance the computational efficiency. Case studies were carried out to validate the effectiveness of the proposed method and to compare its performance with that of local control and optimal power flow-based control.

Chapter 6 presents the conclusions, main findings of the thesis and recommendations for the future work.

Chapter 2. Literature Review

This chapter first presents a literature review on SOPs in distribution networks. The security region-based methodology, which will be referred to in studies on FORs in this thesis for assessing the hosting capacity and for conducting active management in distribution networks with SOPs, is introduced subsequently. The emerging constraint management technologies and their control approaches are also discussed.

2.1. An overview of SOPs

2.1.1. Topologies of SOPs

SOPs are usually used for connecting different alternating current (AC) feeders or buses of an electricity distribution network. The main function of SOPs is AC/AC conversion and accordingly there are four different topologies for SOPs, as shown in Fig. 2.1. These topologies include back-to-back voltage source converters (VSCs), multi-terminal VSCs [83], unified power flow controller (UPFC) [84], [85] and direct AC-to-AC modular multilevel converter (MMC) [86].

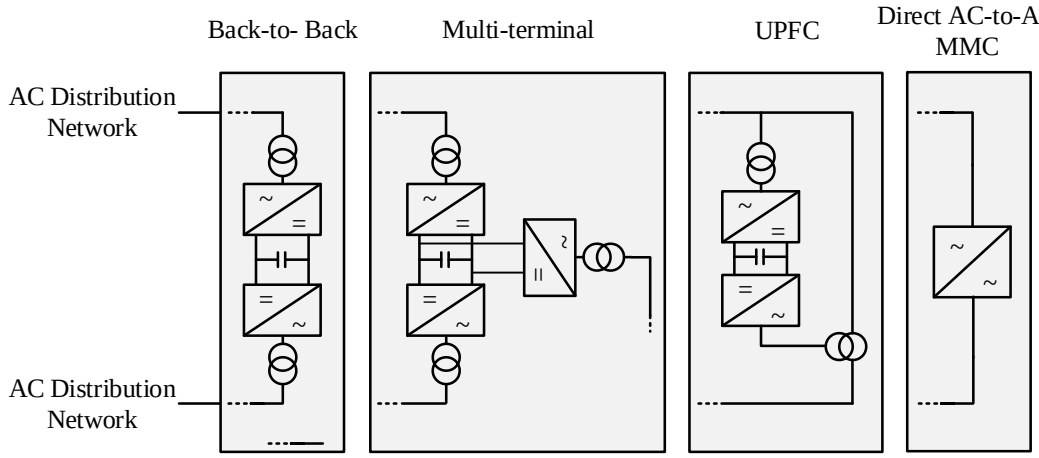

Fig. 2.1. Different topologies of SOPs.

Back-to-back VSCs, multi-terminal VSCs and UPFC are three typical indirect AC-to-AC topologies of SOPs. These three typical topologies exploit multiple VSCs to achieve AC/AC conversion between connected feeders. The main advantages for using VSCs to build SOPs are threefold [12]: 1) the freedom to operate with any combination

of active and reactive power; 2) the ability to limit fault current; 3) the possibility to supply isolated areas of a network and even provide the black-start capability. For these typical topologies, VSCs are connected through a common DC bus. The DC bus is very short so that there is no overhead lines or cables separating the VSCs. This enables high DC current and low DC voltage, thus reducing the insulation requirement and favouring a compact design for SOPs. Through the DC bus, energy storage can be easily connected to provide more flexibility for the operation of distribution networks [87] - [90]. At the interfaces of each VSC with the connected AC feeders, coupling transformers are usually equipped.

Despite the similarities in multi-VSC configuration, there are some different features among back-to-back VSCs, multi-terminal VSCs and UPFC topologies. A major difference lies in whether the connected distribution networks are isolated by the DC bus. As shown in Fig. 2.1, due to the intermediate AC/DC conversion stage, connection between asynchronous distribution networks is viable for back-to-back and multi-terminal VSC based SOPs. Under abnormal network conditions, the fault on one feeder can also be isolated from other feeders by the DC bus. For a UPFC based SOP in comparison, it consists of two VSCs with one in series and the other in shunt, and the feeders interconnected with it are not isolated by the DC bus. Therefore, the connected distribution networks are required to be synchronous and the fault on one feeder will affect the other unless an effective control strategy is developed. However, a UPFC based SOP is able to control power flows greater than its rating (for example, 1MVA rated UPFC based SOP can control maximum 10MVA power exchange between the feeders in Fig. 2.1). Thus, the cost of this type of SOPs can be largely reduced. To make the conventional SOP topologies more competitive in the cost, the

normally bulky and expensive transformers that connect SOP converters can be further removed [23], [91], [92], [93].

J. Pereda et al [18] proposed direct AC-to-AC MMC as an SOP topology, with the idea of keeping the advantage of MMC and simultaneously reducing its cost when applied in distribution networks. For high-voltage direct current transmission, MMC has been proved to be a promising VSC topology due to its high efficiency, fault tolerant operation, and low total harmonic distortion [94], [95]. However, when applied in distribution networks, it occupies big space and has high cost compared to two-level or three-level converters. To solve this problem, the direct MMC topology is an attractive solution. Compared to back-to-back MMC, a direct MMC based SOP has no DC bus and has the same number of semiconductors but half the number of capacitors and inductors, which can reduce the installation space and overall cost. However, it has an important drawback that the currents in the connected two feeders are not independent. The coupling of the currents between the two feeders entails a coupled reactive power and results in a limitation of the converter to assist only one feeder at a time when unbalance voltage or harmonic compensation is desired [18]. These limitations are expected to be addressed by control and hardware development hereafter.

2.1.2. Modelling and benefit quantification of SOPs

In this section, a generic steady-state model of SOPs and various indices for quantifying the benefits of SOPs in distribution networks are given. The model and quantification indices have been widely used in the analysis of distribution networks with SOPs, laying the foundation for the optimal system-level control of SOPs in Section 2.1.3 and the optimal siting and sizing of SOPs in Section 2.1.4. It should be mentioned that due to the space limitations this section does not give the SOP models for all the topologies shown in Section 2.2.1. Instead, the generic model for SOPs with

back-to-back VSCs and multi-terminal VSCs topologies (two commonly used topologies in both research and practice) is given, while the models of SOPs with direct AC-to-AC MMC topology and UPFC topology refer to [86] and [96], respectively.

- **Mathematical model of SOPs**

The steady-state model of SOPs is normally developed as the power injection model, which involves the power injections at SOP terminals and hence enables straightforward incorporation of SOPs into existing power flow analysis without the need of considering detailed controller design. The mathematical model of an SOP is shown in (2-1)-(2-4), expressing the active power exchange, power losses, power constraints and voltage constraints of the SOP respectively.

$$\sum_{i=1}^{N_T}(P_i^{SOP}+P_i^{SOP,\mathrm{L}})=0 \tag{2-1}$$

$$P_i^{SOP,L}=A_i^{SOP}\sqrt{\left(P_i^{SOP}\right)^2+\left(Q_i^{SOP}\right)^2} \tag{2-2}$$

$$\sqrt{\left(P_i^{SOP}\right)^2+\left(Q_i^{SOP}\right)^2}\le S_i^{SOP} \tag{2-3}$$

$$V_i^{\min}\le V_i^{SOP}\le V_i^{\max} \tag{2-4}$$

N_T is the number of the terminals of the SOP. P_i^{SOP} and Q_i^{SOP} are active power and reactive power injections from the *i*th terminal of the SOP to the connected points of the network. $P_i^{SOP,\mathrm{L}}$ is the power losses of the *i*th converter of the SOP whereas A_i^{SOP} is the losses coefficient. S_i^{SOP} is the capacity of the *i*th converter of the SOP. V_i^{SOP} denotes the voltage of the network at the *i*th terminal of SOP, normally restrained by the minimum allowed network voltage $V_i^{\min}$ and the maximum allowed network voltage $V_i^{\max}$ at the SOP terminals. The setting for $V_i^{\min}$ and $V_i^{\max}$ can be customized according to different network conditions. Under normal network condition, $V_i^{\min}$ and $V_i^{\max}$ are

usually defined as the minimum and maximum allowed voltages of the network [97], while in fault conditions, SOPs can serve for voltage support and $V_i^{\min}$ is suggested to be set as 1.0 p.u. [14], [98].

- **Benefit quantification of SOPs**

SOPs can provide accurate and fast bidirectional active and reactive power flow control, which can bring great benefits to electricity distribution networks. Under normal operation of distribution networks, SOPs can help balance the power loads between connected feeders, improve the voltage profile [19], [82], and/or reduce the overall power losses [99], [100], [101]. These three benefits are comprehensively considered in [97], [102], [103], [104] and compared in [21], [79].

In addition, SOPs can increase DG penetration [89], [105], [106] and participate in congestion management [107], [108]. Under three-phase unbalanced operation condition of the network, SOPs can mitigate the three-phase unbalance [109], [110]. When a fault occurs, SOPs can detect the presence of an unbalanced fault [109], help isolate the fault area and split the distribution network into separate self-sufficient partitions [98]. They can also achieve fast supply restoration [14], [111], [112], [113], [114] resulting in the reliability improvement of the network [115].

Quantifying the benefits of SOPs is important for SOP owners to learn their value in an intuitive and comparable way. Moreover, the quantification indices can be selected as objective functions in the optimisation problems for the optimal control and the optimal siting and sizing of SOPs in distribution networks, which will be detailed in Section 2.1.3 and Section 2.1.4 respectively. Due to the importance of benefit quantification for SOPs, this section summarises the existing quantification indices.

The identified indices, although with different unit and function, can be used for evaluating the benefits of SOPs considering different operation targets of distribution

system operators separately. Moreover, multiple indices can be used as objectives in a multi-objective optimisation model for a comprehensive evaluation of the benefits of SOPs. A straightforward way is to weight and summate these indices in one objective function after their standardisation. Based on Pareto-dominance principle [21] [97], a set of solutions with equal interests amongst different objectives can be further obtained and the trade-off between different SOP benefits can be considered. By comparing the values of these indices, technologies used in distribution networks, including SOPs and other technologies such as network reconfiguration and on-load tap changers, can be compared quantitatively.

1) Feeder load balancing

Feeder load balancing of a distribution network can be represented by the line utilisation index – feeder load balancing (FLB), which can be defined either in the form of the line currents [79] [97], [104], or in the form of apparent power flow [21]. The index represented by the line currents is shown in (2-5), while the index represented by the power flow is described as (2-6) or (2-7).

$$FLB = \sum_{ij \in B} \left(\frac{I_{ij}}{I_{ij-rated}} \right)^2 \tag{2-5}$$

I_{ij} is the current flowing through line ij, and $I_{ij\text{-}rated}$ is the rated current of line ij. B is the set of lines.

$$FLB = \sum_{ij \in B} \left(\frac{S_{ij}}{S_{ij,\text{rated}}} \right)^2 \tag{2-6}$$

S_{ij} is the apparent power flow in line ij, and $S_{ij,\text{rated}}$ is the rated capacity of the line.

$$FLB = \sqrt{\frac{1}{n_b} \sum_{ij \in B} \left(\frac{S_{ij}}{S_{ij,\text{rated}}} \right)^2} \tag{2-7}$$

n_b is the number of power lines in the distribution network.

The index shown in (2-7), divided by the total number of lines, reflects the average degree of utilisation of all lines in the distribution network.

2) Voltage profile improvement

Voltage profile index (VP_{index}) is commonly used to measure the voltage improvement of a distribution network. The index reflects the degree of dispersion of all bus voltages from the nominal values, which is described as the following forms.

$$VP_{index} = \sqrt{\frac{1}{n}\sum_{i\in N}\left(V_i - V_{i,\mathrm{ref}}\right)^2} \tag{2-8}$$

$$VP_{index} = \sum_{i\in N}\left(\left|V_i\right| - \left|V_{i,ref}\right|\right)^2 \tag{2-9}$$

$$VP_{index} = \sum_{i\in N}\left|V_i - V_{i,ref}\right| \tag{2-10}$$

V_i and $V_{i,ref}$ are the real and nominal voltage magnitudes at bus i. N is the set of of buses. Equation (2-8) adopts the form of the standard deviation of the bus voltages [21], while it is more simplified in (2-9) [79] and (2-10) [97].

3) Power losses reduction

Power losses reduction is one of the key benefits brought by the SOPs for distribution networks. Power losses index (PL_{index}), as shown in (2-11), is usually calculated for evaluating this benefit and is of great significance for the cost evaluation [21][97].

$$PL_{index} = \sum_{ij\in B} I_{ij}^2 \times R_j = \sum_{ij\in B} \frac{P_{ij}^2 + Q_{ij}^2}{\left|V_j\right|^2} \times R_j \tag{2-11}$$

R_j is the resistance of line ij. P_{ij} and Q_{ij} are the active and reactive power flow through line ij. In [79], energy losses is also adopted as a quantification index by adding up the power losses during a certain period of time.

4) Three-phase balancing

Distribution networks are usually unbalanced due to the asymmetric three-phase line configuration and a large number of single-phase power loads. The asymmetric integration of DGs will further exacerbate the three-phase unbalanced condition in a distribution network. The unbalanced operation of the network will cause inefficient utilisation of network assets and increase losses. The negative sequence components of the unbalanced voltages may also result in distribution equipment operating in an abnormal condition.

SOPs are able to rapidly regulate the three-phase active and reactive power flow to mitigate the three-phase unbalance. In [109], the three-phase balancing indices are proposed in (2-12) and (2-13), while in [110] the index for voltage unbalance adopts a different form as shown in (2-14).

$$f^{\mathrm{V}} = \sum_{i \in N} \sum_{\varphi=a}^{c} \left| V_{\varphi,i} - \frac{1}{3}\left(V_{a,i} + V_{b,i} + V_{c,i}\right) \right| \tag{2-12}$$

$$f^{\mathrm{I}} = \sum_{\varphi=a}^{c} \left| I_{\varphi,0} - \frac{1}{3}\left(I_{a,0} + I_{b,0} + I_{c,0}\right) \right| \tag{2-13}$$

$$f^{\mathrm{V}} = \sum_{i \in N} \sum_{\varphi=a}^{c} \left| \left|V_{\varphi,i}\right|^2 - \frac{1}{3}\left(\left|V_{a,i}\right|^2 + \left|V_{b,i}\right|^2 + \left|V_{c,i}\right|^2\right) \right| \tag{2-14}$$

f^{V} and f^{I} are the index of the voltage unbalanced condition of the network and the current unbalanced condition of the substation. $V_{\varphi,i}$ is the complex voltage on phase φ (φ=a, b, c) at busbar i. $I_{\varphi,0}$ denotes the complex current on phase φ of the substation outlet.

5) DG hosting capacity enhancement

With the strong power and voltage controllability, SOPs are able to coordinate the DG resources connected to the feeders (or networks) and mitigate voltage violation to enable more DG connected to distribution networks. Hosting capacity (HC) [89], [106] is used for quantitatively evaluating this benefit:

$$HC = \sum_{i \in N} S_i^{\mathrm{DG}} \tag{2-15}$$

S_i^{DG} is the capacity of DG at busbar *i*.

Alternatively, DG penetration level (PL) [116] can also be used for quantitative evaluation. One of the widely used DG penetration level definitions is shown below:

$$PL = \frac{\sum_{i \in G} P_{g,i}}{P_{\mathrm{max-load}}} \tag{2-16}$$

$P_{g,i}$ denotes the active power injection from the DG unit at busbar *i*, and G is the set of DG units. $P_{\text{max-load}}$ is the maximum loading of the network under study.

6) Supply restoration

After traditional protection relay acts when a fault happens, SOPs in the distribution network can be controlled for restoring the out-of-service power loads from outages. Restored active power load (RAPL) [14], [111], [112], [113], [114] is normally used for quantifying the performance of SOPs in supply restoration of the distribution network:

$$RAPL = \sum_{i \in N} \lambda_i \pi_i P_i^L \tag{2-17}$$

λ_i is the coefficient associated with the recovery level of load at bus *i*, where $\lambda_i \in [0,1]$. π_i is the weighting factor of the load at bus *i* depending on its importance. P_i^L is the active power load at bus *i*, which can be further expressed as the sum of the three-phase active power at each bus in the unbalanced distribution network [98]. In [98], [113], [114], the restored active power load during the restoration period is also accumulated for the evaluation of the benefits of SOPs.

It is noteworthy that the indices 5) DG hosting capacity enhancement and 6) supply restoration are normally maximised in the optimal operation of the distribution network with SOPs, while the indices 1) feeder load balancing, 2) voltage profile improvement,

3) power losses reduction and 4) three-phase balancing are minimised. Multiple quantification indices above can also be used simultaneously for the optimal operation (or planning) of distribution networks with SOPs.

2.1.3. Control of SOPs

- **Control structure of SOPs**

Fig. 2.2 shows the control structure of SOPs. The control for SOPs encompasses three levels: system-level, converter-level, and switching-level.

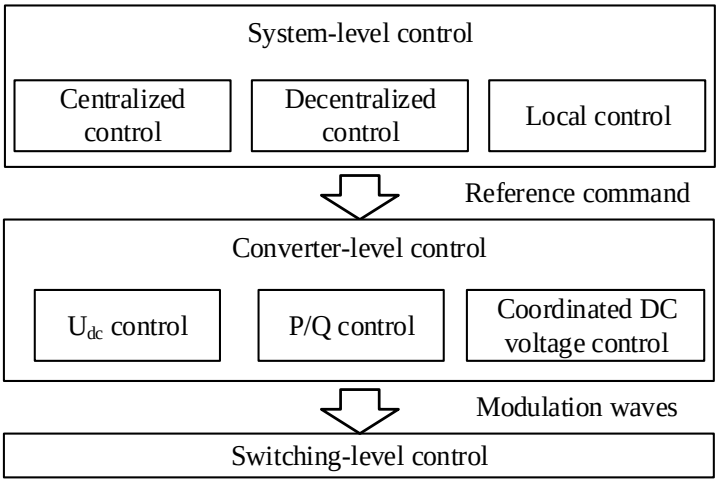

Fig. 2.2. Control structure of SOPs.

The system-level control of SOPs is based on the measured states of the distribution network and subject to communication conditions and computational requirements. Corresponding to different conditions, different system-level control strategies are developed, which can be categorised into centralised, decentralised, and local control strategies (or their mix). In the system-level control, reference values such as active power and reactive power reference values, are determined and are sent to the converter-level control.

According to different reference commands (active power, reactive power, or DC voltage reference), converter-level control can vary. At this level, DC voltage control or active power control are applied at the DC side of SOPs, while reactive power control

or AC voltage control are at the AC side. It is noteworthy that at least one converter should be selected to control the DC voltage. For multi-terminal SOPs, coordinated DC voltage control method is normally used.

Modulation waves are generated from the converter-level control for switches (e.g., Insulated Gate Bipolar Transistors) of SOPs. This section will focus on the system-level and converter-level control of SOPs only.

- **System-level control**

1) Centralised control

The centralised control requires sufficient measurements of the distribution network through fast and reliable communication. Usually, the historical or forecasted power load and solar/wind generation are needed. Based on these measurements, the optimal control strategies of SOPs are normally derived by using optimisation models, of which the objective functions can be selected from the quantification indices in Section 2.1.2 depending on different operation targets of distribution system operators.

Due to the nonlinearity of power flow equations and SOP constraints in the optimisation models, the optimal control of SOPs is nonlinear programming, which can be directly solved by the primal-dual interior-point algorithm [14], the Powell's Direct Set method [104] or intelligent algorithms such as meta-heuristic algorithm [99], particle swarm algorithm [97] and genetic algorithm [28], [112]. To achieve global optimality and computation efficiency, the original problems can also be converted to and solved as convex optimisation problems (e.g., second-order cone programming [82], [98], [107], [111] or semidefinite programming [108], [109]). Considering the uncertainty of distributed energy resources in the distribution network, the chance-constrained programming embedded nonlinear optimisation model is formulated for SOP control [114]. However, a large number of scenarios are required to fully

characterise the uncertain power output of renewable resources, making the model computationally difficult. A further robust optimisation model is formulated for the robust operation of SOPs [102] [110]. Instead of requiring the historical data or probability distribution of the power output of renewable resources, this method requires only the range of the power output. The obtained control strategy of SOPs is conservative, and the network constraints can be satisfied under the uncertainty conditions.

Besides the conventional optimisation-based centralised control for SOPs, X. Xing et al [117] develops a rolling horizon operation model for networks with SOPs on the basis of model predictive control. In [118] and [119], model predictive control is only used for inner-day/intra-day control of SOPs, combined with other methods separately for real-time control.

Despite the fact that the global optimal operation strategies of SOPs might be obtained under centralised control, the heavy communication burden and complex global optimisation might hinder the fast response of SOPs against the frequent power/voltage fluctuations in the network. Moreover, there may be privacy and security concerns in centralised control, resulting in potential data unavailability. In comparison, decentralised and local control methods can fix these problems.

2) Decentralised control

Compared to centralised control, decentralised control usually has the advantages of higher computation efficiency and stronger reliability, only based on local information of each area and boundary interaction among connected areas. Therefore, decentralised control methods are usually more suitable for SOPs to provide responses in real time.

To achieve decentralised control, H. Ji et al [120] firstly split a distribution network into multiple partitions based on voltage-to-power sensitivity analysis, assigning DGs as the partition centres and SOPs or distribution lines as the components between partitions. After network partition, the alternating direction method of multiplier algorithm is applied to realize the decentralised optimisation of the exchange power among connected areas. Different from [120], J. Zhao et al [121] consider SOPs as the centres of each partition and divide the network into sub-areas using a clustering method. This allows independent power control of SOPs in each partition by using an optimisation model for intra-area voltage control. If some nodal voltages still exceed the expected range after the intra-area autonomy, the alternating direction method of multiplier algorithm will be further used to improve the operation strategies of SOPs by inter-area coordination [121].

3) Local control

Local control for SOPs is implemented based on local information, for example the measurements of the bus voltage at each port of SOPs. Despite the difficulty to obtain the global optimal control strategy for SOPs, fast responses can be provided in real time.

To realize local control of SOPs, droop control methods are usually used [122], [123], [124]. In [123], an improved control strategy is further proposed to adjust the droop control coefficient in real time according to the rated active power and the value of active power variation. Optimisation methods could also be used for local control of SOPs. In [125], an optimisation model to minimise the apparent power of SOPs is adopted based on the local voltage data of the common connection point. Apart from the above two methods, Q-V curve is also exploited for local control of the reactive power output of SOPs. The parameters of the Q-V curve is determined by optimisation

using the day-ahead forecasted data of electricity power load and solar/wind generation [126].

- **Converter-level control**

Converter-level control aims to use control loops to generate modulation waves for the ultimate control of SOPs, using the reference values provided (e.g., from the system-level control) as the input to the controllers. Under normal network operating conditions, a dual closed-loop current-controlled strategy is popular because it can not only provide de-coupled control of active and reactive power components, but also inherently limits the converter current during network faults.

The dual closed loop consists of an outer power control loop, an inner current control loop and a phase locked loop as shown in Fig. 2.3 [10], [124], [127], [128]. In the outer power control loop shown in Fig. 2.3 (a), one converter operates with V_{dc}-Q control scheme where the DC voltage error and reactive power error are transformed into the reference d–q current components i_d^*, i_q^* through the proportional-integral (PI) controllers. Other converters normally use P-Q control scheme for active and reactive power control. Under P-Q control scheme, it is in the same way that active and reactive power errors are transformed into the reference d-q current components. In the inner current control loop shown in Fig. 2.3 (b), the d-q current errors are ultimately transformed into the modulation waves for switches of SOPs. Besides the reactive power control at the AC side of SOPs, AC voltage control can also be selected [128] in the dual closed loop. For the dual closed-loop current-control, the phase locked loop is important for synchronizing the output voltage of SOPs with the AC network voltage. As presented in Fig. 2.3 (c), by using the sum of the products of the feedback signals f_α and f_β, and input α-β voltages that are generated through Clark's transformation of the phase voltages [12], the variation of the angular frequency $\Delta\omega$ is obtained. The output

angle θ is then obtained using a PI-controller, a feedback of the base angular frequency ω_b and an integrator.

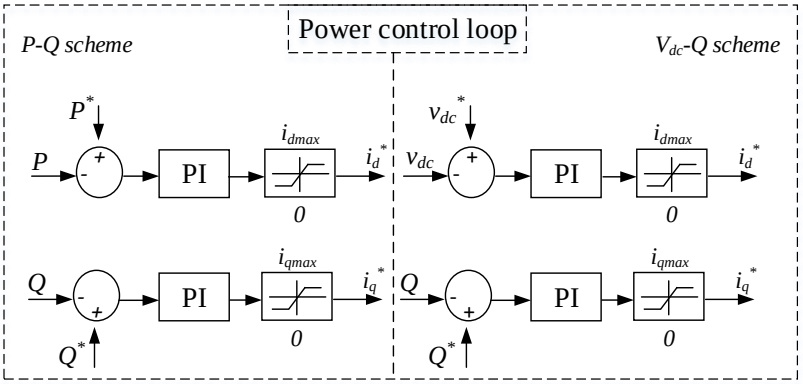

(a)

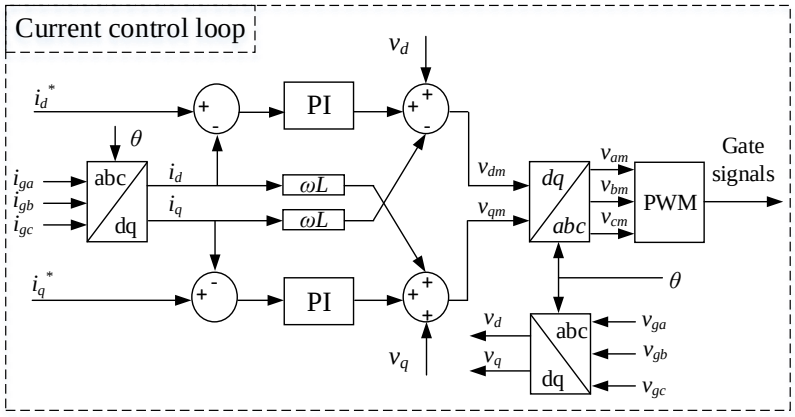

(b)

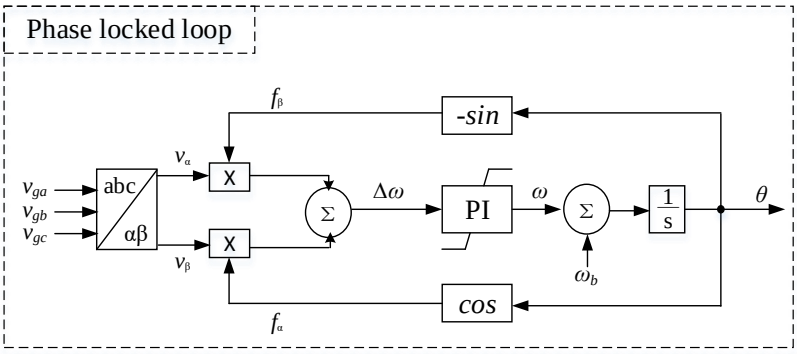

(c)

Fig. 2.3. Schematic diagram of dual closed-loop control schemes for SOPs: (a) outer power control loop; (b) inner current control loop; (c) phase locked loop

Apart from the classic dual closed loop for outer power control and the inner current control, an adaptive voltage droop outer-loop control and a sliding mode inner-loop control with feedback linearisation are further proposed in [129], which shows

better steady-state performance with less fluctuation in the controlled active/reactive power and DC voltage.

2.1.4. Optimal siting and sizing of SOPs

Optimal siting and sizing of SOPs in distribution networks is reviewed and discussed in this section. Since only the topology of back-to-back VSCs has been used in the existing studies on SOP siting and sizing, the selection of SOP topologies is not discussed yet can be a future research topic.

The siting and sizing of SOPs can be well formulated as an optimisation model, which is proved to be able to be solved by various effective algorithms in the corresponding studies. In this section, the optimisation problem for siting and sizing of SOPs is described in two parts: problem formulation (including decision variables, objective functions and constraints) and the algorithms to solve the problem.

- **Problem formulation**

1) Decision variables

The basic decision variables of the optimal siting and sizing problem for SOPs can be categorised into planning variables and operation variables. The planning variables include the installation sites and sizes of SOPs, while the operation variables encompass the active/reactive power injections from SOPs in each scenario or for each time period.

To achieve a better performance of the operation of a distribution network and to reduce the overall cost, other electrical devices or smart technologies are often used with SOPs simultaneously. The electrical devices include but not limited to the switches of the network [130], DGs [131], [132], [133], energy storage [131], and capacitor banks [133]. Therefore, the states of the switches, the sites and sizes of DGs, energy storages and capacitor banks are also considered as decision variables in these articles. In addition, I. Konstantelos et al [134] combine SOPs with other smart technologies

(demand side response and coordinated voltage control), of which the planning variables and operation variables are also decision variables in the planning problem.

2) Objective functions

In existing studies, the objective of siting and sizing of SOPs is to minimise the overall cost including the investment, maintenance, and operation-related cost within the planning horizon. Optimal siting and sizing of SOPs is to find the best trade-off between the investment/maintenance cost and the operation benefits. The total investment/maintenance cost is usually converted into annual cost by timing the capital recovery factor or the present value factor [130], [131], [132], [133]. Among the benefits summarised in Section 2.1.2, power losses reduction can be easily converted into monetary value considering the price of electricity and is commonly considered as a term in the objective function of the optimisation problem for SOP siting and sizing [130], [131]. In addition to the consideration of power losses, an alternative is to consider the cost of the electricity purchased from the upstream grid in the objective function [132], [133].

3) Constraints

The constraints for the planning problem of SOPs encompass SOP power constraints, power flow equations, network constraints and constraints of other electrical devices. In [130] [132], the constraints of SOP capacity are also considered, where SOP in each candidate location is assumed to be constituted by multiple modules or units.

In respect of SOP power constraints, the apparent power output from each SOP terminal should be within the SOP capacity. In [132], [134], an upper limit on reactive power output of SOPs is also considered individually. For power flow equations, distflow branch model [130] is usually used due to the radial topology of the

distribution network. As for network constraints, they are comprised of voltage limits and line current (or line power) limits. Constraints of other devices or technologies can refer to the correlated papers and will not be focused on this study.

4) Single-level/Bi-level optimisation

The optimal siting and sizing problem of SOPs can be formulated in a single-level [130], [131], [134] or a bi-level optimisation model [132], [133]. Compared to the single-level optimisation model, the bi-level one consists of an upper-level optimisation model and a lower-level optimisation model. The upper-level optimisation model optimises the planning variables (sites and capacities of SOPs and other electrical components) and sends them to the lower level. Then based on these optimised results from the upper level, the operation variables (for example power output of SOPs) are optimised and then the cost-related objective in the lower-level optimisation process is fed back to the upper level. The two procedures iterate to achieve better results.

In general, the formulation of the single-level optimisation follows those presented in the above three subsections, while the formulation of the bi-level optimisation differs in three parts. Firstly, despite the investment cost, operation related cost in many cases is also involved in the objective function in the upper level, which will be calculated in the lower-level optimisation process. Secondly, in the lower-level optimisation model, different quantification indices in Section 2.1.2 can be weighted and summated as the objective function. The weights for different indices can be decided through analytic hierarchy process [132]. Thirdly, the constraints considered by the upper level only include the location and capacity constraints of SOPs and other aforementioned electrical devices, such as DGs, energy storage and capacitor banks, while the other constraints are considered in the lower level.

- **Algorithms for solving the optimisation problem**

The optimal siting and sizing problem of SOPs is a mixed integer nonlinear optimisation problem, which is difficult to converge into the global optimum and computationally inefficient. One effective algorithm to solve this optimisation problem is firstly to transform the original model to a mixed integer second-order cone programming model, and then solve it by commercial solvers like CPLEX [130] and MOSEK [132]. Considering the uncertainties of power output of DGs and the power load, a chance-constrained programming model can be embedded in the original model, where genetic algorithm is proved to be effective for solving the problem [133].

The algorithms for the transformation between single-level optimisation problem and bi-level problem can also be used. In [132], the bi-level optimisation model is transformed into a single-level model based on the strong duality theory of conic optimisation [135]. In [131], on the contrary, the single-level optimisation problem is converted to an investment decision-making master problem with integer variables and an operation optimal sub-problem with continuous variables by the Benders decomposition method.

2.1.5. Industrial projects of SOPs

Industrial projects of SOPs have already been carried out across the globe. Fig. 2.4 summarises the development of eighteen major projects in the world, whose information are publicly available. Among these projects, Germany, the UK and China are the three countries leading the industrial development of this technology.

According to the types of distribution networks where SOPs are installed, the implementation of SOPs can be classified into two categories: within public distribution networks and between public and grid edge distribution networks.

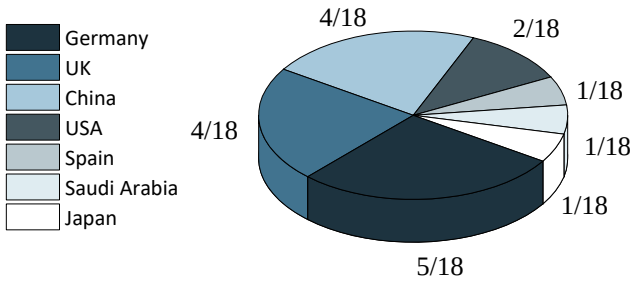

Fig. 2.4. SOP projects worldwide.

- **Within public distribution networks**

The most common topology of SOPs connecting two public distribution networks is back-to-back VSCs. This type of SOPs was firstly developed and named as SIPLINK by Siemens AG, which is an industrial manufacturing company in Germany. Since 2001, the SIPLINK series of product were deployed at the switchgear factory in Frankfurt [16], trialled in the "Ulm" project and the "EDISon" project in Germany [136], and used for 50/60 Hz network connection in Saudi Arabia [137]. Besides SIPLINK of Siemens AG, SOPs were also developed and exploited in other countries. In Japan, two distribution lines in a test distribution network were connected by a 6.6kV/1MVA dual-terminal SOP in 2007 for the purpose of load balancing and voltage improvement [23], [24]. In the USA, back-to-back SOPs designed by ABB company in Switzerland were demonstrated in the "Eagle Pass" project in 2011 [138] and "Mackinac HVDC Flow-Control" project in 2014 [139]. In the UK, back-to-back SOP projects funded by the Office of Gas and Electricity Markets (Ofgem) include "Flexible Urban Network-Low Voltage" project led by UK Power Networks (2014-2016) [140], "Network Equilibrium" by Western Power Distribution (2015-2019) [141] and the ongoing "Active Response to Distribution Network Constraints" by UK Power Networks [142]. Apart from Ofgem projects, another dual-terminal SOP project has also been conducted under the "Active Network Management" program of Northern Power Grid in the UK [143]. Particularly in the ongoing "Active Response to

Distribution Network Constraints" project, remote control switches will be used in coordination with back-to-back SOPs for automatic reconfiguration to optimise distribution networks.

In addition to back-to-back SOPs, four multi-terminal SOPs were applied in different cities of China since 2018. Depending on whether the connection is for AC or DC networks, these multi-terminal SOPs were configured with either AC/DC converters or DC/DC converters. A three-terminal and a four-terminal SOP with only AC/DC converters were demonstrated [144] in Beijing in 2019 and Suzhou in 2018 [145], respectively. On the other hand, with one or more DC/DC converters connecting to the DC distribution networks, two other multi-terminal SOPs were deployed in Hangzhou in 2018 [146] and Tianjin in 2020 [147], respectively. Connecting the DC bus of an SOP to DC networks makes it easy to integrate DC power load and power generation in public distribution networks. Apart from China, multi-terminal SOPs are also seen in other countries. For example, a three-terminal SOP was trialled in the "Flexible Urban Network-Low Voltage" project in the UK to share capacity between substations.

Besides back-to-back SOPs and multi-terminal SOPs, an UPFC-based SOP is used in the ongoing project "Active Response to Distribution Network Constraints" in the UK [142]. This newly designed SOP will be installed to share power loads and optimise capacity between primary substations. Compared to back-to-back and multi-terminal SOPs, converters of UPFC-based SOPs are partially rated so as to reduce converter cost.

- **Between public distribution networks and grid edge networks**

Projects of SOPs were also implemented between public distribution networks and grid edge networks, mainly including shipboard and railway distribution networks.

The shore-to-ship connection through SOPs attributes to the capability of SOPs to connect networks with different frequencies or voltage levels. In “Flender Shipyard” project in 2002, a 1MVA SOP manufactured by Siemens AG enables the power exchange between the shipyard and the shipboard network [136]. It not only enables power supply from the 50 Hz shipyard network to the 50/60Hz on-board network of the vessels, but also the reverse from the marine generator to the shipyard network. In 2007, similar solution was provided for the shipbuilding company FSG in Germany [148]. Through the installed SOP, the 5kV, 50Hz shipyard network could provide ships with different voltages and frequencies (440V/60Hz, 600V/60Hz, 690V/60Hz).

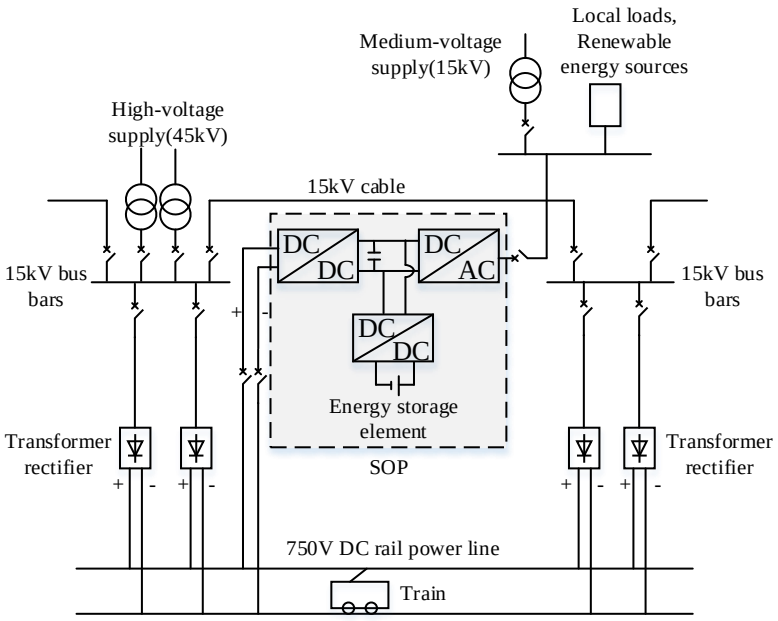

Fig. 2.5. Application of SOP between public and railway distribution networks.

A good example for the SOP implementation between public distribution networks and railway electrification networks is the “E-lobster” project in Spain since 2018. A schematic diagram for this unique SOP is shown in Fig. 2.5 [149]. The SOP consists of an AC/DC converter connecting to a public distribution network and two DC/DC converters connecting to a railway network and the energy storage system, respectively. Such SOP can capture the regenerative energy of rail braking and use it to charge the

energy storage, support the public distribution network, or both. Similarly, the excess of power generation within the public distribution network from renewables but not consumed locally, can also be stored in the energy storage. Therefore, both networks would benefit from this system, being able to reduce electricity losses. Moreover, equipped with the energy storage unit, the surplus energy of both networks can be stored and then used during peak load hours.

- **Discussions on implementation cost of SOPs**

SOPs have not been widely deployed throughout the distribution networks worldwide since its invention in 2001 due to their high cost. In the industrial applications of SOPs, the cost justification is required. To boost SOP implementation, how to reduce the cost of SOPs and increase the revenue from SOP applications need to be further investigated.

To reduce the cost of SOPs, the transformerless UPFC topology is promising, which can be achieved by cascade multilevel inverters [96], [97]. Under this innovative topology, the converters are partially rated. The bulky and expensive zigzag transformers, which are required by conventional UPFC for isolation and reaching high power rating with desired voltage waveforms, can also be removed. Another opportunity is to develop SOPs with reduced number of components by using emerging wide-bandgap power electronic materials such as silicon carbide. Owing to the advantages of much higher breakdown electric field in silicon carbide than in the conventional silicon material, it is practically achievable to implement SOP topology with a reduced number of components.

On the revenue side, implementation of SOPs in extreme meteorological conditions is of great value in future distribution networks. It can be anticipated that distribution networks will face adverse meteorological conditions more frequently due

to climate change. SOPs can play a role in proactive control in both pre-event and post-event stages, which can enhance the network resilience. Compared to the extremely high cost of outages caused by the extreme meteorological events, the cost of SOPs is able to be justified.

With the introduction of new SOP topologies, the development of wide-bandgap power electronic materials, and the increasing importance of resilience requirements in distribution networks, SOPs are set to become an attractive technology in the future.

2.2. Security region-based methodology

The security region of an energy network is denoted as the range of network operating states that comply with the security constraints. The scope of the security constraints considered in existing literature on security regions is extensive, encompassing not only the steady-state operational security but also post-fault stability of energy networks. Although the FORs developed in this thesis are specifically focused on the steady-state operation of distribution networks, the approaches employed to obtain security regions and their applications provide valuable insights applicable to the study of FORs.

To better elucidate the distinctions between security regions and FORs, this section begins with a review of various categories of security regions. Subsequently, the approaches for obtaining security regions and the application of security regions are discussed.

2.2.1. Classification of security regions

Security regions in different energy networks can be classified into different categories based on two factors: whether the network configuration change is considered and the security constraints that are considered. Different categories of

security regions (SRs) are summarised in Fig. 2.6. For clarity, the specific classification is presented as follows.

- **Factor 1: whether the network configuration change is considered**

In the context of electricity transmission networks, SRs can be classified into steady-state SRs and dynamic SRs, based on the consideration of network configuration changes. Steady-state SRs focus on maintaining the security of operating states of transmission networks under a fixed network configuration [41], [48], [73], [74], [75]. On the other hand, dynamic SRs account for the transient stability of transmission networks after short circuit faults [39], [55], [61], defining the range of operating states where transient stability is preserved following such incidents.

With respect to SRs of electricity distribution networks and integrated energy networks, the related security constraints are typically around the N-1 criterion in existing studies [70], [71], [77], which entails the system's ability to withstand the outage of a single feeder or transformer.

- **Factor 2: the security constraints that are considered**

SRs in electricity transmission and distribution networks can be further classified into various subcategories, each focusing on diverse security constraints. These security constraints include thermal constraints, voltage constraints, small-disturbance stability and dynamic stability in electricity networks. Conversely, in the context of integrated energy networks, SRs have not been distinctly subcategorised since the security region-based methodology for these networks was only developed in recent years (as shown in Fig. 1.3) and are yet to be established in the future.

This thesis focuses on developing models for FORs of distribution networks considering both thermal constraints voltage constraints under fixed network configurations. Although previous studies on security regions of electricity networks

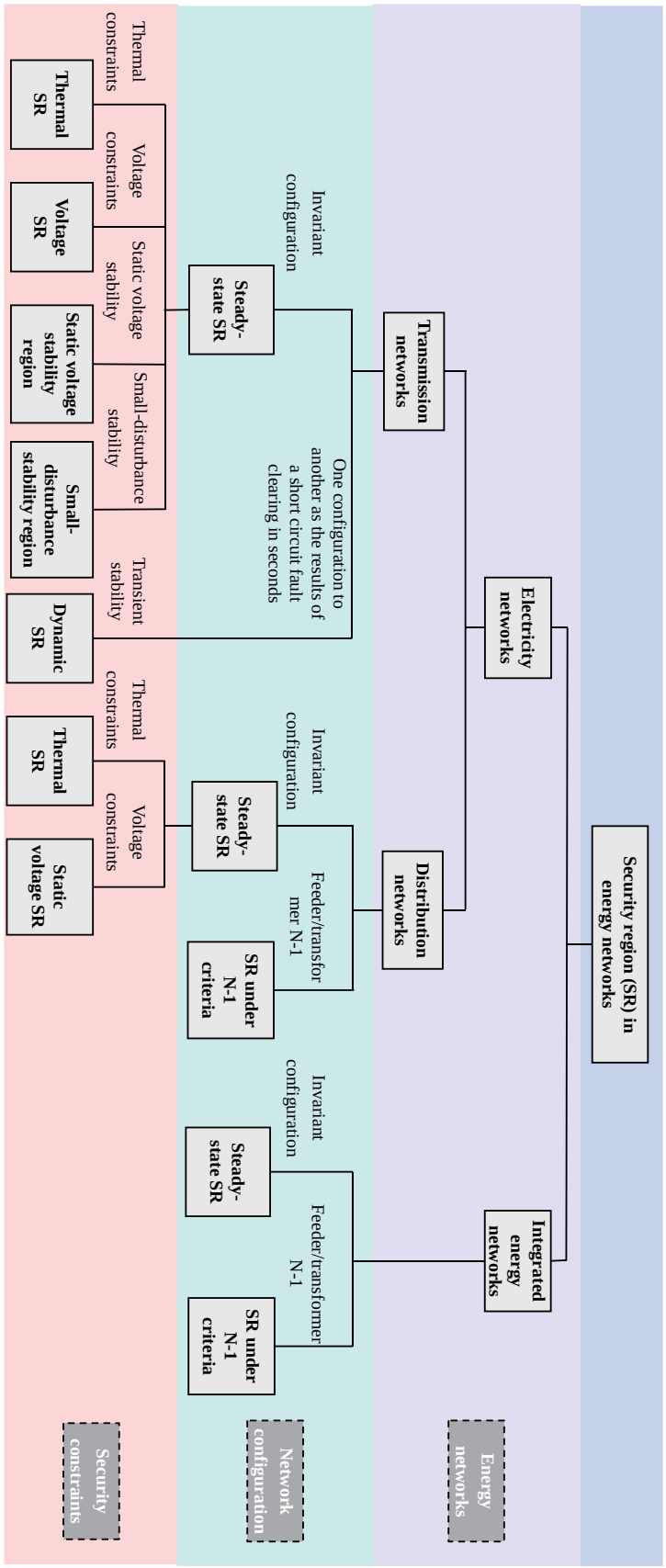

Fig. 2.6. Classification of security region.

primarily concentrated on maintaining network stability following faults or small disturbances, the foundational principles from these studies, particularly the approaches to obtain a region in the power injections space, have enlightened us to develop FORs of distribution networks within this thesis.

2.2.2. Approaches for obtaining security regions

The approaches for obtaining security regions in existing studies can be classified into simulation approaches and analytical approaches.

- **Simulation approaches**

The security regions of energy networks can be obtained by simulation approaches. One can either differentiate secure and insecure operating states [150] or obtain the operating states on security region boundaries [52], [73].

Regarding the first approach, numerous operating states are generated in power injection space and differentiated by the results of power flow calculations. Uniform grid points [150] or points randomly generated in power injection space can serve as these operating states. By executing power flow calculations for these operating states and evaluating their compliance with the network's security constraints, the operating states can be distinctly categorised as either secure or insecure. This approach is easy to implement in a low-dimensional security region or low-dimensional cross-sections of the security region. Here x-dimensional cross-section is the subspace of the security region where x power injections (active, reactive or apparent power injections) are variable, while other power injections are fixed. However, its computational complexity grows exponentially with the increasing dimension of security regions. This rapid escalation of complexity renders the method impractical for application in the high-dimensional security region of a network with many nodes.

The second approach depicts a security region by obtaining accurate boundary points of the security region through simulation. In our published paper (see the paper [3] in other publications in Section 1.5), the boundary points were searched by iteratively changing one power injection with equal intervals while fixing other power injections until reaching the region boundaries. To accelerate the computation, the operating state with the maximum apparent power loading for all nodes of the distribution network was suggested as the initial operating state in the searching process. In [45], Li et al. proposed to use an optimisation method to search for the boundary points on a specified region boundary. Referring to the proposed optimisation method in [45], different boundary points can be obtained along different searching directions with searching angles varying uniformly in the 2-dimensional cross-sections of the security region. To improve the computational efficiency, the authors further proposed to use the previous obtained boundary point as the initial point for the optimisation model in [46], [47] to explore the next boundary point, following an orbiting route around the surface of the security region. The boundary points obtained in [45], [46], [47] rely on changing the searching direction angles, which cannot be easily determined uniformly in the high-dimensional security region, and thus the methods normally apply to 2-dimensional or 3-dimensional cross-sections of the security region.

In summary, the existing simulation approaches for depicting security regions normally compromise on only identifying low-dimensional security regions and demonstrating in two/three-dimensional cross-sections of a security region.

- **Analytical approaches**

Compared to simulation approaches, analytical approaches can easily characterise the security region of an energy network by security region boundaries' analytical expressions, thereby providing the allowable range of power injections in the network.

Moreover, the analytical approaches establish correspondence between region boundaries and network constraints. As a result, the analytical boundaries can be used to replace network constraints in optimal power flow models to accelerate the calculation [42].

The focus of the analytical approaches is to use analytical expressions (of power injections) to approximate the security region boundaries. This can be achieved based on the physical laws of network power flows. In transmission networks, due to the small R/X ratio (i.e., the ratio of network resistance to network reactance) and small phase angles across lines, power flow equations can be simplified as decoupled active/reactive power flow equations [151]. Based on these decoupled power flow equations and the network constraints, the explicit limits on active and reactive power injections at each node can be obtained [38], [152], [153]. In other words, the analytical expressions can be obtained. The studies on developing analytical boundaries for transmission networks cannot be directly applied to distribution networks because distribution networks are with high R/X ratio (i.e., the ratio of network resistance to network reactance) and the power flow equations cannot be simplified as decoupled active/reactive power flow equations. For distribution networks, Yang et al. provided linear approximation (termed as hyperplane expressions) for voltage and thermal boundaries of a security region in [41] and [42], respectively.

Data-driven approaches can also be used to obtain the analytical expressions of security region boundaries. Based on the secure and insecure operating states from the simulation results, a decision tree can be trained, referring to [69], to derive linear analytical expressions of security region boundaries. On the other hand, when boundary points are acquired via simulation, various curve fitting techniques, including the least

square method [150], the piecewise approximation method [46] and the convex hull method [154], can be employed to approximate the security region boundaries.

The two aforementioned analytical approaches possess different features. The approaches based on the physical laws of network power flows can identify the one-to-one correspondence between the network constraints and analytical security region boundaries. However, assumptions made during the determination of the explicit relationship between the electrical elements (such as line currents and node voltages) and power injections may introduce inaccuracies in the derived approximate FOR boundary expressions. In contrast, data-driven methods are straightforward to implement, yet lacking the innate physical correspondence between the network constraints and security region boundaries. Furthermore, the data-driven methods necessitate simulation results, which faces the dimensionality crisis as discussed in the preceding subsection.

2.2.3. Applications

The security region-based methodology has been mainly used in probabilistic security assessment [55], [63], [155], hosting capacity assessment [71], [156] and optimal power flow [54], [64], [68].

- **Probabilistic security assessment**

Electrical power networks often suffer from various disturbances, such as variability of the nodal power injections, unexpected incidents, and component outages. A network is secure if it is able to withstand the disturbances possibly occurring at the next moment. In the context of increasing uncertainties from renewable generation (e.g., solar and wind generation) and electrified demand like electric vehicles, the deterministic security assessment of the power networks becomes unreliable. Probabilistic security assessment is one attractive alternative to solve this problem. It

aims to obtain the probability of the upcoming operating state that satisfies the security constraints of the power network, given that the probability distribution of the operating state (with uncertainty) can be obtained or forecasted.

Probabilistic security assessment is usually conducted through Monte-Carlo simulation [157], [158], [159]. By generating operating states randomly following their probabilistic distributions and analysing the security of these operating states, the probability of the operating states that are secure can be obtained. This method can easily consider multiple uncertain factors (e.g., the uncertain nodal power injections or the component outages) simultaneously. However, to reduce the error of the assessment results, considerable operating states need to be generated thus increasing the computational complexity. In contrast to Monte Carlo simulation, analytical methods based on Markov chain [39][160] and condition probability theory [161] can be used. The results by using analytical methods are more accurate than Monte-Carlo simulation method. However, the analytical methods are hard to be used when the security constraints (e.g., transient stability constraints) are not easy to be written into explicit analytical expressions associated with uncertain factors.

The security region-based methodology can assist in the analytical probabilistic security assessment in two ways. Firstly, explicit expressions associated with uncertain parameters or component outages can be formulated once the analytical expressions of the security region have been established. As a result, the existing analytical methods for probabilistic security assessment can be used. Moreover, since the linear approximation [38], [52], [61] or polynomial approximation [60] can be used to approximate the security region, the computational efficiency of the probabilistic security assessment can be largely improved [155], [161] This advantage can be further employed in converting a chance-constrained optimisation model to a deterministic one

[42]. In summary, the security region-based methodology can improve the analytical methods for probabilistic security assessment.

- **Hosting capacity assessment**

The conventional methods for assessing the hosting capacity of the power networks in integrating low-caron technologies rely largely on the selected scenarios, which lead to conservative or limited results (the detail is discussed in Section 1.1.3). To overcome the deficiency of the conventional scenario-based methods, the methods based on the distribution network's security region, which can describe the whole picture the network capability to integrate generation and demand, provide an alternative.

Specifically, the security region boundaries provide the limitations to the operating states, which contain the whole information of the network hosting capacity. In [71], the total power loading of an operating state on the region boundaries is defined as "boundary supply capability (BSC)". Since BSC values of the operating states on the security region boundaries are different, the BSC curve that depicts the obtained BSC values is further provided in [71]. However, [71] only considers the hosting capacity of power load regardless of power generation. In [156], the capability to accommodate DG is further studied based on the boundaries of the security region. Similar with [71], the hosting capacity of generation is obtained by sampling the operating states on the security region boundaries and calculating the total power generation of each sampled operating state.

Optimal power flow

OPF targets at determining the optimal operation of the power networks such that the power flow equations and the security constraints are satisfied [162]. It can not only coordinate the control of different technologies by modelling them in the optimisation

model but also achieve the optimum of different control objectives. However, the power flow equations are nonlinear, which increases the computational complexity. Additionally, some security requirements, such as transient stability and small-disturbance stability, are hard to be written in security constraints of the OPF model.

The analytical expressions of the security regions considering different security constraints can be obtained (as discussed in Section 2.2.2) and used to replace the power flow equations and the security constraints. In this security region-constrained OPF model, since the security region can be effectively approximated by linear expressions [38] or polynomial expressions [60] and the power flow equations are removed, the solution efficiency of the OPF problems can be improved. Moreover, the security requirements can be refined as the boundary constraints of the security region through the analytical approaches as presented in Section 2.2.2. The obtained analytical region boundaries can be then used as the OPF constraints. In summary, the security region methodology can be used in the OPF model in the cases that the security constraints are not available or/ and the computational efficiency is required.

2.3. Constraint management of distribution networks

Constraint management is required where electrical networks are unable to transmit electricity power from a source of generation to an area of demand, owing to the limitations of the electrical networks. Constraint management is firstly applied in transmission networks, but with the increase of distributed energy resources, the passive distribution networks mainly operated radially will face increasing network constraint problems [163]. For instance, the increase of DG may cause overvoltage problems in the distribution networks. To face the challenge, active network management in distribution networks is developed. Constraint management is aimed at solving constraint violations in distribution networks while ensuring the supply-demand

balance. The constraints mainly include thermal constraints of the substation transformer and power lines and voltage constraints for each node of distribution networks.

Fig. 2.7 provides an overview of different technologies that are used for constraint management in distribution networks in existing studies. Accordingly, three commonly used control methods for these technologies are also identified, including the sensitivity-based control, rule-based control, and optimisation-based control. These technologies and the control methods are discussed in the following two subsections.

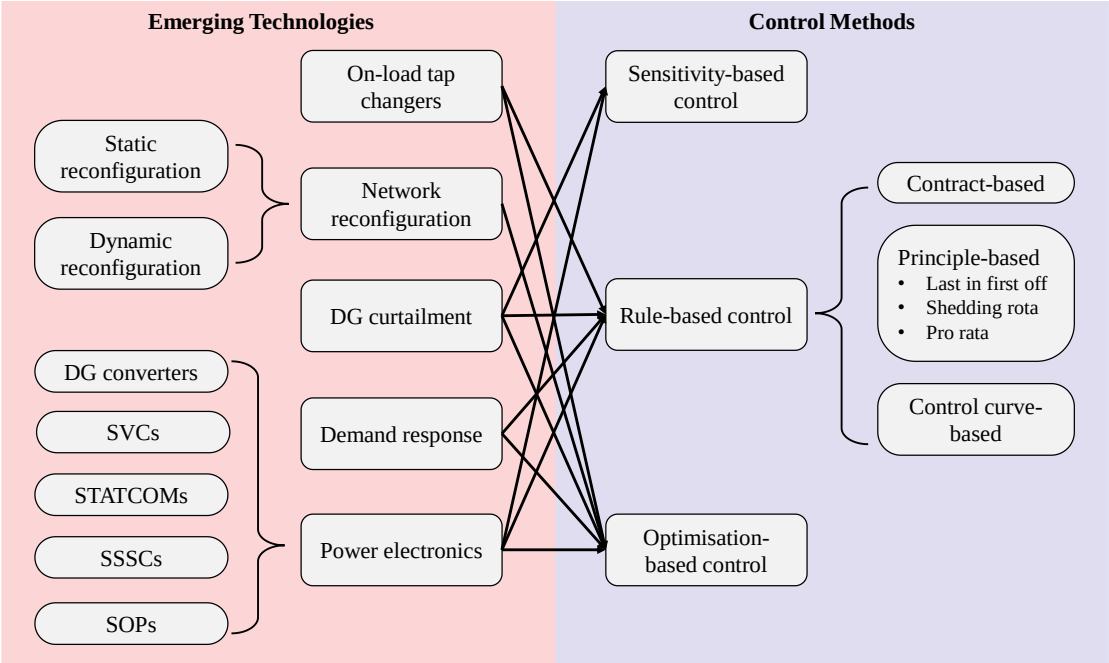

Fig. 2.7. Different technologies and their control methods for constraint management in distribution networks in existing studies.

2.3.1. Emerging technologies involved in constraint management

To avoid the costly and time-consuming reinforcement of distribution networks, different technologies have been proposed for efficient constraint management of distribution networks. The commonly used technologies, including on-load tap changer (OLCT), network reconfiguration, DG curtailment, demand response, and power electronic solutions, are discussed as follows.

- **On-load tap changers**

On-load tap-changers (OLTCs) are mechanical devices capable of adjusting the magnitude of the secondary voltage of the transformer by changing the transformer's tap position while under load [164], [165]. An OLTC is normally equipped with the automatic voltage control relay, which monitors the secondary voltage of a distribution transformer and, when necessary, automatically signals the OLTC to make adjustments [166].

With the increase of DG integration in the distribution network, the OLTCs become less effective in maintaining the voltages across the network [32] [167]. This has sparked considerable interest in exploring coordinated voltage control strategies that synergize OLTCs with other emerging technologies.

- **Network reconfiguration**

Network reconfiguration in distribution networks is effective for constraint management of distribution networks by changing the status of sectionalising switches and tie switches. In [168], the network reconfiguration was exploited to reduce power losses of distribution networks while satisfying the thermal and voltage constraints of distribution networks simultaneously.

[169] further categorises the network reconfiguration into static reconfiguration and dynamic reconfiguration: static reconfiguration improves the topology of distribution networks at the planning and design stage using both manually and remotely controlled switches, while dynamic reconfiguration aims for real-time constraint management thus using only remotely controlled switches.

The effectiveness of static reconfiguration is often challenged by uncertainties in the locations and capacities of connected DG sources. The success of dynamic network reconfiguration, on the other hand, hinges on the efficiency of the measurement and

communication systems and the responses of remote-controlled switching devices [170]. Moreover, practical considerations related to operations and safety typically limit the number of reconfiguration options available in distribution networks [169], [171]. Consequently, network reconfiguration is usually implemented in coordination with other technologies to enhance overall performance in constraint management [32] [172].

- **Distributed generation curtailment**

DG curtailment is the reduction in the output of DG units from what it could otherwise produce given available resources (e.g., wind or sunlight) [173]. The curtailment is typically initiated by DNOs, who instruct DG units to lower their output in order to maintain the network's operation within its specified limits, such as to alleviate voltage constraints.

- **Demand response**

Demand response refers to balancing the demand on power grids by encouraging customers to shift electricity demand to times when electricity is more plentiful or other demand is lower [174]. Towards net zero target, it is projected that by 2030, the market will witness an integration of approximately 500 GW of demand side capacity globally — a significant leap, representing a tenfold increase in deployment levels in 2020 [174]. The projected increase signifies the substantial potential of demand response in service provision within distribution networks.

The location of each demand-responsive load in distribution networks has an impact on its ability to contribute to the management of system constraints [175]. Hence, when considering the application of demand response, it is important to consider the contribution of each load to both local network constraints and overall network energy balancing. Additionally, the effective deployment of demand response necessitates advanced metering infrastructure and robust digital management systems.

- **Power electronic solutions**

Power electronic devices, such as DG converters, static var compensators (SVCs) [176], static synchronous compensators (STATCOMs) [177], static series synchronous compensators (SSSCs) [178] and SOPs, can serve as active compensators in distribution networks. Similar with SOPs discussed in Section 2.1, they are power controllable, thereby capable of improving line flow and node voltage profiles. However, their capabilities in active and reactive power control vary.

SVCs, STATCOMs and SSSCs can only provide reactive power support. While SVCs and STATCOMs provide shunt reactive power compensation within their capacities [179], SSSCs influence network reactive power flows by applying a series voltage between two network nodes to control their in-between impedance [26]. Therefore, the controlled power by SSSCs is determined not only by the capacities of SSSCs, but also by the network topology, the network operating point and the placement of SSSCs [26]. Regarding the differences between SVCs and STATCOMs, SVCs use thyristor-based switching of capacitors and reactors, whereas STATCOMs use voltage-source converters. Although SVCs are less expensive than STATCOMs, they have a limited range of reactive power compensation and may introduce higher harmonics due to the fixed steps of capacitors and reactors [180]. Additionally, the performance of SVCs can degrade under low voltage conditions, while STATCOMs can operate independent of the line voltages at their connected points [181].

DG converters and SOPs can conduct both active and reactive power control [26]. While DG converters can control the power injections at the connection points of DGs, SOPs allow for real power exchange between connected feeders as well as independent reactive power support at SOP terminals. Additionally, the active power injection controlled by DG converters is limited by both the converter capacities and the DG

power output. In contrast, SOPs are constrained primarily by the capacities of their terminal converters.

2.3.2. Control methods used for constraint management

- **Sensitivity-based control**

Sensitivity-based control can be used for DG curtailment [182], [183] and power electronics [121], [184]. It is achieved by using sensitivity factors of the Jacobian matrix to quantify the contribution of P-Q injections from DG units or power electronic devices to the voltage (or thermal) constraints. The sensitivity-based control only requires knowledge of a small number of local network parameters (e.g., the local voltage measurement). However, the linearisation when establishing the Jacobian matrix introduces errors to the control method [183]. Additionally, the results after the sensitivity-based control are usually not the optimum.

- **Rule-based control**

Rule-based control suggests that the control strategy is established and manually configured in accordance with specific contracts, principles, or predefined control curves. With respect to the control of power electronics, a smart contract is used in [103] to determine the transferred power between two distribution networks connected by converters of a medium-voltage direct-current link. Additionally, the Q-V curve can also be obtained for the reactive power control of converters [185], [186]. For DG curtailment, different principles can be used: “last in first off” (curtailing the newest connected DG unit first) [187], “shedding rota” (following a predefined rotation) [188], and “pro rata” (sharing the curtailment by each DG unit equally) [189].

The rule-based control is somehow subjective. To avoid this problem, data-driven methods can be used to refine the rules. For instance, [21] leverages historical

operational data to establish a response curve that correlates the power flow through the substation transformer with the set point of the medium-voltage direct-current link.

- **Optimisation-based control**

Optimisation methods have been widely used for the optimal control of different technologies in constraint management of distribution networks. Compared to the sensitivity-based control and the rule-based control, the optimisation-based control can achieve optimum on different control objectives [97], [112]. Additionally, it is easy to consider the coordination of different technologies by adding them to the constraints and objective functions in the optimisation models [190], [191], [192]

However, the nonlinearity of power flow equations and the introduction of integer variables (e.g., variables representing different tap positions for OLTC) increase the complexity of the optimisation-based control model. This incurs significant computational cost and cannot guarantee the real-time control of the technologies. To solve this problem, the optimisation model is usually converted to a convex programming model [17], [33], [132] with an acceptable error. Another problem is that the optimisation-based control normally requires observability of the entire distribution network. However, the measurements across most distribution networks are not universally available [81]. In [185], [193], a decentralised control based on local information of each area and boundary interaction among connected areas is developed. As discussed in Section 2.2.3, the security region constraints of a given distribution network can be used to replace the power flow equations and the security constraints in the optimisation-based model. This emerging method is especially effective in network constraint management in the cases that the security constraints are not directly available or/ and the computational efficiency is required [153] [155]

2.4. Summary

This chapter first gives a comprehensive overview of both academic research and industrial practice on SOPs in electricity distribution networks. The topologies of SOPs as multi-functional power electronic devices are identified and compared, which include back-to-back voltage source converters, multi-terminal voltage source converters, unified power flow controllers, and direct AC-to-AC modular multilevel converters. The academic research is reviewed in three aspects, i.e., benefit quantification, control, and optimal siting and sizing of SOPs. The benefit quantification indices are categorised into feeder load balancing, voltage profile improvement, power losses reduction, three-phase balancing and DG hosting capacity enhancement. The control of SOPs is summarised as a three-level control structure, where the system-level and converter-level control are further discussed. For optimal siting and sizing of SOPs, problem formulation and solution methods are analysed. Besides the academic research, practical industrial projects of SOPs worldwide are also summarised.

The security region-based methodology that can be referenced in studies on FORs is reviewed subsequently. Security regions has been used in different energy networks and can be classified into different subcategories according to whether the network configuration is invariant and different security constraints considered. Simulation and analytical approaches for obtaining FORs have also been introduced. Compared to simulation approaches, analytical approaches can easily characterise the security region of an energy network) by its boundaries' analytical expressions. The obtained analytical expressions of security region boundaries can be further used in the probabilistic security assessment, hosting capacity assessment, and optimal power flow. Among the approaches for obtaining security regions, the analytical approach based on the physical

laws of network power flows can identify the one-to-one correspondence between the network constraints and analytical security region boundaries. However, the assumptions made in this approach may introduce inaccuracy. Therefore, the validation of the obtained analytical expressions of a security region is important. The analytical security region boundaries with high accuracy should be obtained before being used.

Different technologies for constraint management of distribution networks are summarised, including OLTCs, network reconfiguration, DG curtailment, demand response and power electronic solutions. Their control methods are classified into sensitivity-based, rule-based and optimisation-based control. The identified control methods for different technologies can be used as reference for the control of SOPs in the distribution networks.

Chapter 3. Feasible operation region of an electricity distribution network

3.1. Introduction

In this chapter, higher-order analytical expressions (i.e., quadratic expressions) of the boundaries of the FOR of a distribution network, in contrast to the existing hyperplane expressions, are developed to accurately express the network capability and efficiently exploit the network headroom for integration of more DG/demand.

Furthermore, this chapter provides a high-dimensional error analysis approach for validating any forms of analytical boundaries in high-dimensional power injection space, which is not available in existing literature. It characterises the boundary errors by multiple distance functions and operational indices and quantifies the conservativeness of the analytical boundaries.

The proposed quadratic expressions of FOR boundaries were validated in an 11kV radial distribution network from the United Kingdom Generic Distribution System (UKGDS). The validation results were also compared to those of the existing hyperplane expressions of FOR boundaries.

3.2. Concept of feasible operation regions

3.2.1. Definition of feasible operation regions

A FOR is defined as the set of feasible operation states of a distribution network, where the network constraints are not violated. Considering the operation states are defined as power injections at different nodes of the distribution network, a FOR can be described as follows:

$$FOR := \left\{ \boldsymbol{x}: \ = \begin{bmatrix} \boldsymbol{P} \\ \boldsymbol{Q} \end{bmatrix} \in R^{2n} \middle| \begin{matrix} \boldsymbol{V} \in \boldsymbol{C}_{\boldsymbol{V}}, \boldsymbol{I} \in \boldsymbol{C}_{\boldsymbol{T}} \\ f_{(V_0,\theta_0)}(\boldsymbol{V},\boldsymbol{\theta}) = \boldsymbol{x}, g(\boldsymbol{I},\boldsymbol{V},\boldsymbol{\theta}) = 0 \end{matrix} \right\} \tag{3-1}$$

The FOR is defined in the complex power injection space, where n is the number of nodes (excluding the slack bus) in the distribution network. x is the complex power

injection vector in a distribution network, where $\boldsymbol{P}=(P_1, \ldots, P_n)^T$ and $\boldsymbol{Q}=(Q_1, \ldots, Q_n)^T$ are active power vector and reactive power vector. Since each active/reactive power injection at any node of the distribution network corresponds to one dimension of FOR, the FOR of a n-node distribution network is a 2n-dimensional power injection space. $f_{(V_0,\theta_0)}(\boldsymbol{V},\boldsymbol{\theta})=\boldsymbol{x}$ represents the power flow equations with V_0 and θ_0 as predefined voltage magnitude and phase angle of the slack bus. $g(\boldsymbol{I},\boldsymbol{V},\boldsymbol{\theta})=0$ represents the relationship between line currents and node voltages expressed by Ohm's law. $\boldsymbol{V}$ and $\boldsymbol{I}$ are the node voltage vector and line current vector, which satisfy the voltage constraints $\boldsymbol{C_V}$ and thermal constraints $\boldsymbol{C_T}$, respectively:

$$\boldsymbol{C_V} := \left\{ V_i^m \le V_i \le V_i^M, \forall i \in N \right\} \tag{3-2}$$

$$\boldsymbol{C_T} := \left\{ \left| I_{ij} \right| \le I_{ij}^M, \forall ij \in B \right\} \tag{3-3}$$

V_i is the voltage magnitude at node i, constrained by its lower limit V_i^m and upper limit V_i^M. $\left|I_{ij}\right|$ is the magnitude of the line current constrained by its limit I_{ij}^M. N and B denote the set of the nodes and lines in the network respectively, the number of which are n and n_b respectively.

According to the definition of the FOR, within the boundaries of the FOR are all feasible operation states, while outside of the boundaries any operation states are infeasible (see Fig. 3.1). In this regard, the boundaries of FOR represent all the limits to the power injections that can be hosted by a distribution network, which can provide the information of the network capability. FOR is only associated with the network topology and component parameters. As long as the operation states (i.e., net nodal power injections) are inside FOR, however the generation/consumption vary, the node voltages/line currents will be confined within their upper/lower limits.

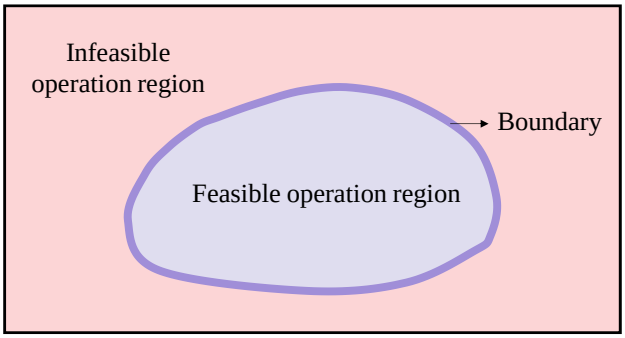

Fig. 3.1. Relationship between hosting capacity and feasible operation region for a distribution network.

3.2.2. Boundaries of feasible operation regions

FOR of a distribution network is enclosed by several high-dimensional surfaces, which are determined by voltage and thermal constraints in (3-2) and (3-3) [153]. These surfaces confine the network to its normal operation without violating the network constraints. In this study, these high-dimensional surfaces are defined as the boundaries of the FOR. Considering the types of constraints in (3-2) and (3-3), the boundaries of the FOR can be further categorized into voltage boundaries and thermal boundaries. In the next section, a new form of analytical expressions of FOR boundaries is proposed in a quadratic form of power injections.

3.3. Analytical expressions for boundaries of feasible operation regions

3.3.1. Analytical expressions of thermal boundaries of feasible operation regions

The schematic diagram of a general radial distribution network is shown in Fig. 3.2. The direction of the arrows at each node of the network represents the net power loading. It is noteworthy that the negative value of the net power loading at one node, in other words the net power injection, indicates that the power generation is larger than the power loading at this node. In this section (and also in Section 3.2), net nodal power loading is used in the deduction process but will be replaced with net nodal power

injection (i.e., the positive direction of active and reactive power at each node is defined as the injection direction) in the final expressions.

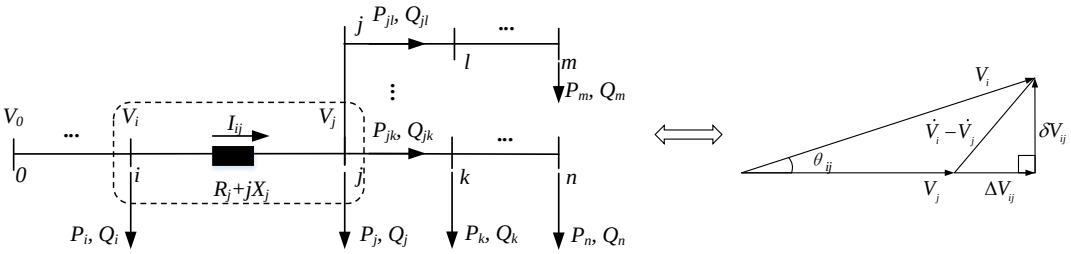

Fig. 3.2. A schematic diagram of a general *n*-node radial distribution network.

For conciseness, $P_{j,eq}$ and $Q_{j,eq}$ are defined as the equivalent power loading at the receiving end node of any line *ij* in the distribution network in Fig. 3.2. The expressions of $P_{j,eq}$ and $Q_{j,eq}$ are as follows:

$$P_{j,eq} = P_j + \sum_{k \in A_j} P_{jk} \tag{3-4}$$

$$Q_{j,eq} = Q_j + \sum_{k \in A_j} Q_{jk} \tag{3-5}$$

P_j and Q_j are the active and reactive power loading at the receiving end node of the line *ij*, while P_{jk} and Q_{jk} are the active and reactive power flow at the line *jk*. A_j denotes the set of the adjoining downstream nodes of node *j* (e.g., nodes *k*, *l* instead of node *i* in Fig. 3.2) in the distribution network.

The voltage drop on the line *ij* can be expressed as the voltage phaser diagram in Fig. 3.2. Compared to the previous study on hyperplane expressions [42] which ignores δV_{ij}, this study considers the impact of the difference of voltage phase angles (i.e., θ_{ij}) and δV_{ij} is retained. Then the relationship between the voltage drop and the power flow on the line in Fig. 3.2 can be expressed as:

$$\dot{V}_i - \dot{V}_j = \Delta V_{ij} + j\delta V_{ij} \tag{3-6}$$

$$\Delta V_{ij} = \frac{P_{j,eq} R_j + Q_{j,eq} X_j}{V_j} \tag{3-7}$$

$$\delta V_{ij} = \frac{P_{j,eq} X_j - Q_{j,eq} R_j}{V_j} \tag{3-8}$$

$\dot{V}_i$ and $\dot{V}_j$ are the voltages at the sending end and the receiving end of the line (V_i and V_j denote the magnitude of them). R_j and X_j are the resistance and reactance of the line.

Based on Ohm's law, the current of the line *ij* can be obtained by:

$$\dot{I}_{ij} = \frac{\dot{V}_i - \dot{V}_j}{R_j + jX_j} \ . \tag{3-9}$$

From (3-6)-(3-9), the magnitude of the line current can be expressed as:

$$\left|\dot{I}_{ij}\right| = \frac{1}{V_j}\sqrt{\left(P_{j,eq}{}^2 + Q_{j,eq}{}^2\right)} \ . \tag{3-10}$$

(3-10) is a symmetric equation in terms of $P_{j,eq}$ and $Q_{j,eq}$, which indicates that $P_{j,eq}$ and $Q_{j,eq}$ have the same degree of influence on the line current. In a distribution network with high R/X ratio, the active power losses are normally larger than reactive power losses. Considering the percentage of active power losses over the power loading is small for a distribution network [194], the power losses at the downstream lines in $P_{j.eq}$ and $Q_{j,eq}$ are ignored. In addition, since the allowable variation of node voltages is small (normally within ±3% or ±5%), the voltage magnitude V_j is assumed to be V_0 [42]. Following these two assumptions, (3-10) can be simplified as:

$$\left|\dot{I}_{ij}\right| = \frac{1}{V_0}\sqrt{\left(\sum_{k\in D_j} P_k\right)^2 + \left(\sum_{k\in D_j} Q_k\right)^2} \ . \tag{3-11}$$

D_j denotes the set of the downstream nodes of node *j* (including node *j* for clarity) in the distribution network. Setting the line current at its upper limit, i.e., $\left|\dot{I}_{ij}\right| = I_{ij}^M$, the analytical expressions for the thermal boundaries of FOR can be derived as:

$$\begin{cases} \left(\sum_{k=1}^{n}\alpha_k P_k\right)^2+\left(\sum_{k=1}^{n}\beta_k Q_k\right)^2 = V_0^2\left(I_{ij}^M\right)^2 \\ \alpha_k^{ij}=\beta_k^{ij}=1, \text{ if } k\in D_j \\ \alpha_k^{ij}=\beta_k^{ij}=0, \text{ if } k\notin D_j \\ \forall ij\in B \ (\textit{set of branches}) \end{cases} \tag{3-12}$$

From (3-12), the thermal boundaries are in the quadratic form of the net power loading at different nodes of the distribution network, which are different from the expressions of hyperplanes such as those in [42]. When defining P_k and Q_k in (3-12) as the net power injection at node k in the deduction process, the form of the analytical expressions of thermal boundaries stays the same as (3-12).

3.3.2. Analytical expressions of voltage boundaries of feasible operation regions

In Fig. 3.3, a circle with radius of V_i (i.e., the voltage magnitude at the sending end node of the line in Fig. 3.2) is drawn to observe the difference of the voltage magnitude between the sending end node and the receiving end node. From Fig. 3.3, (3-6) can be replaced by the following scalar equation:

$$V_i - V_j = \Delta V_{ij} + \overline{BC} \tag{3-13}$$

For conciseness, $\overline{XY}$ denotes the line segment between point ***X*** and point ***Y***. Due to the vertical relation between $\overline{OC}$ and $\overline{AB}$, $\overline{BC}$ in (3-13) can be expressed as:

$$\overline{BC} = \delta V_{ij} \tan\angle BAC \tag{3-14}$$

Extend $\overline{AB}$ to intersect the circle at ***A'***. From the fact that the points ***A*** and ***A'*** on the circle are symmetrical about the $\overline{OB}$, which is perpendicular to $\overline{AA'}$, (3-15) can be obtained.

$$\tan\angle \mathrm{BAC} = \tan\frac{\theta_{ij}}{2} = \frac{\delta V_{ij}}{V_i + V_j + \Delta V_{ij}} = \frac{\delta V_{ij}}{2V_i - \overline{BC}} \tag{3-15}$$

Due to the small difference of the phase angles at the two endpoints of a line (i.e., θ_{ij} is normally small), the numerator ($\delta V_{ij} = V_i \sin\theta_{ij}$) is a first-order element of θ_{ij}, while $\overline{BC} = V_i \sin\theta_{ij} \tan\frac{\theta_{ij}}{2}$, a second-order element of θ_{ij}. The first-order small element is retained yet the second-order one is ignored and Eq. (15) is simplified as:

$$\tan\angle \mathrm{BAC} \approx \frac{\delta V_{ij}}{2V_i} \tag{3-16}$$

Substituting (3-14)-(3-16) in (3-13), the scalar equation of the voltage drop can be expressed as:

$$V_i - V_j = \Delta V_{ij} + \left(\delta V_{ij}\right)^2 \Big/ \left(2V_i\right) \tag{3-17}$$

ΔV_{ij} and δV_{ij} refer to (3-7) and (3-8) respectively. Then consider the same assumptions in Section 3.1 (i.e., the ignorance of power losses at the downstream lines and the voltage magnitude to be V_0 [42]), (3-17) can be simplified as:

$$V_i - V_j = \frac{1}{V_0}\left(P_{j,eq}R_j + Q_{j,eq}X_j\right) + \frac{1}{2V_0^3}\left(P_{j,eq}X_j - Q_{j,eq}R_j\right)^2 \tag{3-18}$$

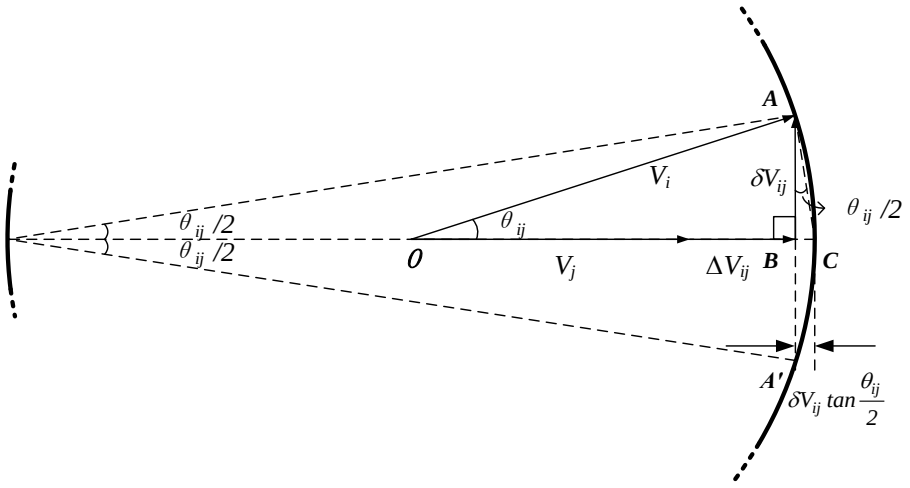

Fig. 3.3 Relations between the voltage magnitudes for voltage drop through a line.

Applying (3-18) to all lines, (3-19) can be obtained.

$$V_0 - V_j = \frac{1}{V_0}\sum_{k\in U_j}\left(P_{k,eq}R_k + Q_{k,eq}X_k\right) + \frac{1}{2V_0^3}\sum_{k\in U_j}\left(P_{k,eq}X_k - Q_{k,eq}R_k\right)^2 \quad (3\text{-}19)$$

U_j denotes the set of the upstream nodes of node j (including node j for clarity) in the distribution network. By substituting (3-4)-(3-5) in (3-19) and considering the effect of the power losses are small (compared with the effect of the power loading), the voltage magnitude for each node can be expressed as:

$$V_j = V_0 - \frac{1}{V_0}\sum_{k\in U_j}\left(R_k\sum_{l\in D_k}P_l + X_k\sum_{l\in D_k}Q_l\right) - \frac{1}{2V_0^3}\sum_{k\in U_j}\left(X_k\sum_{l\in D_k}P_l - R_k\sum_{l\in D_k}Q_l\right)^2 \quad (3\text{-}20)$$

From (3-20), the voltage magnitude at any node includes a first-order term and a second-order term of power loading. In line with the definition of FOR in Section 3.2, here the positive direction of active and reactive power at the node is defined as the injection direction. Then by reversing the signs for all the load terms P_l and Q_l (in both the linear term and the quadratic term of (3-20)), the relationship between the node voltage and power injections can be replaced by (3-21). It should be mentioned that (3-20) and (3-21) are the same except that the positive directions for net power injections are defined differently.

$$V_j = V_0 + \frac{1}{V_0}\sum_{k\in U_j}\left(R_k\sum_{l\in D_k}P_l + X_k\sum_{l\in D_k}Q_l\right) - \frac{1}{2V_0^3}\sum_{k\in U_j}\left(X_k\sum_{l\in D_k}P_l - R_k\sum_{l\in D_k}Q_l\right)^2 \quad (3\text{-}21)$$

Regarding the upper/lower limit of the voltage magnitude at node j, i.e., $V_j \coloneqq V_j^M$ / $V_j \coloneqq V_j^m$, from (3-21) the analytical expressions of voltage boundaries can be obtained as:

$$V_j^M - V_0 = \frac{1}{V_0}\sum_{k\in U_j}\left(R_k\sum_{l\in D_k}P_l + X_k\sum_{l\in D_k}Q_l\right) - \frac{1}{2V_0^3}\sum_{k\in U_j}\left(X_k\sum_{l\in D_k}P_l - R_k\sum_{l\in D_k}Q_l\right)^2, \text{ for } V_j = V_j^M \quad (3\text{-}22)$$

$$V_j^m - V_0 = \frac{1}{V_0}\sum_{k\in U_j}\left(R_k\sum_{l\in D_k}P_l + X_k\sum_{l\in D_k}Q_l\right) - \frac{1}{2V_0^3}\sum_{k\in U_j}\left(X_k\sum_{l\in D_k}P_l - R_k\sum_{l\in D_k}Q_l\right)^2, \text{ for } V_j = V_j^m \quad (3\text{-}23)$$

3.4. High-dimensional error analysis approach

As stated in Section 3.3, the analytical expressions of FOR boundaries in this study are the quadratic expressions of power injections, formulating the surfaces of the FOR. The analytical expressions of FOR boundaries are validated in the high-dimensional power injection space in this section. It should be mentioned that the high-dimensional error analysis is provided to validate or compare the analytical FOR boundaries, but the network operators can directly use the analytical FOR boundaries for practical application.

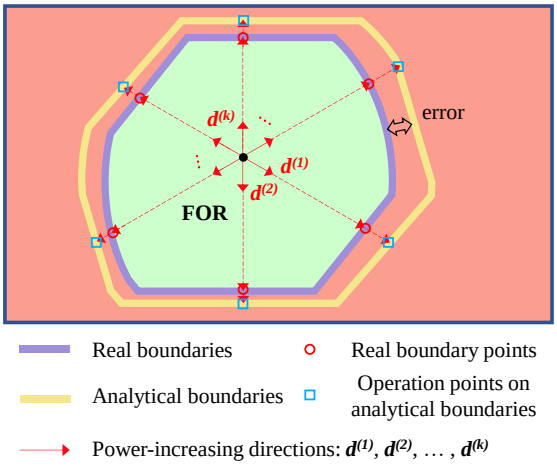

Fig. 3.4. Schematic diagram of high-dimensional error analysis for validating analytical FOR boundaries.

A general validation method is illustrated in Fig. 3.4. Just as a special case for demonstration purpose, the analytical boundaries in Fig. 3.4 are drawn on the outside of FOR. However, caused by the errors, the analytical boundaries might be at both sides of the real boundaries in practice. Supposing a FOR in the high-dimensional space such as that in Fig. 3.4, the validation for the analytical boundaries of the FOR follows four steps:

Step 1: Generate power-increasing directions ($\boldsymbol{d}^{(1)}$, $\boldsymbol{d}^{(2)}$, …, $\boldsymbol{d}^{(k)}$, …) from a point inside the FOR in the power injection space $[\boldsymbol{P}; \boldsymbol{Q}] \in R^{2n}$.

Step 2: Obtain real boundary points of the FOR along the power-increasing directions.

Step 3: Obtain the operation points on the analytical FOR boundaries along the power-increasing directions.

Step 4: Analyse the error of the analytical FOR boundaries through comparing the set of real boundary points (on each thermal/voltage boundary of the FOR) obtained in Step 2 and the set of operation points (on each corresponding analytical thermal/voltage boundary of the FOR) obtained in Step 3.

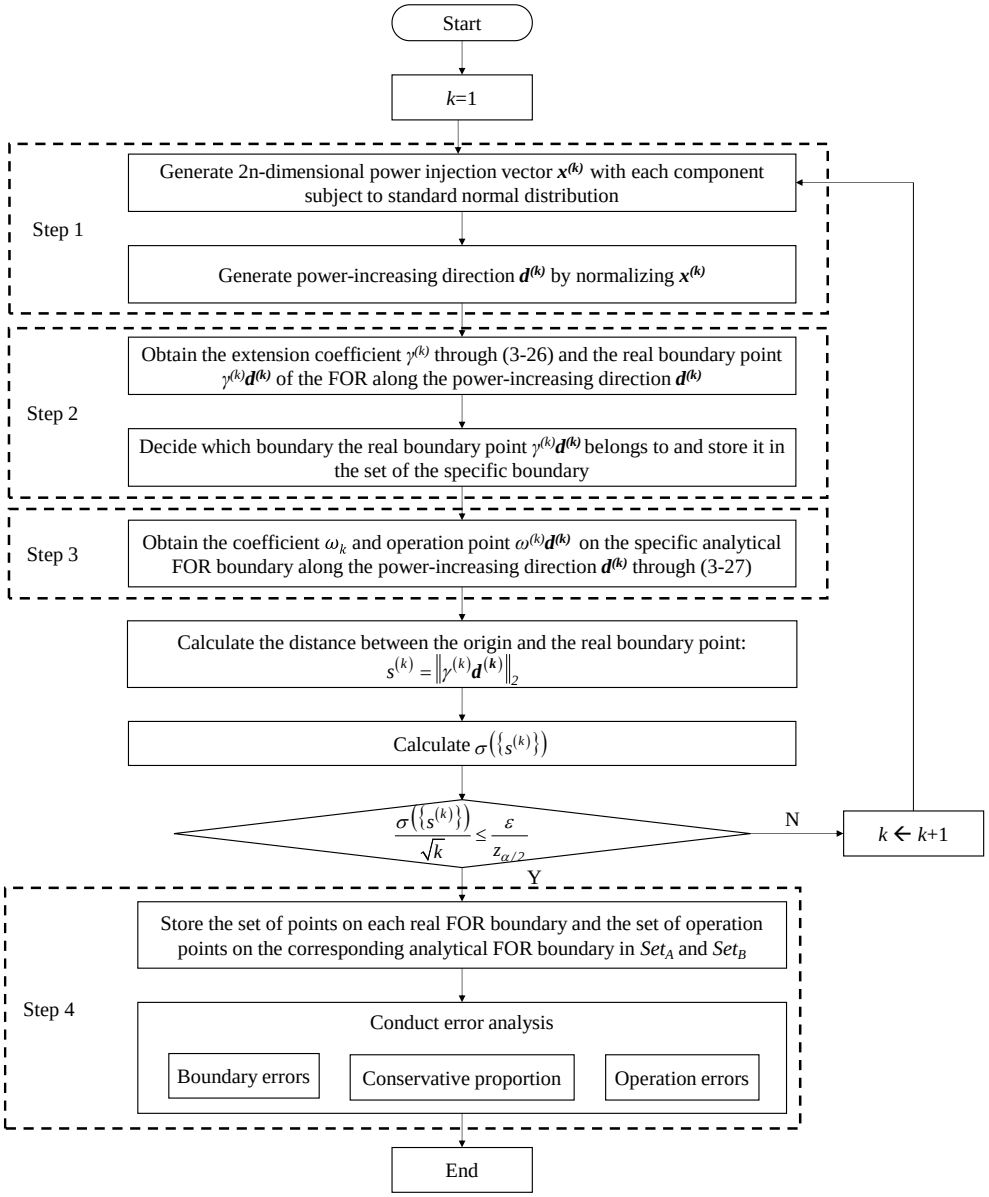

Fig. 3.5. Flow chart of high-dimensional error analysis for analytical FOR boundaries.

The flow chart of the four-step high-dimensional error analysis approach is presented in Fig. 3.5. The four steps are specified in the subsection 3.4.1-3.4.4 respectively, with the stopping rule explained in the subsection 3.4.5.

3.4.1. Generation of power-increasing directions inside feasible operation regions

As with Fig. 3.4, power-increasing directions ($\boldsymbol{d}^{(1)}$, $\boldsymbol{d}^{(2)}$, …, $\boldsymbol{d}^{(k)}$, …) can be represented by power injection vectors in the high-dimensional power injection space of the FOR. Considering power injections at any nodes can be bidirectional (either positive or negative), the origin of the power injection space (i.e., $[\boldsymbol{P}; \boldsymbol{Q}] = [\boldsymbol{0}; \boldsymbol{0}] \in R^{2n}$) is selected as the starting point for all the power injection vectors. For the end points of these power injection vectors, they can be uniformly distributed in the high-dimensional power injection space from the statistical view by exploiting the Marsaglia's algorithm [195]. Marsaglia's algorithm generates uniformly distributed random points on the high-dimensional unit sphere [195]. These uniformly distributed points can then be used as the end points of the targeted power injection vectors.

Following Marsaglia's algorithm, an 2n-dimensional vector (from the origin) is firstly generated:

$$\boldsymbol{x}^{(k)} = \left[p_1^{(k)}, \cdots, p_i^{(k)}, \cdots, p_n^{(k)}, q_1^{(k)}, \cdots, q_i^{(k)}, \cdots, q_n^{(k)} \right]^T \tag{3-24}$$

where each component of the power injection vector $\boldsymbol{x}^{(k)}$ (i.e., $p_i^{(k)}$ or $q_i^{(k)}$) follows normal distribution N (0,1). Then one power-increasing direction can be obtained as:

$$\boldsymbol{d}^{(k)} = \frac{\boldsymbol{x}^{(k)}}{\left\| \boldsymbol{x}^{(k)} \right\|_2}. \tag{3-25}$$

Provided enough power-increasing directions are generated following this step, the real boundary points on all thermal boundaries and voltage boundaries enclosing the FOR can be obtained along these directions. The operation points on different analytical FOR boundaries can also be obtained.

3.4.2. Obtaining real boundary points of feasible operation regions

As shown in Fig. 3.4, along each power-increasing direction in Step 1, one real boundary point can be obtained by extending the initial power injection vector $\boldsymbol{d}^{(k)}$ to its maximum such that the power injection vector is still inside the FOR but a small increase will make it exceed the FOR. A positive constant $\gamma^{(k)}$ is introduced as the coefficient to extend $\boldsymbol{d}^{(k)}$. The real boundary point along any power-increasing direction is calculated through the optimisation model as follows:

$$\max \gamma^{(k)} \quad s.t. \begin{cases} f(\boldsymbol{V},\boldsymbol{\theta}) = \begin{bmatrix} \boldsymbol{P} \\ \boldsymbol{Q} \end{bmatrix} = \gamma^{(k)} \boldsymbol{d}^{(k)} \\ V_i^m \le V_i \le V_i^M, \forall i \in N \\ \left| I_{ij} \right| \le I_{ij}^M, \forall ij \in B \\ \gamma^{(k)} > 0 \end{cases} . \tag{3-26}$$

The objective of the optimisation model is to derive the maximum $\gamma^{(k)}$ towards the predefined power-increasing direction, while the constraints confine the extended power injection vector $\gamma^{(k)}\boldsymbol{d}^{(k)}$ inside the FOR. With the maximum $\gamma^{(k)}$, the power injection $\gamma^{(k)}\boldsymbol{d}^{(k)}$ is on the real boundary of FOR.

Moreover, the critical constraint at the optimum in the model provides the specific FOR boundary to which the obtained real boundary point belongs. By determining which inequality constraint for node voltages/line currents in (3-26) is “active” at the optimal solution, the critical constraint can be found. Here “active” refers to the fact that the optimal solution causes the inequality to be an equality. For example, if

$V_i = V_i^M$ at the optimal solution, the obtained real boundary point (i.e., the maximum power injections along the specified power-increasing direction) causes V_i to reach its upper limit. This indicates that the obtained real boundary point belongs to the voltage upper boundary that is determined by $V_i = V_i^M$. It is worth noting that the optimisation solvers (e.g., solvers in MATLAB) for the constrained optimisation problem normally determine the optimality of the solution in the iteration process by using the Lagrangian function of the optimisation problem. Therefore, a convenient method to decide which constraint is active at the optimal solution is to observe which Lagrangian multiplier for the constraints is not zero. Repeatedly solving the optimisation model considering different power-increasing directions, the set of real boundary points on each thermal/voltage boundary can be obtained.

3.4.3. Obtaining operation points on the analytical feasible operation region boundaries

In the similar way to that in Section 3.4.2, the operation points on the analytical FOR boundaries can be obtained by extending the power injection vector $\boldsymbol{d}^{(k)}$ such that it intersects the analytical FOR boundaries (see Fig. 3.4). The process can be expressed as:

$$\begin{aligned} &solve\ \omega^{(k)} \\ &\text{s.t.}\ \begin{cases} \mathrm{g}(\boldsymbol{P},\boldsymbol{Q}) = g\left(\omega^{(k)}\boldsymbol{d}^{(k)}\right) = 0 \\ \omega^{(k)} > 0 \end{cases} . \end{aligned} \tag{3-27}$$

The positive constant $\omega^{(k)}$ in (3-27) denotes the extension coefficient; $g(\boldsymbol{P}, \boldsymbol{Q})=0$ expresses a specified analytical FOR boundary (see (3-12) for each thermal boundary and (3-22)-(3-23) for each voltage upper/lower boundary respectively). It is noteworthy that this process can be conducted for any forms of analytical expressions of FOR boundaries.

By solving $\omega^{(k)}$, one operation point $\omega^{(k)}\boldsymbol{d}^{(k)}$ on this analytical FOR boundary can be obtained. Selecting different power-increasing directions which are identified towards one particular FOR boundary in Section 3.4.2, the set of operation points on each corresponding analytical FOR boundary can be obtained.

3.4.4. High-dimensional error analysis

- **Boundary errors**

The boundary error for an analytical FOR boundary is defined as the error between the corresponding real boundary and the analytical boundary itself. For clarity, define the set of points on one real FOR boundary and the set of operation points on its corresponding analytical FOR boundary as set_A :={ $a_i \in R^{2n}$ } and set_B :={ $b_i \in R^{2n}$ } respectively. The boundary error for this analytical boundary can be represented by the distance between set_A and set_B, which can be further expressed as the set of the distances between each real boundary point a_i and set_B:

$$\text{Boundary error:=D}\left(\text{set}_A, \text{set}_B\right) = \left\{ D\left(a_i, \text{set}_\text{B}\right) \middle| \forall a_i \in set_A \right\} \tag{3-28}$$

$D(set_A, set_B)$ denotes the distances between set_A and set_B. It is noteworthy that each FOR boundary can be analysed independently when set_A and set_B corresponds to one FOR boundary. $D(a_i, set_B)$ denotes the distance between the ith real boundary point a_i and set_B, which can be represented by the distance between a_i and its nearest operation point in set_B as shown in (3-29):

$$\begin{aligned} &\text{D}\left(a_i, \text{set}_B\right) = \min_{b_j \in \text{set}_B} \text{D}\left(a_i, b_j\right) \\ &where: \\ &\text{D}\left(a_i, b_j\right) = \begin{cases} \max\limits_k \left|a_i(k) - b_j(k)\right|, \text{Chebyshev distance} \\ \sqrt{\sum\limits_{k=1}^{2n} \left|a_i(k) - b_j(k)\right|^2}, \text{Euclidean distance} \\ \sum\limits_{k=1}^{2n} \left|a_i(k) - b_j(k)\right|, \text{Manhattan distance} \end{cases} . \end{aligned} \tag{3-29}$$

$D(a_i, b_j)$ is the distance between the ith real boundary point a_i and the jth operation point b_j on the analytical boundary. In this study, three distance functions in (3-29) are used for the measurement of the distance between two points a_i and b_j. $a_i(k)$ and $b_j(k)$ are the components in the kth dimension of a_i and b_j respectively. Based on the absolute error between $a_i(k)$ and $b_j(k)$, Chebyshev distance function is used for measuring the largest error among the errors in all the dimensions, Euclidean distance function represents the length of the line segment from a_i to b_j in the high-dimensional power injection space, and Manhattan distance function is calculated by the total errors in all dimensions.

To facilitate the comparison of the errors between distribution networks with different scales, $D(a_i, set_B)$ can be normalised by dividing S_{DN} which represents the size of the FOR. In this study, S_{DN} is estimated by the average distance (under different distance functions) between the origin and the FOR boundaries in (3-30):

$$D_{\text{norm}}\left(a_i, \text{set}_B\right) = \frac{D\left(a_i, \text{set}_B\right)}{S_{DN}} \times 100\%$$

$$S_{DN} = \begin{cases} \dfrac{\sum_{i=1}^{N_{total}^R} \max_k \left|a_i(k)\right|}{N_{total}^R}, \text{Chebyshev distance} \\ \dfrac{\sum_{i=1}^{N_{total}^R} \sqrt{\sum_{k=1}^{2n} \left|a_i(k)\right|^2}}{N_{total}^R}, \text{Euclidean distance} \\ \dfrac{\sum_{i=1}^{N_{total}^R} \sum_{k=1}^{2n} \left|a_i(k)\right|}{N_{total}^R}, \text{Manhattan distance} \end{cases} . \quad (3\text{-}30)$$

N_{total}^R denotes the total number of real boundary points of set_A.

Through the normalisation in (3-30), the percentage errors between the real FOR boundaries and the analytical FOR boundaries are obtained and can be analysed statistically. In this study, the mean, minimum, and maximum boundary errors between

the real boundary points and the analytical FOR boundaries in (3-31)-(3-32) are considered for analysis. The calculations in (3-31)-(3-32) can apply to any of the three different distance functions:

$$\bar{\mathrm{e}}\left(\mathrm{set}_A, \mathrm{set}_B\right) = \frac{1}{N_{\mathrm{set}_A}} \sum_{a_i \in \mathrm{set}_A} D_{\mathrm{norm}}\left(a_i, \mathrm{set}_B\right), \tag{3-31}$$

$$\mathrm{e}_{\min}\left(\mathrm{set}_A, \mathrm{set}_B\right) = \min_{a_i \in \mathrm{set}_A} D_{\mathrm{norm}}\left(a_i, \mathrm{set}_B\right), \tag{3-32}$$

$$\mathrm{e}_{\max}\left(\mathrm{set}_A, \mathrm{set}_B\right) = \max_{a_i \in \mathrm{set}_A} D_{\mathrm{norm}}\left(a_i, \mathrm{set}_B\right). \tag{3-33}$$

- **Conservativeness of analytical FOR boundaries**

Since the error indices mentioned above cannot provide the information on whether the analytical FOR boundaries are inside or outside the real FOR (i.e. whether the analytical FOR boundaries are conservative or not), another index, "conservative proportion" (*CP*) is further proposed in (3-34) for measuring the conservativeness of the analytical boundaries, expressed by the proportion of operation points which are inside the real FOR over the total operation points on the analytical FOR boundaries.

$$CP = \frac{N_{in}^{A}}{N_{toal}^{A}} \times 100\% \tag{3-34}$$

N_{in}^{A} is the number of operation points on the analytical FOR boundaries and inside the real FOR. N_{toal}^{A} is the total number of the operation points on the analytical FOR boundaries.

The operation points on the analytical FOR boundaries and inside FOR can be identified by comparing $\gamma^{(k)}$ in Section 3.4.2 and $\omega^{(k)}$ in Section 3.4.3. Towards the same power-increasing direction $\boldsymbol{d}^{(k)}$, if $\omega^{(k)}$ is smaller than $\gamma^{(k)}$, then the operation point $\omega^{(k)}\boldsymbol{d}^{(k)}$ on the analytical boundary is inside the real FOR. Otherwise, the operation point is outside the real FOR.

If the whole analytical FOR enclosed by the analytical boundaries is inside the real FOR, then the analytical FOR is regarded as a conservative approximation of the real FOR, in which all operation points will not violate the constraints of the real distribution network. In most cases, however, approximating the high-dimensional nonlinear real FOR boundaries results in the fact that the analytical FOR boundaries might lie on the safe side or the unsafe side or even both sides of the real FOR. Therefore, the network operators are suggested to conduct offline analysis of the operation errors to learn the worst operating risks.

- **Operation errors**

Operation errors are defined as the physical consequences (including the overvoltage, undervoltage and overcurrent) of boundary errors. According to the definition of the FOR, all the operation points inside a FOR should be feasible and satisfy the network constraints including the thermal and voltage constraints. However, due to the boundary errors in the analytical FOR boundaries, the operation points confined by the analytical FOR boundaries might violate the network constraints. Therefore, it is important to learn how large this kind of violation will be.

The boundary points of a FOR actually correspond to the critical operation states (i.e., the worst operating conditions) of a distribution network. Therefore, the maximum operation errors can be observed by analysing the power flow results of all the analytical boundary points. Specifically, power flow calculation is repeatedly conducted for all the analytical boundary points, so that the overcurrent, overvoltage and undervoltage problems can be observed.

3.4.5. Stopping rule of the error analysis process

Despite the four steps as illustrated in Section 3.4.1-3.4.4, the flow chart also provides the statistical stopping rule for sampling power-increasing directions. Once

the standard deviation of the distances between the origin and the real boundary points along the sampled power-increasing directions satisfies (3-35)-(3-36), the sampling process can stop:

$$s^{(k)} = \left\| \gamma^{(k)} \boldsymbol{d}^{(k)} \right\|_2 \tag{3-35}$$

$$\frac{\sigma\left(\{s^{(k)}\}\right)}{\sqrt{k}} \leq \frac{\varepsilon}{z_{\alpha/2}} \tag{3-36}$$

where $s^{(k)}$ denotes the distance between the origin and the real boundary point $\gamma^{(k)}\boldsymbol{d}^{(k)}$, while $\{ s^{(k)} \}$ represents the set of distances with k samples. $z_{\alpha/2}$ is suggested to be set at 1.96 in accordance with the confidence level of 95%; ε is the acceptable error of the mean of distances to the predefined confidence level and it is set as 0.001MVA in this study.

3.5. Case study

In this section, a 5-node feeder and a 27-node feeder of an 11kV high-voltage underground (HV UG) network from the UKGDS [196] were used for the case study. The FORs of these two feeders were studied, and the analytical expressions of the FOR boundaries were validated.

The computation of the case study was performed in MATLAB R2019b on a PC with an Intel(R) Core(TM) i7-9700 CPU @ 3.00 GHz processor and 16 GB RAM. The simulation method in (3-26) was implemented by fmicon solver in MATLAB and the analytical method in (3-27) used the algebraic solution in MATLAB.

3.5.1. UKGDS 5-node feeder

The 5-node feeder studied is shown in Fig. 3.6. For simplification, the node 301 (slack bus) and nodes 1100-1103 in [196] were numbered as node 1 and nodes 2 to 5 in Fig. 3.6. The line thermal limits and the node voltage limits of the feeder were listed in Table 3.1.

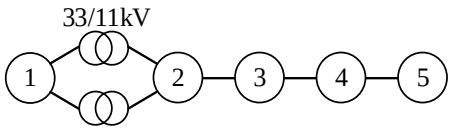

Fig. 3.6. The schematic diagram of the 5-node feeder selected from the 11kV UKGDS distribution network.

Table 3.1. Thermal and voltage limits for the 5-node feeder

Line thermal limits		I_{1-2}=4800A
		I_{2-3}=620A
		I_{3-4}=620A
		I_{4-5}=440A
Node voltage limits	Upper limits	V_x =1.03p.u. (x=2,3,4,5)
	Lower limits	V_x =0.97p.u. (x=2,3,4,5)

- **Results of analytical FOR boundaries**

Since there are 4 power injection nodes (excluding node 1 as the slack bus) in the feeder, the dimension of its FOR in the complex power injection space is eight. In the 8-dimensional operation region, there are twelve boundaries in total, including four thermal boundaries and eight voltage boundaries, which are determined by the thermal limits and voltage limits in Table 3.1, enclosing the FOR of the feeder.

Applying the proposed analytical expressions of thermal boundaries in (3-12) and voltage boundaries in (3-22) and (3-23), these twelve boundaries can be approximated. Considering the difficulties of visualization in the high-dimensional complex power injection space, Fig. 3.7 illustrates the twelve analytical FOR boundaries in a 2-dimensional P_4-P_5 cross-section. Fig. 3.7 also shows how these analytical boundaries

proposed in this chapter characterize the FOR (i.e., the allowable range of power injections in yellow) of the feeder.

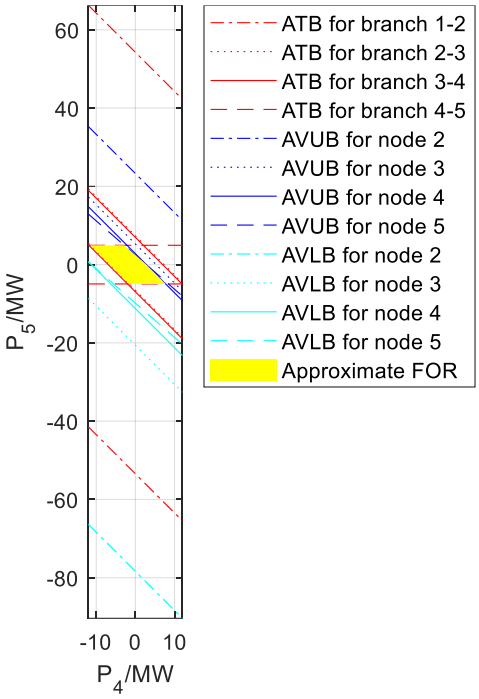

Fig. 3.7. Results of quadratic analytical FOR boundaries of the 5-node feeder in P_4-P_5 cross-section.

(ATB: analytical thermal boundary; AVUB: analytical voltage upper boundary; AVLB: analytical voltage lower boundary.)

The real FOR of the feeder and the FOR obtained by the hyperplane analytical expressions in 2-dimensional cross-sections are further depicted (including P_4-P_5, P_4-Q_5, P_5-Q_4 and Q_4-Q_5 cross-sections) for comparison. The results are shown in Fig. 3.8. The results in these four cross-sections show that the quadratic analytical boundaries are more accurate than hyperplane ones, especially considering the impact of reactive power injections on the line currents. However, these conclusions cannot be made in the whole power injection space since the errors between the analytical FOR boundaries and the real FOR boundaries differ in different cross-sections. This requires the high-

dimensional error analysis of the analytical FOR boundaries in the whole power injection space.

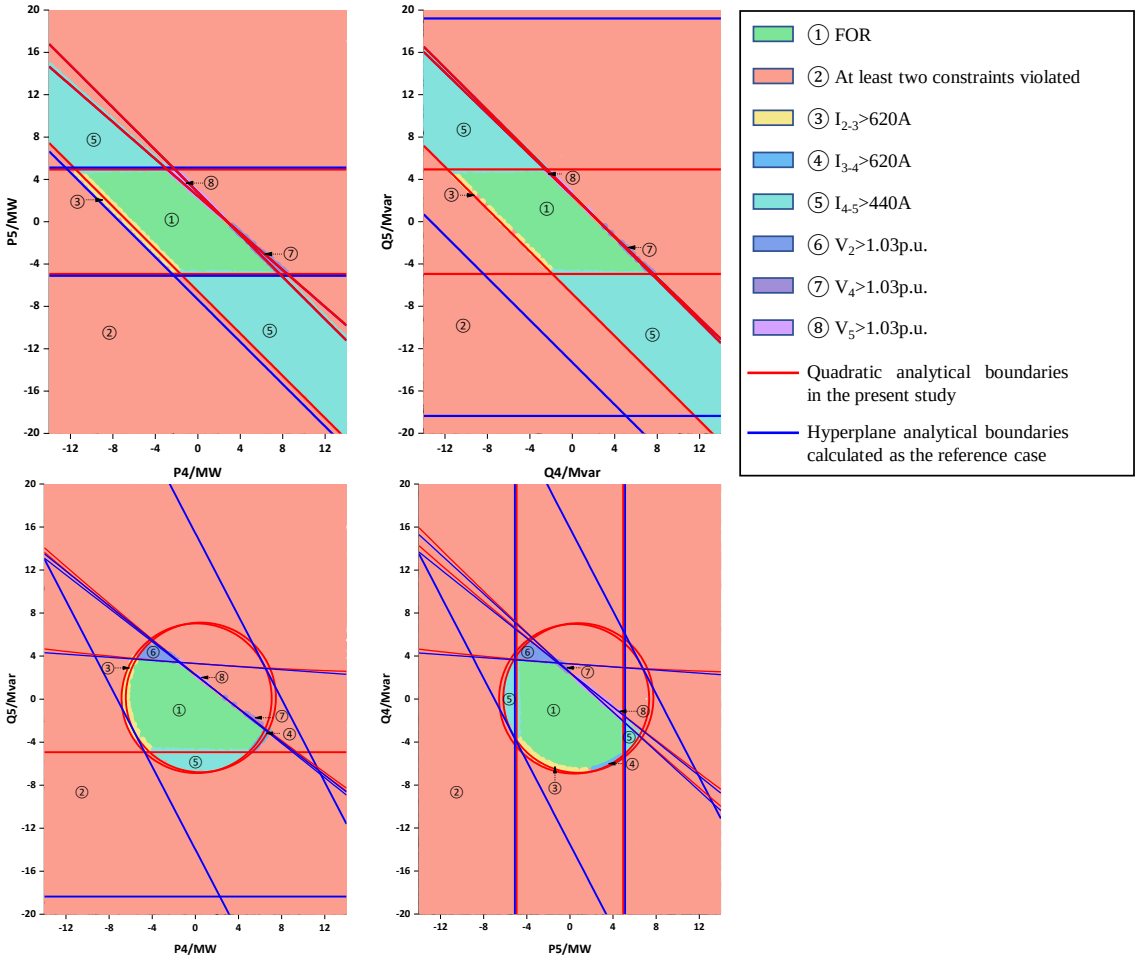

Fig. 3.8. Comparison of the approximate FOR enclosed by analytical boundaries with the real FOR in 2-dimensional cross-sections.

- **Demonstration of high-dimensional error analysis**

In this subsection, the high-dimensional error analysis method developed in this study was demonstrated in the 2-dimensional P_4-P_5 cross-section as shown in Fig. 3.9. In Fig. 3.9, 50 power-increasing directions were generated by Marsaglia's algorithm [195] for Step 1 of the method (see Section 3.4), along which the real boundary points and the operation points on the analytical FOR boundaries can be obtained following Step 2 and Step 3 respectively. The FOR and the innermost analytical boundaries in P_4-P_5 cross-section are also displayed in Fig. 3.9 for reference. It is noteworthy that the

developed high-dimensional error analysis can apply to any forms of analytical FOR boundaries besides the quadratic analytical FOR boundaries presented in Fig. 3.9. Following Step 4 in Section 3.4, the errors of the analytical FOR boundaries can be analysed through comparing the set of the real boundary points and the set of the operation points on the analytical FOR boundaries. The error analysis results in the whole power injection space were presented in the following section.

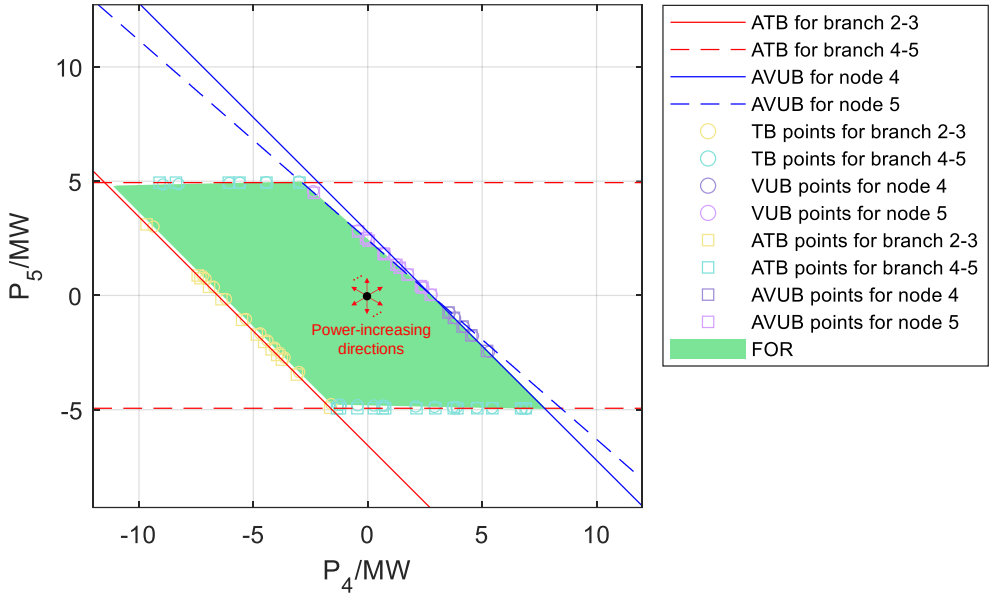

Fig. 3.9. Demonstration of the error analysis method in 2-dimensional P_4-P_5 cross-section.

(ATB: analytical thermal boundary; AVUB: analytical voltage upper boundary; AVLB: analytical voltage lower boundary; TB: thermal boundary; VUB: voltage upper boundary; VLB: voltage lower boundary.)

- **Error analysis results**

100,000 power-increasing directions were generated in the whole power injection space for the high-dimensional error analysis. Through obtaining and analysing the real boundary points, eight boundaries (three thermal boundaries and five voltage boundaries that are determined by thermal limits of lines 2-3, 3-4 and 4-5, voltage upper

limits of nodes 2-5 and voltage lower limit of node 5) were found to constitute the real FOR for the 5-node feeder. The composition of FOR boundaries indicates that the allowable rage of the power injections of the case network is confined by these thermal/voltage limits. It is noteworthy that the lower voltage boundaries that are determined by the lower voltage limits for nodes 2-4 are beyond the FOR and are thus not FOR boundaries. The reason for this is that the increase of power loading will first increase the line currents to their limits before triggering low voltages at nodes 2-4.

The error analysis for the quadratic expressions of the eight FOR boundaries was presented as follows. The quadratic expressions proposed in this study were also compared with the hyperplane expressions used.

1) Boundary errors

Fig. 3.10 shows the boundary errors for quadratic and hyperplane analytical thermal/voltage boundaries of FOR. The minimum, mean and maximum boundary errors for analytical boundaries are expressed in the boxes in Fig. 3.10. The detailed boundary errors for each analytical thermal/voltage boundary are attached in Fig. A.1 of Appendix for reference.

From a statistical point of view, the analytical expressions of FOR boundaries in Fig. 3.10 shows similar error results with different distance functions (i.e., Chebyshev, Euclidean and Manhattan). Whichever distance function is used, the mean boundary errors for quadratic thermal boundaries and voltage boundaries are less than 3.0% and 1.6%, respectively. The maximum boundary errors of quadratic thermal boundaries can be confined within 12.8%, while the maximum boundary errors for quadratic expression of voltage boundaries are 14.9%.

In comparison, the results of hyperplane expressions show larger boundary errors in both thermal and voltage boundaries. In particular, hyperplane expressions are not

able to describe thermal boundaries accurately, whereas the boundary errors of the voltage boundaries are close to those of quadratic expressions.

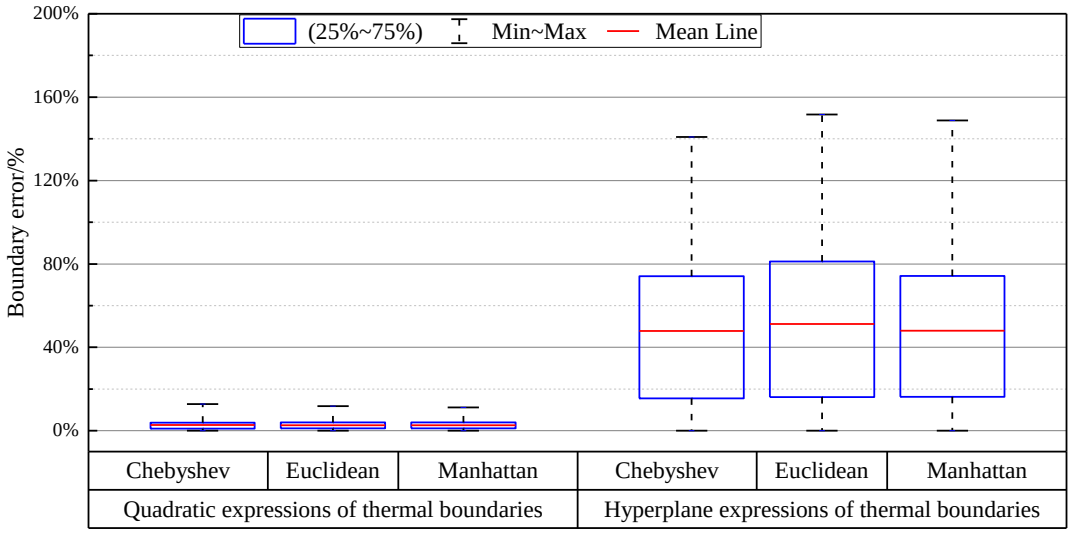

(a)

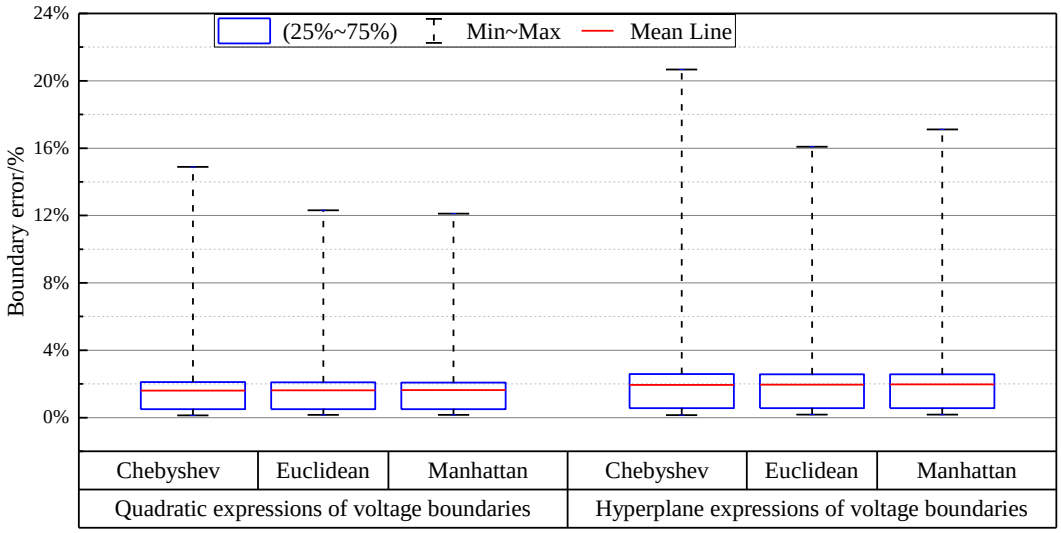

(b)

Fig. 3.10. Comparison of the boundary errors between quadratic expressions and hyperplane expressions of (a) thermal boundaries and (b) voltage boundaries in the 5-node feeder measured by multiple distance functions

2) Conservativeness of analytical FOR boundaries

The analytical boundary points which are inside FOR can be identified by determining whether the obtained $\omega^{(k)}$ in (3-27) is smaller than $\gamma^{(k)}$ in (3-26) along the

same power-increasing directions. By counting the number of the analytical boundary points which are inside the FOR, the conservativeness of the analytical FOR boundaries can be assessed with detailed results listed in Table 3.2.

Table 3.2. Conservative proportion of analytical FOR boundaries

FOR boundaries		Quadratic expressions		Hyperplane expressions	
		Conservative proportion/%	Overall conservative proportion/%	Conservative proportion/%	Overall conservative proportion/%
Thermal boundary corresponding to:	$\|I_{2,3}\|$=620A	6.9	61.5	0	56.3
	$\|I_{3,4}\|$=620A	10.9		0.3	
	$\|I_{4,5}\|$=440A	19.8		0.7	
Voltage boundary corresponding to:	V_2=1.03p.u.	100		100	
	V_3=1.03p.u.	100		100	
	V_4=1.03p.u.	100		100	
	V_5=1.03p.u.	100		100	
	V_5=0.97p.u.	0		0	

For the 5-node feeder, 61.5% of the quadratic analytical FOR boundaries is conservative, while 56.3% of the hyperplane analytical boundaries is conservative. Since the overall conservative proportion of the analytical FOR boundaries is not 100% (for both quadratic and hyperplane expressions), there must be some critical operation points, which are within analytical FOR boundaries but will violate the network constraints. Therefore, analysing the operation errors is important to decide whether the errors of the analytical FOR boundaries are acceptable in practice.

3) Operation errors

The network operating states of the analytical boundary points were calculated to observe the maximum operation errors. The results for quadratic expressions and hyperplane expressions are compared in Fig. 3.11. The maximum operation errors of

quadratic expressions of FOR boundaries for the overcurrent are up to 105.3% and for the undervoltage are down to 0.968 p.u.. This level of thermal and voltage violation is acceptable in practice.

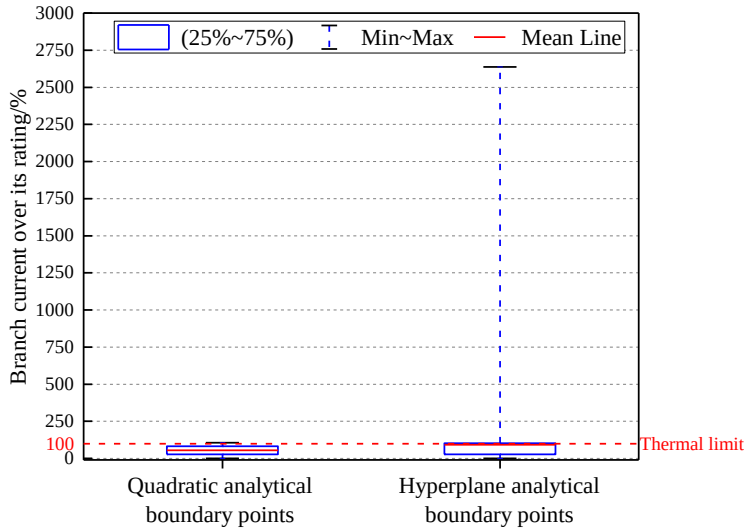

(a)

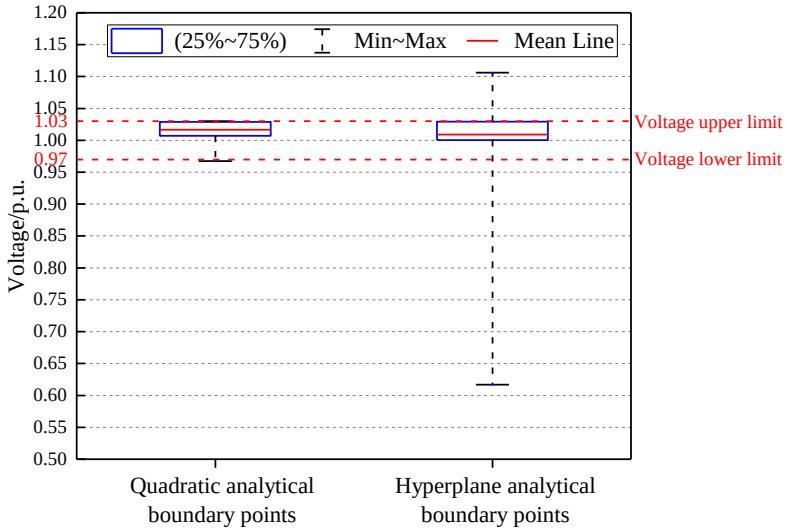

(b)

Fig. 3.11. Network operating states of analytical FOR boundary points for the 5-node feeder: (a) line currents and (b) node voltages. Note that power flow calculations through the Newton-Raphson algorithm cannot converge for 3% extreme operation points with very large power injections for the hyperplane thermal boundary points

The results in Fig. 3.11 show that there are some aggressive operation points on hyperplane analytical boundaries, which cause the network constraint violation up to an unacceptable level. Most aggressive operation points come from the significant boundary errors in the hyperplane thermal boundaries.

3.5.2. UKGDS 27-node feeder

The longest feeder from the UKGDS HV UG network (i.e., the 27-node feeder) [196] is shown in Fig. 3.12, where nodes 1-27 denote the node 301 (slack bus), node 1100 and nodes 1151-1175 respectively in [196]. The line thermal limits and the node voltage limits of the feeder refer to [196]. Since the 27-node feeder is much longer than the 5-node feeder in Section 3.5.1, the total power losses and the voltage difference between the power injection nodes (especially the end node) and the slack bus can be larger. Hence, this feeder is used to further verify the accuracy of the quadratic expressions of FOR boundaries in this study.

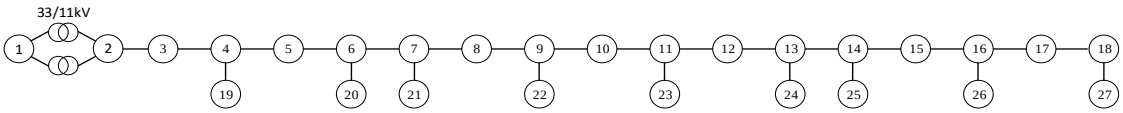

Fig. 3.12. The schematic diagram of the 27-node feeder selected from the 11kV UKGDS distribution network.

In the 27-node feeder there are 26 power injection nodes and 26 lines. As a result, 26 thermal boundaries and 52 voltage boundaries in the 52-dimensional complex power injection space can be identified to characterize the FOR of the feeder. The quadratic analytical expressions for these boundaries can be written as in (3-12), (3-22) and (3-23).

The validation for these analytical boundaries can be conducted by the high-dimensional error analysis method in Section 3.4. 100,000 power-increasing directions were used for searching the real boundary points of the FOR and the operation points

on the analytical FOR boundaries. By comparing the set of real boundary points and the set of operation points on analytical boundaries, the boundary errors were obtained in Fig. 3.13.

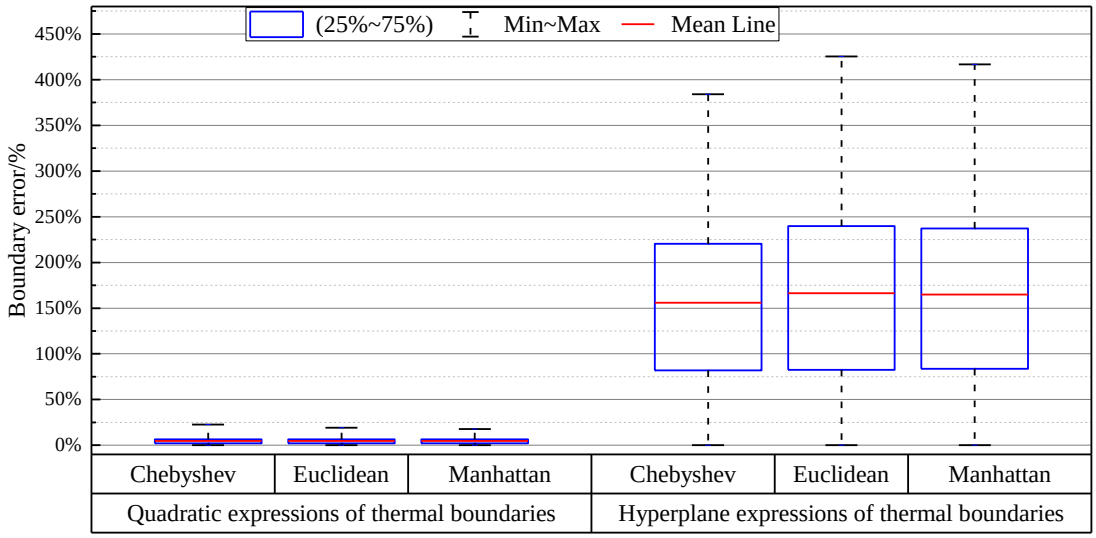

(a)

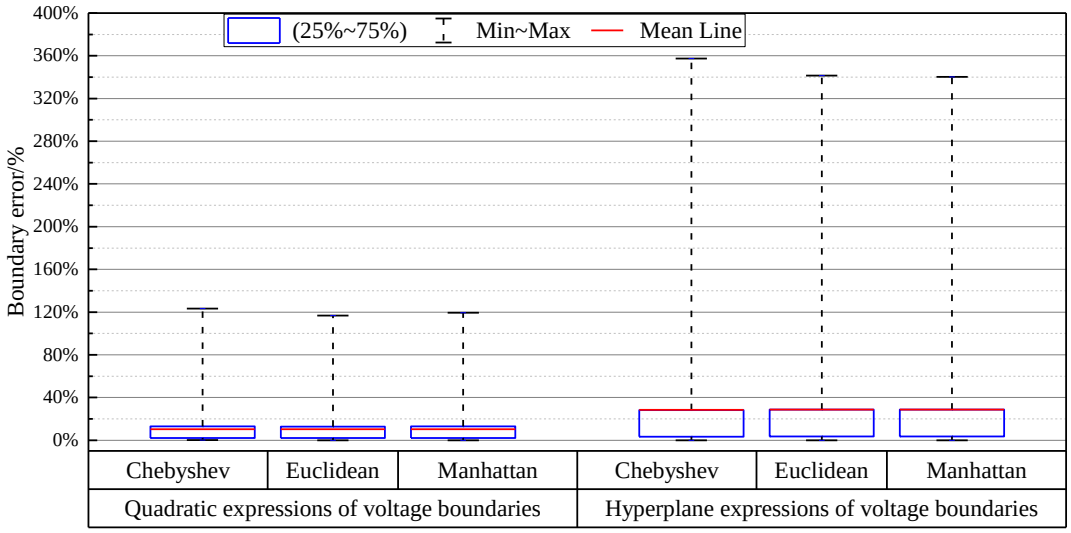

(b)

Fig. 3.13. Comparison of the boundary errors between quadratic expressions and hyperplane expressions of (a) thermal boundaries and (b) voltage boundaries in the 27-node feeder measured by multiple distance functions

Comparing to the results of the 5-node feeder, the mean boundary errors increase to 4.6% and 10.3% for quadratic expressions of thermal and voltage boundaries

respectively, while the maximum boundary errors to 22.7% and 123.3%. However, the quadratic expressions proposed in this study show greater advantages over the hyperplane expressions in characterizing the FOR of the longer 27-node feeder.

The conservative proportion of the quadratic analytical boundaries is 77.4%, while the conservative proportion of the hyperplane analytical boundaries is 51.4%. Hence the operation errors were further analysed and the results were shown in Fig. 3.14. The maximum operation errors of the quadratic analytical boundaries for the overcurrent are up to 116.0% and for the undervoltage are down to 0.960 p.u., which is also acceptable in practice. The reason why the maximum boundary error reaches 123.3% but the operation errors are small is that the maximum boundary error happens at the lower voltage boundary of node 20, where the conservativeness of the corresponding analytical boundary is 100%. For hyperplane analytical boundaries, most aggressive operation points come from the significant boundary errors in the hyperplane thermal boundaries.

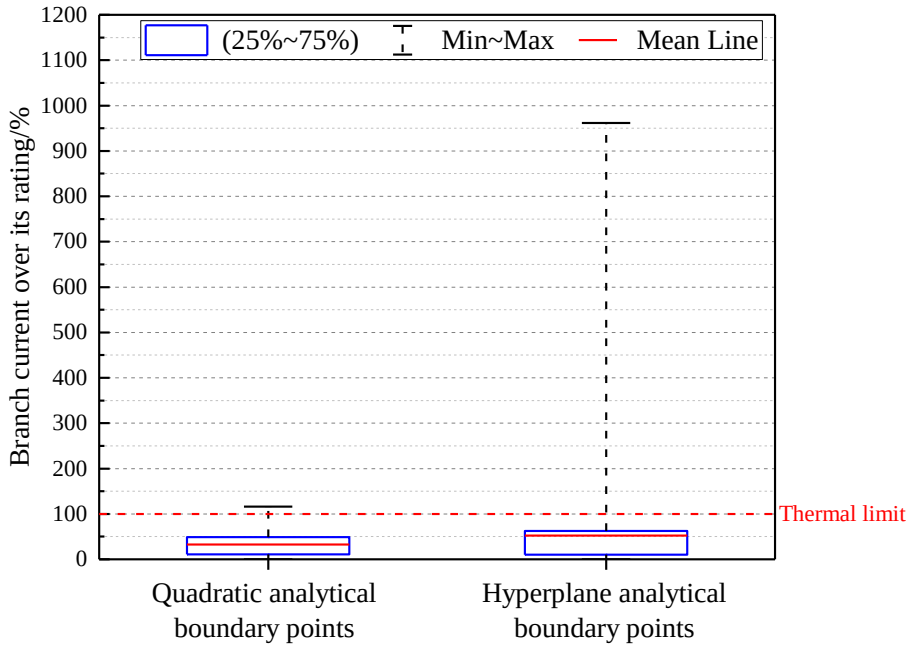

(a)

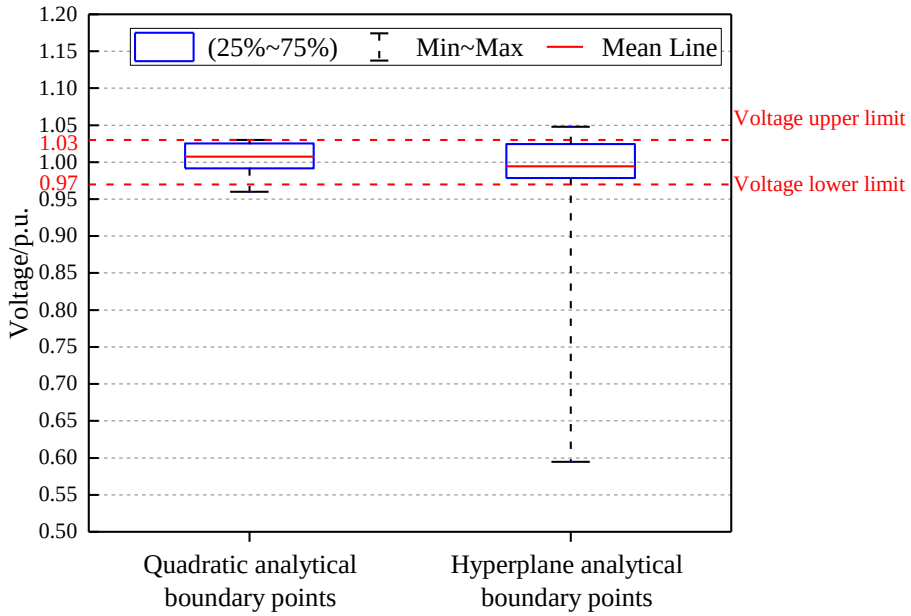

(b)

Fig. 3.14. Network operating states of analytical FOR boundary points for the 27-node feeder: (a) line currents and (b) node voltages. Note that power flow calculations through the Newton-Raphson algorithm cannot converge for 11% extreme operation points with very large power injections on the hyperplane thermal boundaries

3.5.3. Computation time

The computation time for obtaining the FOR boundary points by the simulation method in (3-26) and the proposed analytical FOR boundaries in (3-27) is summarised in Table 3.3.. As observed in Table 3.3., the analytical method spent 0.08ms to calculate one FOR boundary point for the UKGDS 5-node feeder while the simulation method took 41.97ms, achieving five-hundred-fold speed up. Regarding the UKGDS 27-node feeder, the proposed analytical method is even thousand-fold faster than the simulation method. The reason is that compared to the simulation method, the proposed analytical method can directly obtain the boundary point through algebraic computation, avoiding repeatedly iterations in the simulation method. In addition, the proposed method can directly use analytical expressions for complete characterization of the FOR of the

network, while the simulation method requires much more work on point-based simulation.

Table 3.3. Comparison of the time consumption between the analytical method and the simulation method

Method	Average time consumption for obtaining one FOR boundary point	
	UKGDS 5-node feeder	UKGDS 27-node feeder
Simulation method in (3-26)	41.97ms	843.56ms
Analytical method in (3-27)	0.08ms	0.53ms

3.5.4. Error analysis of power losses assumption

The overall error analysis results in Section 3.5.1 have shown that the errors caused from the assumptions of the analytical FOR boundaries are acceptable in practice. This section provides further analysis of the impact of power losses assumption on the results of line currents and node voltages.

Power losses are assumed to be ignored in the line current equation (3-11) and node voltage equation (3-20). Under this assumption, the equivalent power loading at node j (i.e., $P_{j,eq}/Q_{j,eq}$) can be estimated by the summation of the power loading at the downstream nodes of node j (i.e., $\sum_{k\in D_j} P_k$ / $\sum_{k\in D_j} Q_k$). With the actual peak power loading conditions in the test systems, the errors of the equivalent power loading caused by the ignorance of power losses were summarised in Table 3.4. Since the maximum errors should appear at the first PQ node of the system, Table 3.4 only presents the errors for $P_{j,eq}$ and $Q_{j,eq}$ at the first PQ node in different test systems.

Table 3.4. Errors of the equivalent power loading at the first PQ node in different test systems

Test system	Equivalent active power loading				Equivalent reactive power loading			
	True value /MW	Estimated value /MW	Error /MW	Percentage error /%	True value /Mvar	Estimated value /Mvar	Error /Mvar	Percentage error /%
UKGDS 5-node	0.902	0.900	0.002	0.22	0.181	0.180	0.001	0.55
UKGDS 27-node	7.760	7.512	0.248	3.20	1.693	1.502	0.191	11.28

From Table 3.4, the maximum errors for both equivalent active and reactive power are increased as the feeder length of the test systems increases. In addition, the percentage error for the equivalent reactive power loading seems very large especially in long-feeder system. However, the magnitude of the error for the equivalent reactive power loading is actually smaller than that for active power loading since the reactance is smaller than the resistance in the distribution networks.

Table 3.5. Impact of ignorance of power losses on the results of line currents and node voltages

Test system	Maximum error of the line currents /%	Maximum error of the node voltages /%
UKGDS 5-node	0.336	0.002
UKGDS 27-node	4.259	0.264

The errors of all line currents and the errors of all node voltages are further calculated, which result from the ignorance of power losses in calculating the equivalent power loading in Table 3.4. The results of the maximum error of all the line currents and node voltages were summarised in Table 3.5. From the obtained results, the errors

of the line currents and the node voltages are acceptable (even if the error of the equivalent reactive power loading in Table 3.4 can be 11.28% in the UKGDS 27-node test system).

3.6. Summary

This chapter develops a novel FOR method to characterise the range of operating states of a distribution network, within which no network constraints are violated. The boundaries of FOR provide the limitations to operating the network and contain the whole information of the capability of the network to integrate generation and demand. Therefore, the mathematical expressions of the FOR boundaries are investigated.

The analytical expressions of both thermal and voltage boundaries of a FOR are formulated in the quadratic form of the power injections at the nodes of a distribution network. To validate the analytical expressions of FOR boundaries in a high-dimensional operation region, a high-dimensional error analysis approach is further developed. The boundary errors are obtained by comparing the distance between the set of real boundary points and the set of operating points on the analytical FOR boundaries. The operational errors that define the physical consequences (including the overvoltage, undervoltage and overcurrent) of boundary errors are also obtained.

The proposed quadratic expressions of FOR boundaries can well approximate the real boundaries of the FOR from the results of case studies in the UKGDS 5-node and 27-node feeders. The maximum errors for thermal and voltage boundaries would maximally cause an overcurrent up to 116 % and an undervoltage down to 0.96p.u., which are able to satisfy the requirements of engineering practice.

The proposed quadratic expressions of FOR boundaries proposed in this chapter are also compared with the existing linear approximation (i.e., hyperplane expressions) of FOR boundaries. The results show that the quadratic expressions of FOR boundaries

outperform the hyperplane expressions. With the increase of the scale of distribution networks, hyperplane expressions of thermal boundaries may have large errors, while quadratic expressions are more accurate and can be a better choice.

Chapter 4. Characterisation of feasible operation regions with SOPs

4.1. Introduction

This chapter investigates the impact of SOPs on the FOR^{DN} and develops analytical expressions for characterising FOR^{SOP}. Through numerous simulations on the two-dimensional cross-sections of FOR^{SOP} and FOR^{DN}, an underlying geometric relationship between their boundaries was observed. Initially, there was no clear approach to understanding this geometric relationship until another concept used in robot motion planning was come across incidentally. Excitingly, the relationship between the tunnel boundaries and the shortest path of a robot, when the robot moves a volume through a tunnel, bears great similarity to our problem. This insight led to the identification of the Minkowski Sum as the governing principle in this study.

To ensure precision and avoid any intuitive pitfalls, this finding was rigorously proven. Consequently, a strict geometry model for the FOR^{SOP} is established. The model interprets the FOR^{SOP} as the Minkowski Sum of the FOR of the distribution network and the operating range of SOPs. Furthermore, a practical Minkowski Sum algorithm is developed to derive the analytical expressions of FOR^{SOP} boundaries, which exploits the translation and fitting methods within the algorithm.

To clearly demonstrate the Minkowski Sum-based model and the solving algorithm, a three-dimensional FOR is constructed for a three-node distribution network with a SOP. Additionally, the effectiveness of the proposed method is validated using the IEEE 33-node distribution network.

Since the development of FORs in this thesis focuses on the steady-state power flow feasibility of network operating states considering thermal and voltage violations, security of distribution networks under transient events is not considered. This indicates that maintaining the operating states within the FOR of the distribution network does

not guarantee network security during transient events like short-circuit faults. However, the same methodology can be utilised to formulate the security region that satisfies different network security constraints under transient events, which can be referred to the discussion in Section 2.2.

4.2. Preliminaries

The FOR of a distribution network is enclosed by several high-dimensional surfaces, which are determined by thermal and voltage constraints. These surfaces, termed as the boundaries of the FOR, confine the network to its normal operation without violating the network constraints. Considering the types of network constraints, the boundaries of the FOR can be further categorized into thermal boundaries and voltage boundaries.

In this study, the quadratic expressions are used in Chapter 3 to approximate the thermal boundaries as shown in (4-1), while using linear/hyperplane expressions in [42] to approximate the voltage boundaries of FOR as shown in (4-2)-(4-3).

$$\left(\sum_{k=1}^{n}\alpha_k^{I_{ij}}P_k\right)^2+\left(\sum_{k=1}^{n}\beta_k^{I_{ij}}Q_k\right)^2=\left(V_0I_{ij}^M\right)^2,\forall ij\in B \tag{4-1}$$

In (4-1), B is the set of lines of the distribution network. n is the number of nodes (excluding the slack bus) in the distribution network. P_k and Q_k are the active and reactive power injections at node k of the distribution network. Their coefficients $\alpha_k^{I_{ij}}$ = $\beta_k^{I_{ij}}$ =1 if node k is the downstream node of node j (or node k= node j); otherwise $\alpha_k^{I_{ij}}$ = $\beta_k^{I_{ij}}$ =0. I_{ij}^M is the upper limit to the current on the power line ij. V_0 is the voltage magnitude at the slack bus, which is used to approximate the voltage at node j.

$$\sum_{k=1}^{n}\left(\alpha_k^{V_{i,M}}P_k+\beta_k^{V_{i,M}}Q_k\right)=1,\forall i\in N$$

$$\text{where}\begin{cases}\alpha_k^{V_{i,M}}=\dfrac{r_k^i}{V_0\left(V_i^M-V_0\right)}\\ \beta_k^{V_{i,M}}=\dfrac{x_k^i}{V_0\left(V_i^M-V_0\right)}\end{cases} \tag{4-2}$$

$$\sum_{k=1}^{n}\left(\alpha_k^{V_{i,m}}P_k+\beta_k^{V_{i,m}}Q_k\right)=1,\forall i\in N$$

$$\text{where}\begin{cases}\alpha_k^{V_{i,m}}=\dfrac{r_k^i}{V_0\left(V_i^m-V_0\right)}\\ \beta_k^{V_{i,m}}=\dfrac{x_k^i}{V_0\left(V_i^m-V_0\right)}\end{cases} \tag{4-3}$$

In (4-2) and (4-3), N is the set of nodes of the distribution network. $\alpha_k^{V_{i,M}}$ and $\beta_k^{V_{i,M}}$ are the coefficients of P_k and Q_k for upper voltage boundaries in (4-2) and $\alpha_k^{V_{i,m}}$ and $\beta_k^{V_{i,m}}$ are the coefficients of P_k and Q_k for lower voltage boundaries in (4-3). The resistance r_k^i and the reactance x_k^i are obtained according to the topology and component parameters of the network as presented in (4-4):

$$r_k^i+jx_k^i=\begin{cases}R_{0,i}+jX_{0,i}, & \text{if } k\in D_i \text{ or } k=i\\ R_{0,k}+jX_{0,k}, & \text{if } i\in D_k\\ R_{0,s}+jX_{0,s}, & \text{if } k\notin D_i \text{ and } i\notin D_k\end{cases} \tag{4-4}$$

where D_x (x=i or k in (4-4)) denotes the set of the downstream nodes of x. $R_{0,x}$ + $X_{0,x}$ (x=i, k or s in (4-4)) is the total impedance of the lines from the slack node to node x. Here node s is the first intersection of the upstream nodes of node i and node k.

Equations (4-1)-(4-3) are expressions of the FOR boundaries for a distribution network. However, the effect of SOPs on the FOR of a distribution network has not been studied. In the next section, the Minkowski Sum-based model will be established for the analysis of the impact of SOPs on the FOR.

4.3. Mathematic model of the feasible operation region of a distribution network with SOPs

For conciseness, the FOR of the distribution network is termed as FOR^{DN}, whereas the FOR of a distribution network with SOPs is termed as FOR^{SOP} in this study. The modelling of the FOR^{SOP} of a distribution network with SOPs is targeted at obtaining the FOR that is expanded by SOPs due to their strong power controllability. Therefore, the relationship between the FOR^{SOP} and the FOR^{DN} must be associated with the operating range of SOPs (SOP^{OR}).

In this section, the Minkowski-Sum based model is established for describing the FOR of a distribution network with SOPs. The concept of Minkowski Sum will be introduced first. Subsequently, the mathematical relationship between the FOR of distribution networks with and without SOPs will be discussed and the Minkowski Sum-based model will be developed. Finally, the physical meaning of the model will be further illustrated to enhance the understanding of the model.

4.3.1. Concept of Minkowski Sum

Minkowski Sum was defined by Hermann Minkowski and has been used in various domains such as robotic motion planning, computer-aided design, penetration depth estimation and solid modelling [197]. Given two sets of position vectors *A* and *B*, the Minkowski Sum of them is defined as the set of vectors that are formed by adding each position vector from set *A* to each position vector from set *B*. Here a position vector is a vector that represents the position of a point in relation to the origin (i.e., the reference point). Following this definition, the Minkowski Sum can be expressed as:

$$A \oplus B = \{a + b | a \in A, b \in B\} \tag{4-5}$$

where $\oplus$ denotes the Minkowski Sum. *a* and *b* are the position vectors from the two sets *A* and *B* respectively.

Based on the definition, the Minkowski Sum can be further obtained by (4-6) that reflects on the geometry property of Minkowski Sum:

$$A \oplus B = \bigcup_{a \in A} B_a \tag{4-6}$$

where $\cup$ denotes the set union operation. B_a denotes the set obtained by translating the entire set B by a position vector a from the set A. The translating operation refers to moving every vector in set B the same distance in the same direction, as specified by the position vector a.

From a geometric perspective, the Minkowski Sum of the two sets A and B (as shown in Fig. 4.1 [197]) can be obtained by sweeping the end points of all position vectors of A by B. The sweeping operation denotes moving B along the end points of all position vectors of A. From Fig. 4.1, the sweeping operation for obtaining the Minkowski Sum of the sets A and B finally combine the two sets to produce a new set C. It is worthy of noting that the Minkowski Sum boundaries can be obtained by sweeping the boundary of A by B and taking the union of the outermost resulting points.

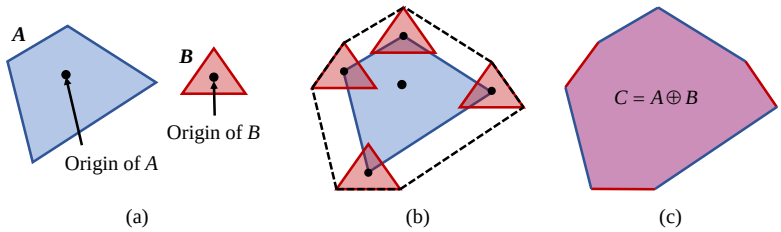

Fig. 4.1. An example of the Minkowski Sum of two sets: (a) Two sets A and B; (b) The sweeping of set A by set B; (c) The Minkowski Sum of sets A and B.

From Fig. 4.1, the Minkowski Sum boundaries are expanded from the two parts of A: the boundaries of A and the intersection point of the adjacent boundaries of A (i.e., the four vertices of A in Fig. 4.1). Specifically, the blue Minkowski Sum boundaries are translated from the original boundaries of A, while the red Minkowski Sum boundaries are originated from the intersection point of adjacent boundaries of A. Though Fig. 4.1

only provides a two-dimensional example, this rule can be extended to higher-dimensional Minkowski Sum.

Referring to [197], the translation vector associated with each blue Minkowski Sum boundary can be obtained by firstly identifying the point in set *B* that is the farthest from the boundary of *A* in the direction of the boundary's outer normal (denoted as b^{farthest}). Then the translation vector is the vector starting at the origin of *B* (i.e., the common initial point of all the position vectors in *B*) and ending at the point b^{farthest}. The red Minkowski Sum boundaries can be obtained based on 2/3-dimensional geometry methods proposed in [197] yet hard to be applied in computation of high-dimensional Minkowski Sum.

In the next section, the impact of SOPs on the FOR of a distribution network will be explored using Minkowski Sum.

4.3.2. Definition of the feasible operation region of a distribution network with SOPs

FOR^{SOP} describes the allowable range of nodal power injections in a distribution network with SOPs, where both network and SOP constraints are not violated.

$$FOR^{SOP} := \left\{ \begin{bmatrix} \boldsymbol{P} \\ \boldsymbol{Q} \end{bmatrix} \in R^{2n} \middle| \begin{array}{c} \boldsymbol{V} \in \boldsymbol{C_V} \\ \boldsymbol{I} \in \boldsymbol{C_I} \\ \begin{bmatrix} \boldsymbol{P^{SOP}} \\ \boldsymbol{Q^{SOP}} \end{bmatrix} \in SOP^{OR} \\ f\left(\boldsymbol{V}, \boldsymbol{I}, \boldsymbol{P^{SOP}}, \boldsymbol{Q^{SOP}}, \boldsymbol{P}, \boldsymbol{Q}\right) = 0 \end{array} \right\} \tag{4-7}$$

where $\boldsymbol{P}=[P_1, \ldots, P_n]^T$ and $\boldsymbol{Q}=[Q_1, \ldots, Q_n]^T$ are vectors of active power injections and reactive power injections respectively. $f\left(\boldsymbol{V}, \boldsymbol{I}, \boldsymbol{P^{SOP}}, \boldsymbol{Q^{SOP}}, \boldsymbol{P}, \boldsymbol{Q}\right) = 0$ represents the power flow equations (e.g., Distflow branch equations [168]). $\boldsymbol{V}$ and $\boldsymbol{I}$ are the node

voltage vector and line current vector, which satisfy the voltage constraints $\boldsymbol{C_V}$ and thermal constraints $\boldsymbol{C_T}$, respectively:

$$\boldsymbol{C_V} := \left\{ V_i^m \le V_i \le V_i^M, \forall i \in N \right\} , \tag{4-8}$$

$$\boldsymbol{C_T} := \left\{ \left| I_{ij} \right| \le I_{ij}^M, \forall ij \in B \right\} , \tag{4-9}$$

where V_i is the voltage magnitude at node *i*, constrained by its lower limit V_i^m and upper limit V_i^M. $\left| I_{ij} \right|$ is the magnitude of the line current constrained by its limit I_{ij}^M. Different from the definition of FOR^{DN}, FOR^{SOP} considers SOPs as components of the distribution network. $\boldsymbol{P^{SOP}}$ and $\boldsymbol{Q^{SOP}}$ denote the active power and reactive power injections from SOPs. SOP^{OR} is the operating range of SOPs, which can be expressed as in (4-10).

$$SOP^{OR} := \left\{ \begin{bmatrix} \boldsymbol{P^{SOP}} \\ \boldsymbol{Q^{SOP}} \end{bmatrix} \in R^{2m} \middle| \begin{array}{l} \sqrt{\left(P_k^{SOP}\right)^2 + \left(Q_k^{SOP}\right)^2} \\ \le S^{SOP}, \forall k \in \Omega_{SOP} \\ \sum_{k \in \Omega_{SOP}} P_k^{SOP} = 0 \end{array} \right\} \tag{4-10}$$

where *m* is the number of SOP terminals. Ω_{SOP} is the set of nodes that SOPs connect. P_k^{SOP} and Q_k^{SOP} are the power injections from SOPs at node *k* of the distribution network. S^{SOP} is the capacity of the converters of SOPs. From (4-10), SOP^{OR} is a 2*m*-dimensional geometry symmetric about the origin in the 2m-dimensional $\left[\boldsymbol{P^{SOP}}; \boldsymbol{Q^{SOP}} \right]$ space.

4.3.3. Modelling of the feasible operation region of a distribution network with SOPs

The implementation of SOPs can expand the FOR of a distribution network. It can be proved that FOR^{SOP} is the Minkowski Sum of FOR^{DN} and SOP^{OR}:

$$FOR^{SOP} = FOR^{DN} \oplus SOP^{OR} \tag{4-11}$$

Equation (4-11) is equivalent to the two propositions outlined in (4-12), of which the proofs are provided as below.

$$\begin{cases} \text{Proposition 1: } FOR^{DN} \oplus SOP^{OR} \subset FOR^{SOP} \\ \text{Proposition 2: } FOR^{SOP} \subset FOR^{DN} \oplus SOP^{OR} \end{cases} \tag{4-12}$$

- **Proof of Proposition 1**

Unless otherwise specified in the subsequent text, let us assume $\boldsymbol{u}$, $\boldsymbol{v}$ and $\boldsymbol{w}$ represent the power vectors within FOR^{DN}, SOP^{OR} and FOR^{SOP} respectively. For brevity, let $\boldsymbol{u}+\boldsymbol{v}$ （where $\boldsymbol{u} \in R^{2n}$, $\boldsymbol{v} \in R^{2m}$, $m<n$） express the nodal power injections considering the addition of the power injections from SOPs. From a mathematic perspective, $\boldsymbol{u}+\boldsymbol{v}$ signifies that $\boldsymbol{u}$ is added by $\boldsymbol{v}$ at the *P*/*Q* dimension corresponding to the *m* nodes connected by SOPs.

Following the definition of Minkowski Sum in (4-5), Proposition 1 can be interpretated as:

$$\begin{gathered} \forall \boldsymbol{u} \in FOR^{DN}, \forall \boldsymbol{v} \in SOP^{OR}, \text{we have:} \\ \left(\boldsymbol{w}=\boldsymbol{u}+\boldsymbol{v}\right) \in FOR^{SOP} \end{gathered} \tag{4-13}$$

Without loss of generality, assume $\boldsymbol{u}^*$ is any given power vector within FOR^{DN} and $\boldsymbol{v}^*$ is any given power vector within SOP^{OR}. The condition for (4-13) to hold is that their sum $\boldsymbol{w}^*=\boldsymbol{u}^*+\boldsymbol{v}^*$ should be within the set of FOR^{SOP}. In other words, (4-13) is satisfied if and only if there exists a power control strategy for the SOPs in the distribution network such that the power vector $\boldsymbol{w}^*=\boldsymbol{u}^*+\boldsymbol{v}^*$ does not violate the network constraints.

Since SOP^{OR} is symmetric about the origin. ($-\boldsymbol{v}^*$) that is symmetric with $\boldsymbol{v}^*$ is also within SOP^{OR}. If ($-\boldsymbol{v}^*$) is exploited as the power control strategy for SOPs, then the power injections $\boldsymbol{w}^*$ in the network can be regulated by SOPs, i.e., the net power

injections into the distribution network will be $\boldsymbol{w}^* - \boldsymbol{v}^* = \boldsymbol{u}^*$. Since $\boldsymbol{u}^*$ is within FOR^{DN}, the power injections $\boldsymbol{u}^*$ will not violate the network constraints.

In conclusion, for $\boldsymbol{u}^* \in FOR^{DN}$ and $\boldsymbol{v}^* \in SOP^{OR}$, their sum $\boldsymbol{w}^*$ (considering using (-$\boldsymbol{v}^*$) as the power control strategy for SOPs) is a feasible operating point within FOR^{SOP}. Proposition 1 is proved.

- **Proof of Proposition 2**

Proposition 2 can be interpretated as:

$$\begin{aligned} &\forall \boldsymbol{w} \in FOR^{SOP}, \exists \boldsymbol{u} \in FOR^{DN}, \exists \boldsymbol{v} \in SOP^{OR} \\ &s.t.\ \boldsymbol{w} = \boldsymbol{u} + \boldsymbol{v} \end{aligned} \tag{4-14}$$

Given a power vector $\boldsymbol{w}^*$ within FOR^{SOP}, the condition for (4-14) to hold is that at least a power vector within FOR^{DN} and a power vector within SOP^{OR} can be found such that their sum is equivalent to $\boldsymbol{w}^*$.

Since $\boldsymbol{w}^*$ is within FOR^{SOP}, there is at least one SOP control strategy $\boldsymbol{v}^*$ such that the net power injections $\boldsymbol{w}^* + \boldsymbol{v}^*$ satisfy the network constraints. Let the power vector $\boldsymbol{u}^*$ be the sum of $\boldsymbol{w}^*$ and $\boldsymbol{v}^*$ (i.e., $\boldsymbol{u}^* = \boldsymbol{w}^* + \boldsymbol{v}^*$), then the power vector $\bar{u}^*$ is within FOR^{DN}. Additionally, (-$\boldsymbol{v}^*$) that is symmetric with $\boldsymbol{v}^*$ is within SOP^{OR}.

From the above deduction, for the given power vector $\boldsymbol{w}^*$ within FOR^{SOP}, a power vector $\boldsymbol{u}^*$ can be found within FOR^{DN}, and a power vector $\left(-\boldsymbol{v}^*\right)$ within SOP^{OR} such that $\boldsymbol{w}^* = \boldsymbol{u}^* + \left(-\boldsymbol{v}^*\right)$. Proposition 2 is proved.

Equation (4-11) establishes the geometric relationship among FOR^{DN}, FOR^{SOP} and SOP^{OR}. From (4-11), it can be concluded that FOR^{SOP} is the Minkowski Sum of the 2n-dimensional FOR^{DN} and the 2m-dimensional SOP^{OR} of which the 2m dimensions correspond to the connected nodes of SOPs. Another interpretation of (4-11) is that SOPs expand the FOR of a distribution network in the way that the FOR^{DN} is swept by

the SOP^{OR} in the 2m-dimensional cross-sections related to the nodes connected by SOPs.

4.3.4. Categories of feasible operation region boundaries

As with the results of the Minkowski Sum boundaries of *A* and *B* in Fig. 4.1, the boundaries of FOR^{SOP} can either be translated from the original FOR^{DN} boundaries (including thermal and voltage boundaries) or originated from the intersections of the FOR^{DN} boundaries.

From a physical perspective, each boundary translated from the original FOR^{DN} boundary is determined by the same thermal/ voltage constraint as the original FOR^{DN} boundaries. In contrast, boundaries that originated from the intersections of adjacent boundaries of the FOR^{DN} are determined by two or more thermal/voltage constraints. For clarity throughout this study, the former boundaries will be termed as "single-constraint thermal/voltage boundaries" and the latter as "multi-constraint boundaries".

4.4. Minkowski Sum algorithm

Based on the mathematical model of FOR^{SOP} presented in the previous section, this section provides a practical Minkowski Sum algorithm to generate the analytical expressions of FOR^{SOP} boundaries. The single-constraint boundaries can be obtained using the translation algorithm in [197], while the multi-constraint boundaries (that are hard to be derived using the geometry algorithm in [197] due to the high dimensionality) can be derived through fitting methods. Since the thermal boundaries of FOR^{DN} in (4-1) and the quadratic boundaries of SOP^{OR} in (4-10) are both in circular form, the polygonal inner-approximation method in [32] can be used to linearise these boundaries at first.

4.4.1. Linearisation of the quadratic boundaries of FOR^{DN} and SOP^{OR}

In this study, regular polygons with 12 edges are used for the linearisation of the quadratic boundaries of FOR^{DN} and SOP^{OR} that are in circular form. Because the

vertices of an inscribed polygon in a circle are all located at the circumference of the circle, the linearisation of the inner region of FOR^{DN} and SOP^{OR} is conservative. The results of the linear expressions of FOR^{DN} and SOP^{OR} are shown in (4-15) and (4-16) respectively.

$$FOR^{DN} := \left\{ \begin{bmatrix} \mathbf{P} \\ \mathbf{Q} \end{bmatrix} \in R^{2n} \left| \begin{array}{l} \alpha_c \sum_{k=1}^{n} \alpha_k^{I_{ij}} P_k + \beta_c \sum_{k=1}^{n} \beta_k^{I_{ij}} Q_k \\ +\delta_c V_0 I_{ij}^{M} \le 0, \ \forall c \in \{1,2,...,12\}, \forall ij \in B \\ \sum_{k=1}^{n} \left(\alpha_k^{V_{i,M}} P_k + \beta_k^{V_{i,M}} Q_k \right) \le 1, \forall i \in N \\ \sum_{k=1}^{n} \left(\alpha_k^{V_{i,m}} P_k + \beta_k^{V_{i,m}} Q_k \right) \le 1, \forall i \in N \end{array} \right. \right\} \quad (4\text{-}15)$$

$$SOP^{OR} := \left\{ \begin{bmatrix} \boldsymbol{P}^{SOP} \\ \boldsymbol{Q}^{SOP} \end{bmatrix} \in R^{2m} \left| \begin{array}{l} \alpha_c P_k^{SOP} + \beta_c Q_k^{SOP} \\ +\delta_c S^{SOP} \le 0, \ \forall c \in \{1,2,...,12\}, \forall k \in \Omega_{SOP} \\ \sum_{k \in \Omega_{SOP}} P_k^{SOP} = 0 \end{array} \right. \right\} \quad (4\text{-}16)$$

After the linearisation, the quadratic boundaries of FOR^{DN} and SOP^{OR} are approximated in polygonal form, where the values of the coefficients α_c, β_c and δ_c for the *c*th edge of the polygon can refer to [32].

The Minkowski Sum of FOR^{DN} in (4-15) and SOP^{OR} in (4-16) is also polyhedron, which is enclosed by multiple hyperplanes. Unless otherwise specified in the following text, the approximate expressions of FOR^{DN} and SOP^{OR} in (4-15) and (4-16) will be used.

4.4.2. Obtaining single-constraint boundaries of FOR^{SOP}

Each thermal/voltage boundary of FOR^{DN} is expanded by the SOP to a single-constraint thermal/voltage boundary of FOR^{SOP}. Based on the Minkowski Sum algorithm in [197], the single-constraint boundaries of FOR^{SOP} can be easily obtained by translating the thermal/voltage boundaries of FOR^{DN}. Fixing the origin of SOP^{OR} on

the boundaries of FOR^{DN}, the translation vector associated with each boundary of FOR^{DN} can be determined. This is achieved by identifying the point within SOP^{OR} that lies farthest away from the boundary of FOR^{DN}. The translation vector is then represented by the vector that starts at the origin of SOP^{OR}, where there is no power transfer from SOPs, and ends at the farthest point. In this regard, the calculation of the translation vector associated with the *k*th boundary of FOR^{DN} can be established as an optimisation model below:

$$\max \left\langle \boldsymbol{n}_k^{FOR}, \boldsymbol{v}_k \right\rangle$$
$$s.t. \begin{cases} \boldsymbol{v}_k = \begin{bmatrix} \boldsymbol{P}^{SOP} \\ \boldsymbol{Q}^{SOP} \end{bmatrix} \\ \boldsymbol{v}_k \in SOP^{OR} \end{cases} \tag{4-17}$$

where $\boldsymbol{n}_k^{FOR}$ denotes the projection of the normal vector of the *k*th FOR^{DN} boundary onto the subspace defined by the power injections at the nodes connected by the SOP. For example, if node *i* and node *j* are connected by a two-terminal SOP, $\boldsymbol{n}_k^{FOR}$ is the projection of the normal of the *k*th FOR^{DN} boundary onto the P_i-P_j-Q_i-Q_j power injection space. The vector $\boldsymbol{v}_k$ represents the vector of the point inside SOP^{OR}, which starts at the origin of SOP^{OR} and ends at the point.

In (4-17), the decision variable is $\boldsymbol{v}_k$, which satisfies the constraints of SOP^{OR} (see (4-16)). The objective function of the optimisation model is to maximise the dot product of $\boldsymbol{n}_k^{FOR}$ and $\boldsymbol{v}_k$, which expresses the maximal distance between a point within SOP^{OR} and the *k*th boundary of FOR^{DN}.

The solution of $\boldsymbol{v}_k$ from (4-17) can then determine the expression of the *k*th boundary of FOR^{SOP} that is translated from FOR^{DN}. Take a two-terminal SOP that connects node *i* and node *j* for example. Assume the *k*th boundary of FOR^{DN} is

$f_k(\boldsymbol{P},\boldsymbol{Q})=0$. After translation, the corresponding single-constraint boundary of FOR^{SOP} can be obtained by simply replacing the symbols of P_x and Q_x in $f_k(\boldsymbol{P},\boldsymbol{Q})=0$ (where x is the node number) with P_x' and Q_x' as below:

$$\begin{cases} P_x' = P_x, \ if \ \ x \neq i, j \\ Q_x' = Q_x \ if \ \ x \neq i, j \\ \left(P_i', P_j', Q_i', Q_j'\right)^T = \left(P_i, P_j, Q_i, Q_j\right)^T - \boldsymbol{v_k} \end{cases} \tag{4-18}$$

4.4.3. Obtaining multi-constraint boundaries of FOR^{SOP}

Besides single-constraint boundaries, multi-constraint boundaries of the FOR^{SOP} contain operating points which reach two or more thermal/voltage limitations of the distribution network.

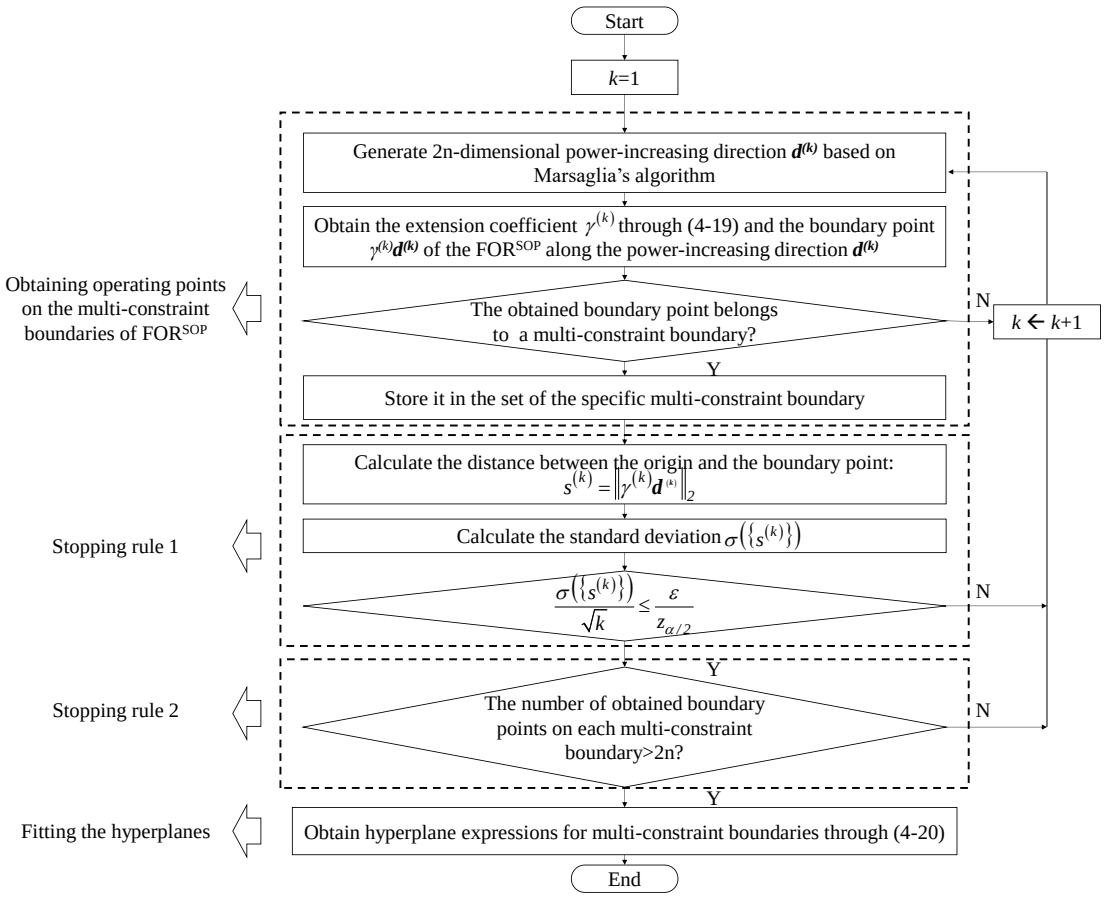

Fig. 4.2. Flow chart for obtaining multi-constraint boundaries of FOR^{SOP}.

To obtain the multi-constraint boundaries, an optimisation-based simulation method is first developed referring to Section 3.4 of Chapter 3 to obtain at least 2*n* operating points on each multi-constraint boundary which enclose FOR^{SOP}. Based on the operating points on each specific multi-constraint boundary, the fitting method to obtain its hyperplane expression is exploited.

The overall process for obtaining the mathematical expression of the multi-constraint boundaries of the FOR^{SOP} is summarised in Fig. 4.2. In this section, the method for obtaining operating points on the multi-constraint boundaries of FOR^{SOP} and the method for fitting the hyperplanes as shown in Fig. 4.2 are specified firstly, followed by the two stopping rules to ensure the required number of operating points on multi-constraint boundaries can be obtained.

- **Obtaining operating points on the multi-constraint boundaries of the FOR^{SOP}**

As shown in Fig. 4.2, the boundary points of the FOR^{SOP} can be obtained by the following three steps:

Step 1: Generate power-increasing directions ($\boldsymbol{d}^{(1)}$, $\boldsymbol{d}^{(2)}$, …, $\boldsymbol{d}^{(k)}$, …) from the origin of the power injection space $[\boldsymbol{P}; \boldsymbol{Q}] \in R^{2n}$ based on Marsaglia's algorithm. Here the origin of the power injection space is selected as $[\boldsymbol{0}; \boldsymbol{0}] \in R^{2n}$.

Step 2: Obtain boundary points of the FOR^{SOP} along the power-increasing directions. This step can be conducted by maximising the power increasement in each power-increasing direction until hitting the boundaries as modelled in (4-19), where $\gamma^{(k)}$ is a positive variable to extend $\boldsymbol{d}^{(k)}$. $\left[\boldsymbol{P}^{ext}; \boldsymbol{Q}^{ext}\right]^T$ denotes the extended power injection vector along the power-increasing direction $\boldsymbol{d}^{(k)}$.

$$\max \gamma^{(k)}$$
$$s.t.\begin{cases} \begin{bmatrix} \boldsymbol{P}^{ext} \\ \boldsymbol{Q}^{ext} \end{bmatrix} = \gamma^{(k)} \boldsymbol{d}^{(k)} \\ P_i = P_i^{ext} + \quad P_i^{SOP} \\ \qquad\qquad\qquad if\ SOP\ at\ node\ i \\ Q_i = Q_i^{ext} + \quad Q_i^{SOP} \\ \qquad\qquad\qquad if\ SOP\ at\ node\ i \\ \begin{bmatrix} \boldsymbol{P} \\ \boldsymbol{Q} \end{bmatrix} \in FOR^{DN} \\ \begin{bmatrix} \boldsymbol{P}^{SOP} \\ \boldsymbol{Q}^{SOP} \end{bmatrix} \in SOP^{OR} \end{cases} \tag{4-19}$$

Step 3: Match the boundary points with the corresponding multi-constraint boundaries of the FOR^{SOP}.

From Section 4.3.4, the points on the multi-constraint boundaries of the FOR^{SOP} violate multiple network constraints. By determining which inequality constraints for thermal/voltage boundaries of the FOR^{DN} in (4-19) are "active" at the optimal solution, a boundary point obtained from the optimisation model in (4-19) can be matched with the corresponding multi-constraint boundary of the FOR^{SOP}. Here "active" refers to the fact that the optimal solution causes the inequality to be an equality. For example, if $\sum_{k=1}^{n}\left(\alpha_k^{V_{i,M}} P_k + \beta_k^{V_{i,M}} Q_k\right) = 1$ (i.e., the voltage boundary determined by the upper limit to V_i is "active") and $\sum_{k=1}^{n}\left(\alpha_k^{V_{j,M}} P_k + \beta_k^{V_{j,M}} Q_k\right) = 1$ (i.e., the voltage boundary determined by the upper limit to V_j is "active") at the optimal solution, the obtained boundary point causes both V_i and V_j to reach their upper limit. This indicates that the obtained boundary point belongs to the multi-constraint boundary that is determined by the upper limits to V_i and V_j.

It is noteworthy that for fitting a hyperplane in *x*-dimensional space, at least *x* points on the hyperplane are required. Therefore, at least 2*n* boundary points, where 2*n* is the dimension of the FOR^{SOP}, are required to fit the hyperplane expression of each multi-constraint boundary.

- **Fitting the hyperplanes**

After obtaining N_b (> 2*n*) boundary points on one multi-constraint boundary as required in the flow chart in Fig. 4.2, its hyperplane expression can be obtained as the form of $\sum_{k=1}^{n}\left(\alpha_k^{multi}P_k+\beta_k^{multi}Q_k\right)=1$, where the coefficients can be obtained by solving the linear equations in (4-20) through the method like Gauss-Jordan elimination. The coefficient matrix of (4-20) is formulated by the N_b boundary points.

$$\begin{bmatrix} P_1(1) & \cdots & P_n(1) & Q_1(1) & \cdots & Q_n(1) \\ \vdots & \vdots & \vdots & \vdots & \vdots & \vdots \\ P_1(N_b) & \cdots & P_n(N_b) & Q_1(N_b) & \cdots & Q_n(N_b) \end{bmatrix} \begin{bmatrix} \alpha_1^{multi} \\ \vdots \\ \alpha_n^{multi} \\ \beta_1^{multi} \\ \vdots \\ \beta_n^{multi} \end{bmatrix} = I_{N_b\times 1} \qquad (4\text{-}20)$$

- **Stopping rules**

Two stopping rules as presented in Fig. 4.2 should be satisfied at the same time in the process. Stopping rule 1 requires that the number of the obtained boundary points (i.e., *k* in Fig. 4.2) is large enough and the standard deviation of the distances between the origin and the obtained boundary points is small enough such that a statistical stopping rule is satisfied. For the statistical stopping rule setting, the *z*-value $z_{\alpha/2}$ is suggested to be set at 1.96 in accordance with the confidence level of 95%; ε is the acceptable error of the mean of distances between the origin and the boundary points to the predefined confidence level and it is set as 10^{-5} p.u. Stopping rule 2 is used to

ensure at least 2*n* points on each boundary are obtained for the generation of the hyperplane in 2n-dimensional power injection space.

4.5. Case studies

In this section, firstly an SOP-connected 3-node distribution network is used to construct a three-dimensional FOR^{SOP} for the purposes of: 1) comparison of the FORs of the distribution networks with and without an SOP; 2) demonstration of the Minkowski Sum model for FOR^{SOP}; 3) demonstration of the analytical expressions of FOR^{SOP} boundaries. Secondly, the IEEE 33 node network is used to further validate the effectiveness of the proposed Minkowski-sum based method. The computation of the case study was performed in MATLAB R2019b on a PC with an Intel(R) Core(TM) i7-9700 CPU @ 3.00 GHz processor and 16 GB RAM. The linear and nonlinear optimisations are implemented by linprog and fmicon solvers respectively in MATLAB.

4.5.1. 3-node distribution network

The topology of the 3-node distribution network is exhibited in Fig. 4.3. The grid supply point (GSP) is chosen as the slack node with voltage assumed as 1.02 p.u. The allowable range of voltages at other nodes is 0.97 p.u.-1.03 p.u.

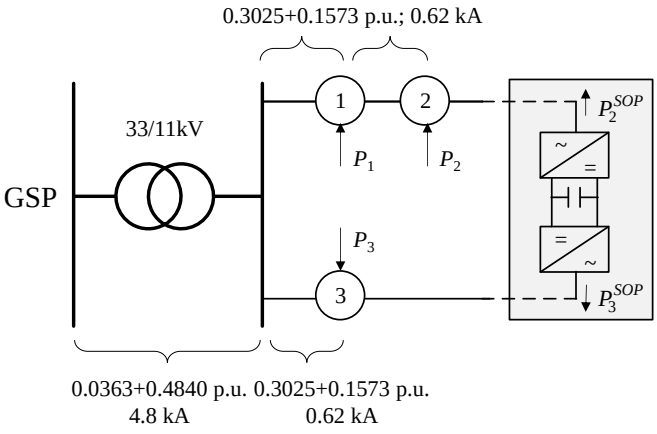

Fig. 4.3. A 3-node test distribution network with an SOP.

For simplicity, in the 3-node test network, unity power factors are assumed for the nodal power injections. The simplified model of the SOP with only active power control

is used to demonstrate the SOP performance on expanding the FOR of the network, considering both thermal and voltage constraints.

- **Comparison of the FOR of the distribution network with and without SOPs**

The FOR of the test network is three-dimensional associated with P_1-P_2-P_3. Simulation can be conducted by the method proposed in Section 3.4 to obtain FOR^{DN} and FOR^{SOP}. The results are compared in Fig. 4.4. It shows that the boundaries of FOR^{DN} are located inside the boundaries of FOR^{SOP}. This observation suggests that implementing an SOP can expand the boundaries of the FOR of the distribution network, resulting in an increased hosting capacity for the network.

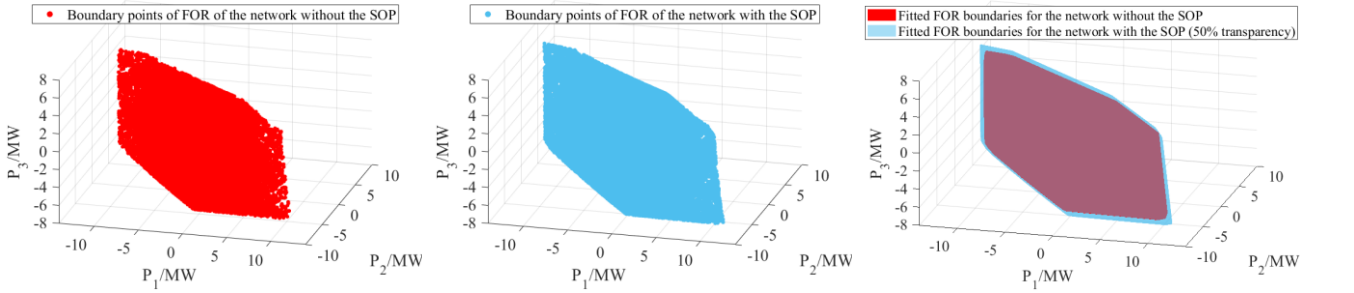

(a) Simulation results of FOR of the network without the SOP (b) Simulation results of FOR of the network with the SOP (c) Comparison of the simulation results of FORs with and without the SOP

Fig. 4.4. Simulation results of the FOR of the 3-node test distribution networks with and without SOP.

- **Demonstration of the Minkowski Sum model for FOR^{SOP}**

To better understand the relationship between FOR^{DN} and FOR^{SOP}, Fig. 4.5 presents some different examples of P_2-P_3 cross-sections of the FOR in Fig. 4.4. Here P_2-P_3 cross-sections are the P_2-P_3 subspaces of the FOR, where P_2 and P_3 are variable while P_1 is fixed. It can be concluded that for any of the P_2-P_3 cross-sections, the boundaries of FOR^{SOP} can be obtained by sweeping the boundaries of FOR^{DN} by the operating range of the SOP. In other words, FOR^{SOP} is the Minkowski Sum of FOR^{DN} and SOP^{OR}. It is noteworthy that the top-right and bottom-left corner of FOR^{DN} cannot be expanded by the SOP in Fig. 4.5. This results from the fact that the SOP can only exploit the available capacity of one feeder to transfer the active power to relieve the

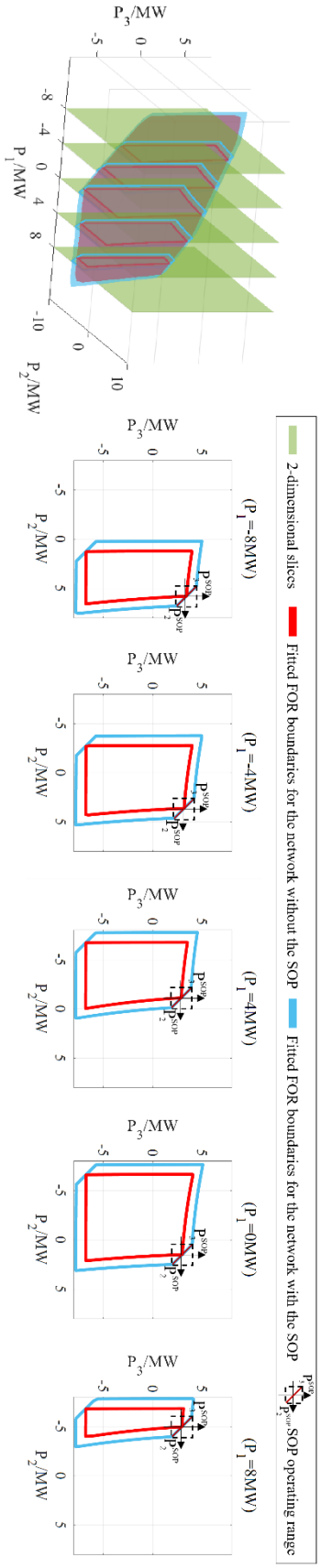

Fig. 4.5. Demonstration of different P_2-P_3 cross-sections of the boundaries of FOR^{DN} and FOR^{SOP}.

thermal/voltage problem at the other feeder. Therefore, when the operating points on both connected feeders by the SOP reach their thermal/voltage limitations (i.e., the operating point is at the top-right/bottom-left corner in Fig. 4.5), SOP cannot increase the nodal power injections in the network anymore and FOR of the network cannot be expanded.

- **Demonstration of the analytical expressions of FOR^{SOP} boundaries**

There are 4 single-constraint thermal boundaries, 3 single-constraint voltage boundaries and 7 multi-constraint boundaries that enclose the FOR^{SOP} of the network. Following the Minkowski Sum algorithm proposed in the paper, their analytical expressions are presented in Fig. 4.6.

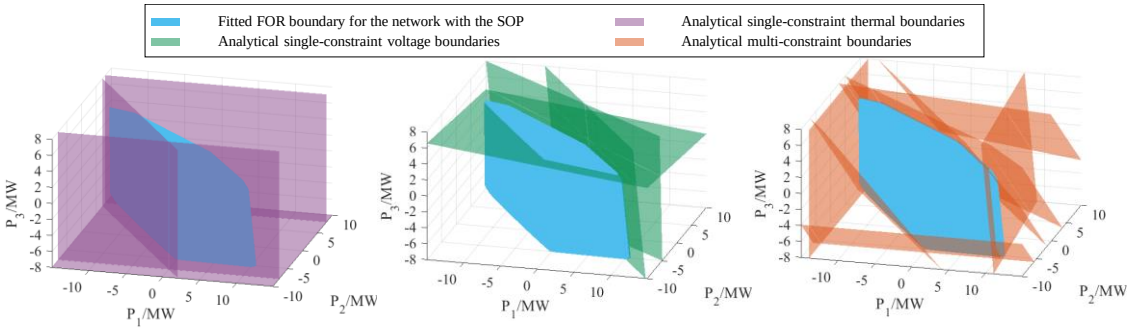

Fig. 4.6. Comparison of the analytical FOR^{SOP} boundaries with the real FOR^{SOP} boundaries in the 3-node test distribution network.

The key to obtaining the single-constraint thermal/voltage boundaries of FOR^{SOP} is the calculation of the translation vector associated to each thermal/voltage boundary of FOR^{DN} based on Minkowski-Sum algorithm in Section 4.4.2. Since the operating range of the SOP in this case is a line segment with only two vertices (i.e., (-1, 1) and (1, -1)), the translation vectors should be one of them. Take the single-constraint voltage boundary for node 2 for an example. Without the SOP, the boundary can be approximated as $0.332P_1 + 0.629P_2 + 0.036P_3 \leq 1$ using the hyperplane expression in (4-2). After the implementation of SOP, the voltage boundary is expanded through translation by (1, -1) on P_2-P_3 cross-sections. Therefore, the analytical expression of the

single-constraint voltage boundary of FOR^{SOP} should be $0.332P_1 + 0.629P_2 + 0.036P_3 \leq 1.593$ (see (4-18) for reference).

Each multi-constraint boundary of FOR^{SOP} is fitted by at least three operating points (consistent with the dimension number) on the boundary in this test network. The multi-constraint boundaries are different from the boundaries of FOR^{DN} in the way that the operating points on the multi-constraint boundaries violate at least two thermal/voltage constraints.

The results of the boundary errors for analytical FOR^{SOP} boundaries are shown in Fig. 4.7, where the percentage boundary error is calculated as the Euclidean distance between the sets of points on the real FOR^{SOP} boundaries and the analytical FOR^{SOP} boundaries, divided by the average Euclidean distance between the origin and the real FOR^{SOP} boundaries. From Fig. 4.7, the maximum boundary error is 14%, primarily resulting from the inaccuracies of the analytical FOR^{DN} boundaries.

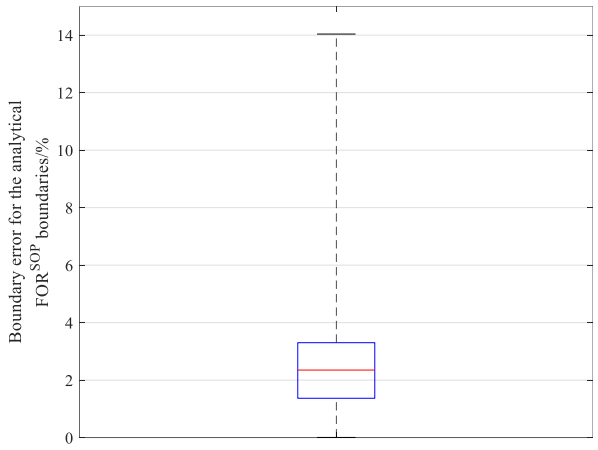

Fig. 4.7. Boundary errors for the analytical FOR^{SOP} boundaries in the 3-node distribution network.

Power flow calculation is run to further analyse the corresponding line currents (or node voltages) on each obtained analytical single-constraint thermal (or voltage) boundary. The results are presented in Fig. 4.8. The analysis for multi-constraint analytical boundaries is very similar and the results are presented in Fig. 4.9.

Comparing to the theoretical 100% of the line currents and 1.03p.u. of the node voltages, it can be concluded from Fig. 4.8 and Fig. 4.9 that the errors of the line currents and the node voltages on the analytical FOR^{SOP} boundaries are less than 5% and 0.002p.u. respectively.

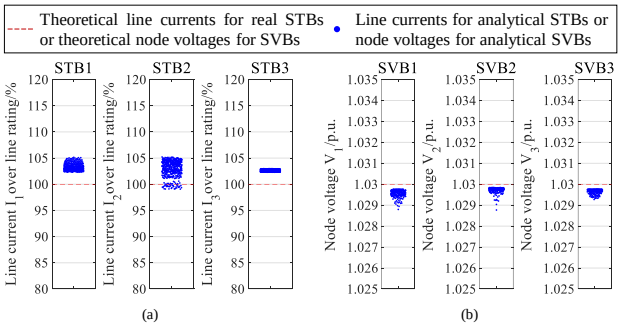

Fig. 4.8. Beeswarm plots of (a) line currents on analytical STBs and (b) node voltages on analytical SVBs. (STB: single-constraint thermal boundary; SVB: single-constraint voltage boundary)

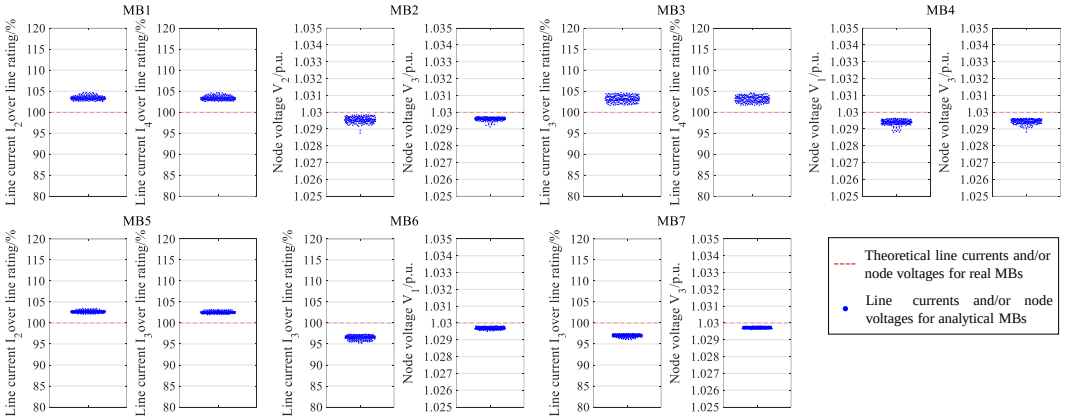

Fig. 4.9. Beeswarm plots of line currents and/or node voltages for analytical MBs. (MB: multi-constraint boundary. MB1/MB2/MB3 are determined by two thermal constraints; MB4/MB5 are determined by two voltage constraints; MB6/MB7 are determined by one thermal constraint and one voltage constraint).

4.5.2. IEEE 33-node distribution network

To validate the effectiveness of the Minkowski-Sum based algorithm to generate the analytical expressions of FOR^{SOP} boundaries, the IEEE 33-node benchmark distribution network [198] is used. In this case, both active and reactive power

injections at nodes 2-33 are considered. An SOP (rated at 1 MVA) is assumed to be installed at the tie-line B, controlling both active and reactive power injections at nodes 18 and node 33. The FOR^{SOP} of the 33-node distribution network considering both thermal and voltage constraints will be formulated based on the methodology proposed in the paper.

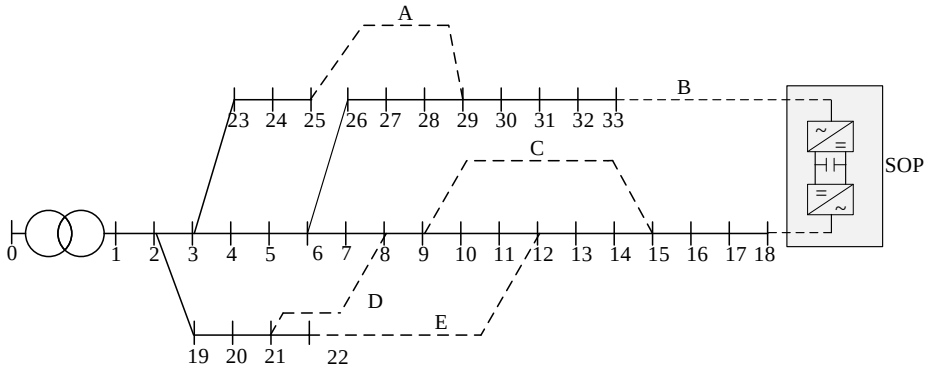

Fig. 4.10. Modified IEEE 33-node distribution network with an SOP.

- **Results of the analytical FOR^{SOP} boundaries**

To obtain the analytical expressions of FOR^{SOP} boundaries, the quadratic thermal boundaries of FOR^{DN} and quadratic constraints of SOP^{OR} are linearised as a regular polygon (as shown in (4-15) and (4-16)) with 12 edges. The results are summarised in Table 4.1.

Table 4.1. Summary of the boundaries of FOR^{SOP}

Boundaries of FOR^{SOP}		Number
Single-constraint thermal boundaries		32×12=384
Single-constraint voltage boundaries	Upper boundaries	32
	Lower boundaries	32
Multi-constraint boundaries		1252

The number of the single-constraint thermal boundaries are 32×12=384, where 32 is the number of lines in the network and 12 is the number of edges in the linearisation.

The number of the single-constraint voltage boundaries is consistent with the number of nodes (excluding the slack node) in the network. Note that the number of multi-constraint boundaries may slightly vary due to the precision of the statistical stopping rule setting in the fitting flow chart, as outlined in Section 4.4.3.

- **Error analysis**

The results of the analytical FOR^{SOP} boundaries in IEEE 33-node distribution network are shown in Fig. 4.11. From Fig. 4.11 (a), the mean boundary error is 13%, while the maximum boundary error is 30%. By analysing the line currents and node voltages of the boundary points on analytical FOR^{SOP} boundaries, the statistical results in Fig. 4.11 (b)(c) can be obtained. The results show that the obtained analytical expressions are conservative since the line currents/node voltages do not reach or exceed their limits. This mainly results from the polygonal inner approximation of quadratic boundaries of FOR^{DN} and SOP^{OR} in (4-15) and (4-16).

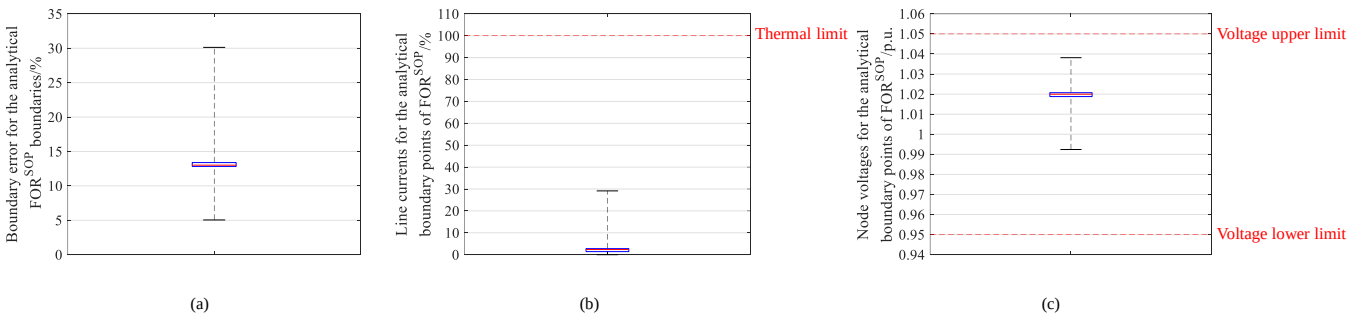

Fig. 4.11. (a) Boundary errors (b) line currents (c) node voltages for analytical FOR^{SOP} boundaries in the IEEE 33-node distribution network.

In general, the boundary errors (and the resulting errors of line currents/node voltages) come from the errors of the analytical expressions of FOR^{DN} and the linearisation of the quadratic boundaries of FOR^{DN} and SOP^{OR} in (4-15) and (4-16).

4.6. Summary

This chapter investigates the impact of SOPs on FOR of an electricity distribution network. The relationship between the FORs of a distribution network with and without

SOPs is obtained through a strict mathematical proof. From a mathematical perspective, the FOR^{SOP} can be interpreted as the Minkowski Sum of the FOR^{DN} and the SOP^{OR}.

Depending on whether the operating points on the FOR^{SOP} boundaries reach single or multiple limits of line currents/node voltages, the boundaries of FOR^{SOP} are classified into single-constraint thermal/voltage boundaries and multi-constraint boundaries. To solve the analytical expressions of these boundaries, a practical Minkowski Sum-based algorithm is developed. Specifically, the analytical expressions of the single-constraint boundaries can be obtained by translating from the thermal/voltage boundaries of FOR^{DN} directly, while the multi-constraint boundaries can be determined by obtaining boundary points and fitting them.

A three-dimensional FOR^{SOP} is constructed using an SOP-connected 3-node distribution network. The results show that the FOR of the distribution network can be expanded by SOPs satisfying the Minkowski Sum model. Following the solution algorithm, the mean and maximum errors of the obtained analytical expressions of FOR^{SOP} boundaries are 3% and 14% respectively, causing maximal 5% and 0.002p.u. errors in line currents and node voltages on the analytical FOR^{SOP} boundaries respectively.

The effectiveness of the proposed Minkowski-sum based method is further validated using a modified IEEE 33 node network with SOPs. Compared to the 3-node case network, the mean and maximum boundary error increase to 13% and 30% respectively. The proposed analytical FOR^{SOP} boundaries are conservative through the results of the errors of the line currents and the node voltages, which results from the linearisation of quadratic boundaries of FOR^{DN} and SOP^{OR}.

Chapter 5. Constraint management of distribution networks with SOPs

5.1. Introduction

SOPs can improve the distribution of the power flows and the voltage profile across the networks through flexible power transfer and independent reactive power compensation. These features facilitate SOPs to be a good choice for constraint management of distribution networks.

In this chapter, a novel SOP control method is developed for network constraint management, leveraging the FOR methodology. Specifically, the FOR constraints are exploited in the formulation of the optimal SOP control. Due to the one-to-one correspondence between FOR boundaries and the network constraints, the FOR constraints of the components equipped with real-time measurements are simply needed to be included into the constraints of the optimisation model. This ensures that the FOR-based constraint management method is scalable, adapting to various measurement conditions. Additionally, the method can rapidly generate SOP set points, with the cost of time being solely dependent on the number of SOP terminals and measurement units, rather than the scale of the distribution network.

The proposed method was demonstrated and validated using a three-node distribution network. The performance of the FOR-based method was also compared with that of local control and OPF-based control using the IEEE 33-node distribution network.

5.2. Expressions of feasible operation regions

By integrating the thermal boundaries as given in (4-1) with the voltage boundaries presented in (4-2)-(4-3), the FOR of a distribution network within the power injection space can be expressed as follows:

$$FOR := \left\{ \begin{bmatrix} \boldsymbol{P} \\ \boldsymbol{Q} \end{bmatrix} \in R^{2n} \left| \begin{array}{l} \left(\sum_{k=1}^{n} \alpha_k^{I_{ij}} P_k \right)^2 + \left(\sum_{k=1}^{n} \beta_k^{I_{ij}} Q_k \right)^2 \le \left(V_0 I_{ij}^M \right)^2, \forall ij \in B \\ \sum_{k=1}^{n} \left(\alpha_k^{V_{i,M}} P_k + \beta_k^{V_{i,M}} Q_k \right) \le 1, \forall i \in N \\ \sum_{k=1}^{n} \left(\alpha_k^{V_{i,m}} P_k + \beta_k^{V_{i,m}} Q_k \right) \le 1, \forall i \in N \end{array} \right. \right\} \quad (5\text{-}1)$$

5.3. Mathematic formulation of FOR-based constraint management using SOPs

In this section, an optimisation model for constraint management of a distribution network with SOPs is established. Compared to the conventional OPF-based model, constraints represented by FOR boundaries, instead of power flow equations and network constraints, are considered in the model. Due to one-to-one correspondence between FOR boundaries and thermal/voltage constraints, the formulated optimisation model can adapt to various measurement conditions. Before introducing the developed model, the requirements of constraint management using SOPs are presented first.

5.3.1. Requirements of constraint management using SOPs

In medium-voltage distribution networks, the real-time measurements encompass line currents/line flows and node voltages [81]. However, the power flows through each secondary substation (represented as the nodes in the distribution network) are generally not available in real-time. Given the significant expenses associated with measurement and communication units, the available measurements under current conditions are limited. These measurements are predominantly situated at the high-voltage/medium-voltage (HV/MV) substation, such as the MV bus and feeder outlets. Furthermore, key line segments are also furnished with real-time measurement and communication equipment to guarantee the uninterrupted operation of the distribution network.

Within the context of constraint management using SOPs, the limited online measurement data is forwarded to the SOPs' control system. Utilising these measurements, reference values (i.e., the change to the SOP set point) are determined by the SOP control algorithm (e.g., an optimisation algorithm) and sent as a control signal to the SOP controllers. In response, the SOP converters make adjustments to the power set points, leading to improved performance of the distribution network.

For effective constraint management using SOPs, three critical requirements must be considered:

1) SOP control should be effective with real-time (yet limited) measurements of line currents/line flows and node voltages.

2) The control algorithm is designed for managing constraints within the distribution network. Upon detecting violations, such as thermal overloading in power lines or overvoltage/undervoltage issues at busbars via network state measurements, the algorithm should efficiently address and rectify these issues using SOPs.

3) The SOP control should adapt to real-time measurement. Specifically, the cumulative time cost, including the communication delay, the generation of SOP set points, and the hardware control of the SOP, should not exceed a measurement interval. With the advancements in communication technologies, such as the adoption of micro phaser measurement units, and the capability of SOPs to adjust their power output within milliseconds, the primary emphasis should be on developing an efficient model and algorithm for generating SOP set points rapidly.

To meet the above three requirements, an effective optimisation model is established in the following subsections of this section, while an algorithm to expedite the solution of the model is developed in Section 5.4

5.3.2. Constraints

- **SOP constraints**

In a general case, *m* (*m*≥2) feeders of the distribution network can be connected by an SOP with *m* converters, which share the same DC bus. While active power can be transferred among the interconnected feeders, the reactive power can be either provided or absorbed at the various SOP terminals independently.

Assuming the positive direction of the active power of each SOP terminal is from the SOP terminal towards the connected node of the distribution network, the active powers controlled by SOP should follow the constraint as below:

$$\sum_{k\in\Omega_{SOP}} \left(P_{k,t}^{SOP} + \Delta P_{k,t+\Delta t}^{SOP}\right) = 0 \tag{5-2}$$

where $P_{k,t}^{SOP}$ is the active power output from the SOP at node *k* at time *t*. Ω_{SOP} denotes the set of nodes connected by the SOP. $\Delta P_{k,t+\Delta t}^{SOP}$ is the adjustment in the active power set point of the SOP after a total elapsed time Δt since time *t*. The shorter the time cost, the more prompt the SOP control will be. It should be noted that with the use of the modular multi-level converter technology, the operating loss of a converter is relatively low, approximately 1% per converter [25]. Therefore, for simplicity, the SOP losses are neglected.

Though the reactive power set points for different SOP terminals are independent, they, together with the active power set points, are constrained by the converter capacity:

$$\left(P_{k,t}^{SOP} + \Delta P_{k,t+\Delta t}^{SOP}\right)^2 + \left(Q_{k,t}^{SOP} + \Delta Q_{k,t+\Delta t}^{SOP}\right)^2 \le S^{SOP}, \forall k \in \Omega_{SOP} \tag{5-3}$$

where $Q_{k,t}^{SOP}$ is the reactive power output from the SOP at node *k* at time *t*. $\Delta Q_{k,t+\Delta t}^{SOP}$ is the adjustment in the reactive power set point of the SOP after a total elapsed time Δt since time *t*. S^{SOP} is the capacity of the converters.

- **FOR constraints**

From the previous study [42], each FOR boundary is determined by one thermal/voltage constraint of the distribution network. The one-to-one correspondence between FOR boundaries and thermal/voltage constraints allows the use of FOR to establish the operational constraints under incomplete measurements of line flows/node voltages. For instance, when concerned with the line flow on a specific line segment, it is sufficient to incorporate the constraint of the thermal boundary, which is determined by the thermal constraint of the line flow, into the constraints of the optimisation model. This feature makes the constraints of FOR boundaries more advantageous than the conventional OPF constraints which necessitate global measurements or predictions of all the power generation and load.

However, prior studies depict FOR boundaries as equations of nodal power injections, which are not directly applicable since the measurements taken are line flows and node voltages. This subsection transforms the FOR boundaries into a format based on line flows and node voltages.

1) Thermal constraints

With respect to the thermal boundary of any line segment ij, (5-4) can be obtained.

$$\left(P_{ij,t}-\underbrace{\Delta P_{k,t+\Delta t}^{SOP}}_{\text{if } k\in\Omega_{SOP}\cap D_j}\right)^2+\left(Q_{ij,t}-\underbrace{\Delta Q_{k,t+\Delta t}^{SOP}}_{\text{f } k\in\Omega_{SOP}\cap D_j}\right)^2=\left(V_0 I_{ij}^M\right)^2 \tag{5-4}$$

which directly employs the measured active power flow $P_{ij,t}$ and reactive power flow $Q_{ij,t}$ on line ij, subtracting the downstream power injection from the SOP to indicate the line flows. D_j denotes the set of the downstream nodes of node j (including node j for conciseness). It is noteworthy that in (5-4) node i is the sending node of line ij which is closer to the HV/MV substation than the receiving node j. The power losses of the SOP power injections through the network are very small compared to $P_{ij,t}$ and

$Q_{ij,t}$, which are ignored in (5-4). Additionally, a threshold for the line capacity I_{ij}^{M} can be defined in the FOR constraints afterwards to avoid its impact on the performance of SOP control.

Assuming Ω_B as the lines equipped with measurement units, the constraints of thermal boundaries of FOR regarding these lines then can be expressed as:

$$\begin{aligned}&\left(P_{ij,t}-\underbrace{\Delta P_{k,t+\Delta t}^{SOP}}_{\text{if } k\in\Omega_{SOP}\cap D_j}\right)^2+\left(Q_{ij,t}-\underbrace{\Delta Q_{k,t+\Delta t}^{SOP}}_{\text{if } k\in\Omega_{SOP}\cap D_j}\right)^2\\&\le\left(V_0 I_{ij}^{M}\right)^2,\quad \forall ij\in\Omega_B\end{aligned} \tag{5-5}$$

2) Voltage constraints

Based on the voltage boundaries of FOR in (4-2)-(4-4), the constraints for each node voltage can be obtained as follows:

$$V_i^m \le V_i = V_0+\frac{1}{V_0}\sum_{k=1}^{n}\left(r_k^i P_k + x_k^i Q_k\right)\le V_i^M, \forall i\in\Omega_N \tag{5-6}$$

where Ω_N are the nodes equipped with measurement units. The resistance r_k^i and the reactance x_k^i, which are coefficient of nodal power injections P_k and Q_k at node k, can be obtained from (4-4). The change of P_k and Q_k ($k\in\Omega_{SOP}$) due to the adjustment of SOP power injections will result in the change of V_i at time $t+\Delta t$ as below:

$$\Delta V_{i,t+\Delta t}=\frac{1}{V_0}\sum_{k\in\Omega_{SOP}}\left(r_k^i\Delta P_{k,t+\Delta t}^{SOP}+x_k^i\Delta Q_{k,t+\Delta t}^{SOP}\right) \tag{5-7}$$

Considering Δt is short, $V_{i,t+\Delta t}$ (i.e., V_i at time $t+\Delta t$ under the SOP control) can be:

$$V_{i,t+\Delta t}=V_{i,t}+\Delta V_{i,t+\Delta t} \tag{5-8}$$

$V_{i,t+\Delta t}$ should satisfy the voltage constraints as:

$$V_i^m \le V_{i,t+\Delta t}\le V_i^M, \forall i\in\Omega_N \tag{5-9}$$

Through (5-7)-(5-9), following constraint can be obtained:

$$\begin{aligned} V_i^m &\le V_{i,t} + \frac{1}{V_0} \sum_{k \in \Omega_{SOP}} \left(r_k^i \Delta P_{k,t+\Delta t}^{SOP} + x_k^i \Delta Q_{k,t+\Delta t}^{SOP} \right) \\ &\le V_i^M, \forall i \in \Omega_N \end{aligned} \tag{5-10}$$

From the foregoing deduction, the FOR constraints associated with nodal power injections can be transformed into new expressions based on measurements of line flows and node voltages and the adjustments of SOP power set points as shown in (5-5) and (5-10).

5.3.3. Objective functions

For optimal constraint management of the distribution network, three objectives, including the feeder load balancing, voltage profile improvement, and power losses reduction are used for real-time control of SOP. It should be noted that the objective functions are transformed from those in the existing studies into the form associated with the active/reactive power adjustments of SOPs.

- **Feeder load balancing**

The goal for feeder load balancing is to balance the line flows on different lines of the distribution network. With the measurement of the line flows and the power adjustments of SOPs, the FLB index can be expressed as:

$$FLB = \sum_{ij \in \Omega_B} \frac{\left(P_{ij,t} - \underbrace{\Delta P_{k,t+\Delta t}^{SOP}}_{\text{if } k \in \Omega_{SOP} \cap D_j} \right)^2 + \left(Q_{ij,t} - \underbrace{\Delta Q_{k,t+\Delta t}^{SOP}}_{\text{if } k \in \Omega_{SOP} \cap D_j} \right)^2}{S_{ij,rate}^2} \tag{5-11}$$

where $S_{ij,rate}$ is the rated capacity of the line ij.

- **Voltage profile improvement**

Voltage profile index (VP_{index}) is commonly used to measure the voltage improvement of a distribution network. The index reflects the degree of dispersion of

all concerned node voltages (that are monitored by measurement units) from the nominal values, which is described as:

$$VP_{index} = \sum_{i \in \Omega_N} \left(V_{i,t+\Delta t} - V_{i,ref} \right)^2 \tag{5-12}$$

$V_{i,ref}$ is the nominal voltage magnitude at bus *i*, which is set as 1.0 p.u. in this chapter. $V_{i,t+\Delta t}$ is expressed as in (5-7) and (5-8).

- **Power losses reduction**

Power losses index (PLI), as shown in (5-13), is used as an objective function in the optimisation model to reduce the power losses of the distribution network.

$$PLI = \sum_{ij \in \Omega_B} R_{ij} \frac{\left(P_{ij,t} - \underbrace{\Delta P^{SOP}_{k,t+\Delta t}}_{\text{if } k \in \Omega_{SOP} \cap D_j} \right)^2 + \left(Q_{ij,t} - \underbrace{\Delta Q^{SOP}_{k,t+\Delta t}}_{\text{if } k \in \Omega_{SOP} \cap D_j} \right)^2}{V_0^2} \tag{5-13}$$

R_{ij} is the resistance of line *ij*. V_0 is used for approximating the node voltages at node *i* for calculating the losses of line *ij*.

5.3.4. Optimisation Model

The decision variables of the optimisation problem are $\Delta P^{SOP}_{k,t+\Delta t}$ and $\Delta Q^{SOP}_{k,t+\Delta t}$ ($\forall k \in \Omega_{SOP}$). The full optimisation model for the real-time control of SOPs is shown below:

minimise (5-11) or (5-12) or (5-13)

subject to (5-2), (5-3), (5-5), (5-10)

The model solves the power adjustments of SOPs at time *t* with a time delay Δt. The model demonstrates scalability as the corresponding thermal/voltage constraint can be appended for each concerned line/node with a measurement. Consequently, the optimisation model can be implemented regardless of the number of measurement units

installed in the distribution network, especially applicable to current situation with incomplete measurement.

Due to the quadratic objective functions in (5-11)-(5-13) and quadratic constraints in (5-3) and (5-5), it is a nonlinear optimisation model. In the next section, the nonlinear optimisation model will be converted to a quadratic programming model, which can be effective in real-time constraint management of the distribution network with SOPs.

5.4. Quadratic programming conversion

In this section, auxiliary state variables for the SOP set points, line flows, and node voltages are introduced firstly. Subsequently, the quadratic constraints within the model are linearised to facilitate its transition to a quadratic programming framework. As a result, the optimisation model is formulated in matrix form, where the matrices and coefficient vectors irrelevant to the measurements are segregated. Because these segregated matrices and coefficient vectors can be prepared offline, the computation time of the optimisation problem can be further reduced.

5.4.1. Introduction of state variables

Before the conversion, auxiliary state variables of SOP set points, line flows and node voltages are firstly introduced to simplify the expressions of the model in Section 5.3.4.

Regarding the SOP set points, the state variables of SOP set points at time $t+\Delta t$ are defined as below:

$$P_{k,t+\Delta t}^{SOP} = P_{k,t}^{SOP} + \Delta P_{k,t+\Delta t}^{SOP} \tag{5-14}$$

$$Q_{k,t+\Delta t}^{SOP} = Q_{k,t}^{SOP} + \Delta Q_{k,t+\Delta t}^{SOP} \tag{5-15}$$

The state variables of line flows are introduced in (5-16)-(5-17). The variables express the approximate line flows on each measured line at time $t+\Delta t$.

$$P_{ij,t+\Delta t} = P_{ij,t} - \underbrace{\Delta P_{k,t+\Delta t}^{SOP}}_{\text{if } k\in\Omega_{SOP}\cap D_j} \tag{5-16}$$

$$Q_{ij,t+\Delta t} = Q_{ij,t} - \underbrace{\Delta Q_{k,t+\Delta t}^{SOP}}_{\text{if } k\in\Omega_{SOP}\cap D_j} \tag{5-17}$$

With respect to node voltages, the voltage variable $V_{i,t+\Delta t}$ is obtained by substituting (5-7) in (5-8) as below:

$$V_{i,t+\Delta t} = V_{i,t} + \frac{1}{V_0}\sum_{k\in\Omega_{SOP}}\left(r_k^i \Delta P_{k,t+\Delta t}^{SOP} + x_k^i \Delta Q_{k,t+\Delta t}^{SOP}\right) \tag{5-18}$$

With the introduction of state variables, both the objective functions and the constraints in the model of Section 5.3.4 can be simplified, facilitating their conversion into the standard matrix form of the quadratic programming model.

5.4.2. Linearisation of the quadratic constraints

A polygonal inner-approximation method is employed to linearise the capacity constraints for SOP in (5-3) and the thermal constraints in (5-5) since they are both in circular form. In this chapter, a regular polygon with 12 edges is used for the linearisation. After substituting (5-14)-(5-15) into (5-3) and (5-16)-(5-17) into (5-5), (5-3) and (5-5) can be linearised via polygonal inner-approximation as follows:

$$\alpha_c P_{k,t+\Delta t}^{SOP} + \beta_c Q_{k,t+\Delta t}^{SOP} + \delta_c S^{SOP} \le 0,\ \forall c \in \{1,2,...,12\} \tag{5-19}$$

$$\alpha_c P_{ij,t+\Delta t} + \beta_c Q_{ij,t+\Delta t} + \delta_c \left(V_0 I_{ij}^M\right) \le 0,\ \forall c \in \{1,2,...,12\} \tag{5-20}$$

where the values of the coefficients can refer to [32] and are no longer repeated in this chapter.

Since the linearisation through the polygonal inner-approximation method is conservative, the operating state of the distribution network that satisfies (5-19) and (5-20) will not violate the capacity constraints for SOP in (5-3) and the thermal constraints in (5-5).

5.4.3. Formulation of the quadratic programming model

Through the above conversion, the three objective functions (5-11)-(5-13) of the optimisation model can be simplified as:

$$FLB = \sum_{ij \in \Omega_B} \frac{\left(P_{ij,t+\Delta t}\right)^2 + \left(Q_{ij,t+\Delta t}\right)^2}{S_{ij,rate}^2} \tag{5-21}$$

$$VPI = \sum_{i \in \Omega_N} \left(V_{i,t+\Delta t} - V_{i,ref}\right)^2 \tag{5-22}$$

$$PLI = \sum_{ij \in \Omega_B} R_{ij} \frac{\left(P_{ij,t+\Delta t}\right)^2 + \left(Q_{ij,t+\Delta t}\right)^2}{V_0^2} \tag{5-23}$$

The optimisation model is then formulated as follows:

$$\min \text{ (5-21) or (5-22) or (5-23)}$$

$$s.t. \begin{cases} \sum_{k \in \Omega_{SOP}} P_{k,t+\Delta t}^{SOP} = 0 \\ \alpha_c P_{k,t+\Delta t}^{SOP} + \beta_c Q_{k,t+\Delta t}^{SOP} + \delta_c S^{SOP} \le 0, \ \forall c \in \{1,2,...,12\} \\ \alpha_c P_{ij,t+\Delta t} + \beta_c Q_{ij,t+\Delta t} + \delta_c \left(V_0 I_{ij}^M\right) \le 0, \ \forall c \in \{1,2,...,12\} \\ V_i^m \le V_{i,t+\Delta t} \le V_i^M, \forall i \in \Omega_N \\ P_{k,t+\Delta t}^{SOP} = P_{k,t}^{SOP} + \Delta P_{k,t+\Delta t}^{SOP}, \ \forall k \in \Omega_{SOP} \\ Q_{k,t+\Delta t}^{SOP} = Q_{k,t}^{SOP} + \Delta Q_{k,t+\Delta t}^{SOP}, \ \forall k \in \Omega_{SOP} \\ P_{ij,t+\Delta t} = P_{ij,t} - \underbrace{\Delta P_{k,t+\Delta t}^{SOP}}_{\text{if } k \in \Omega_{SOP} \cap D_j}, \ \forall ij \in \Omega_B \\ Q_{ij,t+\Delta t} = Q_{ij,t} - \underbrace{\Delta Q_{k,t+\Delta t}^{SOP}}_{\text{if } k \in \Omega_{SOP} \cap D_j}, \ \forall ij \in \Omega_B \\ V_{i,t+\Delta t} = V_{i,t} + \frac{1}{V_0} \sum_{k \in \Omega_{SOP}} \left(r_k^i \Delta P_{k,t+\Delta t}^{SOP} + x_k^i \Delta Q_{k,t+\Delta t}^{SOP}\right), \forall i \in \Omega_N \end{cases} \tag{5-24}$$

The variables of the model in (5-24) include the decision variables $\Delta P_{k,t+\Delta t}^{SOP}$ and $\Delta Q_{k,t+\Delta t}^{SOP}$ and the state variables $P_{k,t+\Delta t}^{SOP}$, $Q_{k,t+\Delta t}^{SOP}$, $P_{ij,t+\Delta t}$, $Q_{ij,t+\Delta t}$, and $V_{i,t+\Delta t}$. Defining the vector of the decision variables as $\boldsymbol{X_1}$ and the vector of the state variables as $\boldsymbol{X_2}$, the compact form of the model (5-24) is shown below:

$$\min \frac{1}{2} \boldsymbol{X}_2^T \boldsymbol{H} \boldsymbol{X}_2 + \boldsymbol{f}^T \boldsymbol{X}_2 + c$$
$$\text{s.t.} \begin{cases} \boldsymbol{A}_{eq} \boldsymbol{X}_2 = \boldsymbol{b}_{eq} \\ \boldsymbol{A} \boldsymbol{X}_2 \le \boldsymbol{b} \\ \boldsymbol{l}_b \le \boldsymbol{X}_2 \le \boldsymbol{u}_b \\ \boldsymbol{X}_2 = \boldsymbol{D} \boldsymbol{X}_1 + \boldsymbol{e}_t \end{cases} \tag{5-25}$$

(5-25) includes the linear equality from the first constraint of (5-24), the linear inequality from the second and third constraints of (5-24), the lower and upper bounds from the fourth constraint of (5-24) and the linear relationship between $\boldsymbol{X_1}$ and $\boldsymbol{X_2}$, which is shown in the last five constraints of (5-24). Here $\boldsymbol{e_t}$ is the vector of state variables (i.e., $\boldsymbol{e_t} = (P_{k,t+\Delta t}^{SOP}, Q_{k,t+\Delta t}^{SOP}, P_{ij,t+\Delta t}, Q_{ij,t+\Delta t}, V_{i,t+\Delta t})^T$). By substituting $\boldsymbol{X_2}=\boldsymbol{DX_1}+\boldsymbol{e_t}$ in the model, the quadratic programming model can be finally obtained as in (5-26).

$$\min \frac{1}{2} \boldsymbol{X}_1^T \tilde{\boldsymbol{H}} \boldsymbol{X}_1 + \tilde{\boldsymbol{f}}_t^T \boldsymbol{X}_1 + \tilde{c}_t$$
$$\text{s.t.} \begin{cases} \left(\boldsymbol{A}_{eq} \boldsymbol{D}\right) \boldsymbol{X}_1 = \boldsymbol{b}_{eq} - \boldsymbol{A}_{eq} \boldsymbol{e}_t \\ \left(\boldsymbol{A} \boldsymbol{D}\right) \boldsymbol{X}_1 \le \boldsymbol{b} - \boldsymbol{A} \boldsymbol{e}_t \\ \boldsymbol{D}^{-1}\left(\boldsymbol{l}_b - \boldsymbol{e}_t\right) \le \boldsymbol{X}_1 \le \boldsymbol{D}^{-1}\left(\boldsymbol{u}_b - \boldsymbol{e}_t\right) \end{cases} \tag{5-26}$$

$\tilde{\boldsymbol{H}}$ and $\tilde{\boldsymbol{f}}_t$ can be obtained as follows:

$$\tilde{\boldsymbol{H}} = \boldsymbol{D}^T \boldsymbol{H} \boldsymbol{D} \tag{5-27}$$

$$\tilde{\boldsymbol{f}}_t = \boldsymbol{D}^T \boldsymbol{H}^T \boldsymbol{e}_t + \boldsymbol{D}^T \boldsymbol{f} \tag{5-28}$$

In (5-26), $\tilde{\boldsymbol{f}}_t$, $\tilde{c}_t$ and $\boldsymbol{e_t}$ are associated with the measurements at time *t*. $\tilde{c}_t$ is a constant and can be removed from the objective function. $\tilde{\boldsymbol{f}}_t$ and $\boldsymbol{e_t}$ should be updated during each measurement interval as the input of the optimal control. In contrast, $\tilde{\boldsymbol{H}}$, $\boldsymbol{A_{eq}}$, $\boldsymbol{b_{eq}}$, $\boldsymbol{A}$, $\boldsymbol{b}$, $\boldsymbol{l_b}$, $\boldsymbol{u_b}$ and $\boldsymbol{D}$ are irrelevant to the measurements at time *t* and can be prepared offline.

Compared with (5-25), the number of variables and the number of constraints in (5-26) are largely reduced. In general, there are only 2*m* (*m* is the number of SOP terminals) variables of $\Delta P_{k,t+\Delta t}^{SOP}$ and $\Delta Q_{k,t+\Delta t}^{SOP}$, while the number of constraints are determined by the number of SOP terminals and the number of lines and nodes that are equipped with measurement units. This indicates that the proposed model is almost not affected by the scale of the distribution network. The complexity of solving the model is only determined by the number of SOP terminals and the number of the measurement units.

5.5. Case studies

In this section, first an SOP-connected 3-node distribution network is used to initially demonstrate and validate the proposed FOR-based real-time SOP control for the constraint management of the case network. The IEEE 33-node benchmark distribution network is further used to compare the developed FOR-based method with local control and OPF-based control. The impact of the measurement conditions on the performance of the FOR-based control is also analysed. The computation of the case study was performed in MATLAB R2019b on a PC with an Intel(R) Core(TM) i5-9300H CPU @ 2.40 GHz processor and 8 GB RAM. The quadratic programming is implemented by the Quadprog solver in MATLAB.

5.5.1. Three-node distribution network

Fig. 4.3 shows a 33/11-kV three-node test distribution network. The impedances and thermal capacities of the transformer and the two feeders, and the capacities of the PV unit and SOP are given in Fig. 4.3. The grid supply point (GSP) is chosen as the slack bus with voltage assumed as 1.02 p.u.. The top feeder is heavily loaded (with twice the peak load of the bottom feeder), while the bottom feeder is allocated with

large PV generation. The load profile (per unit of the peak load) and the PV generation profile (per unit of the nominal capacity) are given in Fig. 5.2.

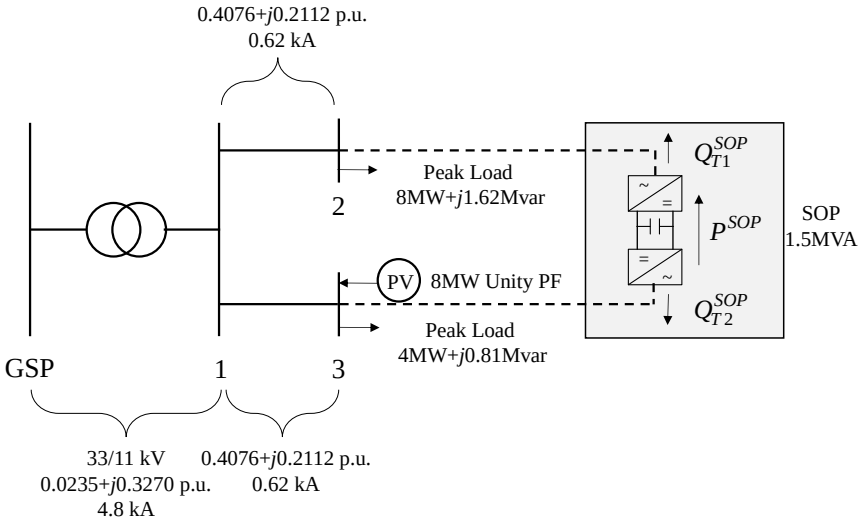

Fig. 5.1. A 3-node test distribution network with a SOP (100-MVA base).

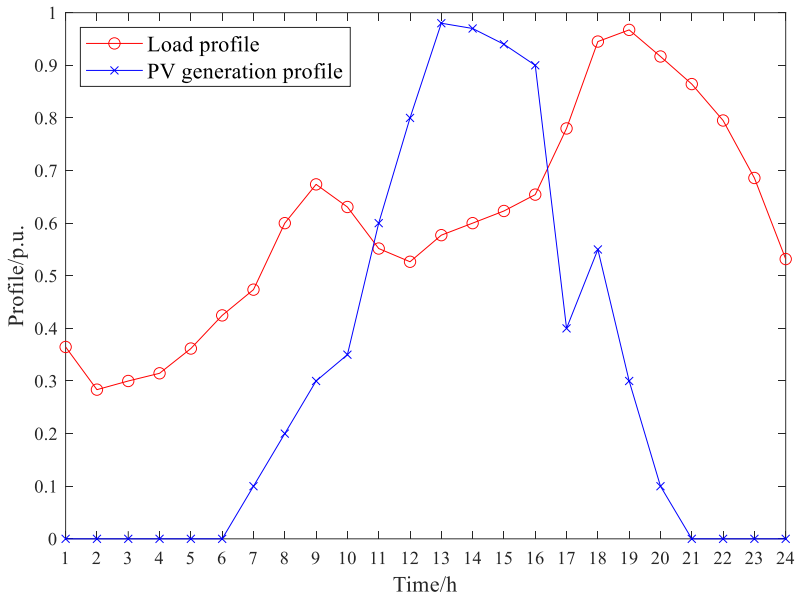

Fig. 5.2. Daily load profile and PV generation profile.

By running power flow, two constraint violation problems can be identified if without constraint management by using the SOP: a) V_3 (voltage at node 3) exceeds the upper limit of 1.03 p.u. during 12:00-16:00 due to the peak generation of the PV unit; b) $|I_{12}|$ (line current on line 1-2) exceeds its thermal capacity during 18:00-21:00 due to

the peak load but small generation of the PV unit during the period. These violation problems can be seen in the black curves in Fig. 5.3.

Considering real-time measurements of V_3 and line flows on line 1-2 are collected, the violation problems can be solved by using the FOR-based constraint management method in this chapter. The results are shown by the coloured curves in Fig. 5.3, where different coloured curves present the performance under different SOP control objectives, i.e., feeder load balancing (FLB), voltage profile improvement (VPI) and power losses reduction (PLR). From the results in Fig. 5.3, both FLB control and PLR control present the very similar performance. Compared to VPI control that improves the voltage profile to the most extent, FLB control and PLR control can reduce more line current on line 1-2. Whatever the control strategy is used for controlling the SOP, V_3 and $|I_{12}|$ can be managed within their limitations.

The results of SOP set points considering different control objectives are obtained and shown in Fig. 5.4. It should be noted that this chapter only focuses on the system-level control of SOPs and does not delve into the converter-level or switching-level control as presented in Fig. 2.2. In other words, the dynamic process in the converter/switching-level control is not considered, in assumption that only steady-state outcomes of SOP control, i.e., SOP set points, are obtained.

From the results in Fig. 5.4, the power control of SOP under the FLB control objective and PLR control objective are nearly the same, exploiting the SOP capacity to transfer the active power from the bottom feeder to the top feeder to try to reduce the line current/line losses on the top feeder. In contrast, VPI control changes the reactive power remarkably, while transferring the active power from the bottom feeder to the top feeder to improve V_3 and reduce $|I_{12}|$ within the line capacity.

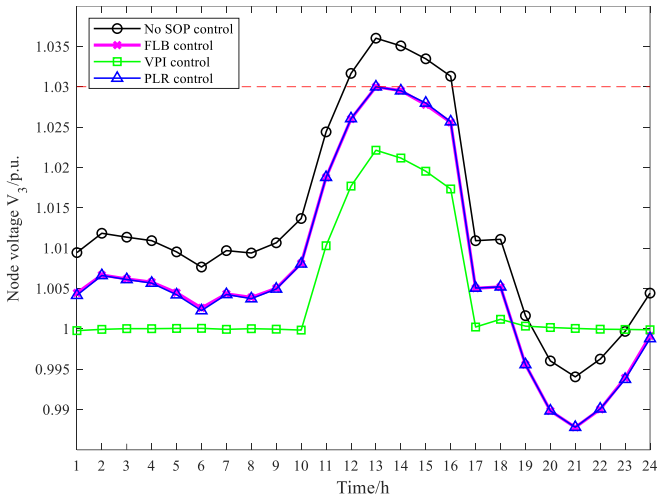

(a)

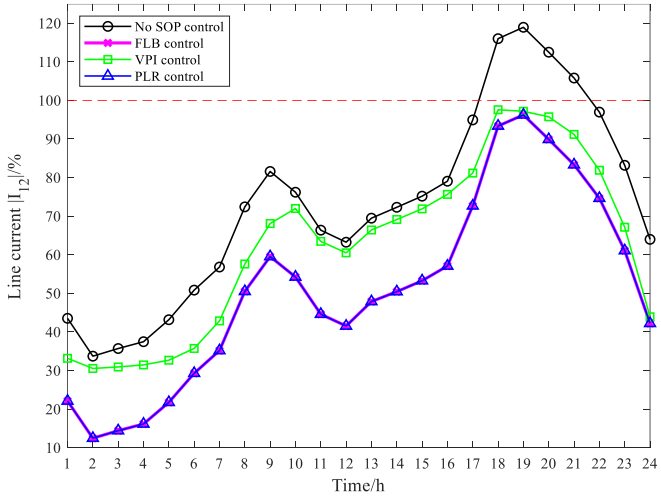

(b)

Fig. 5.3. SOP performance on (a) voltage and (b) thermal management.

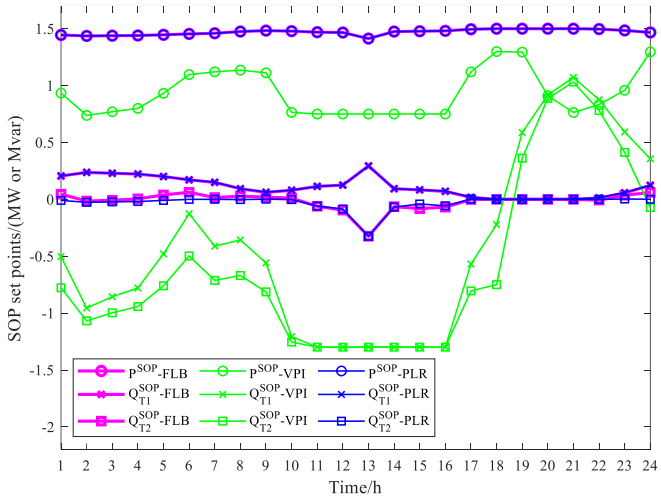

Fig. 5.4. SOP set points under different control objectives.

It should be noted that Fig. 5.4 presents only the steady-state SOP set points from the system-level control of SOPs as described in Section 2.1.3. Given that this chapter focuses on the steady-state results of line currents and node voltages of the distribution network under SOP control, the dynamic responses associated with converter-level and switching-level control of SOPs are neither studied nor discussed.

5.5.2. IEEE 33-node distribution network

- **Assumptions**

The 12.66 kV IEEE 33-node benchmark distribution network [198] is further used to validate the effectiveness of the FOR-based constraint management method. The total active and reactive power loads of the power network are 3.715MW and 2.3MVar, respectively.

As shown in Fig. 5.5, four PV units (each rated at 1.2 MW) are installed in the network. One 1MVA SOP is also employed at one normally open tie line to connect the ends of two feeders (i.e., node 18 and node 33). Two nodes (node T_1 and node T_2) are added at the two terminals of SOP, assuming the impedance of the tie line at 0.25+j0.25 Ω.

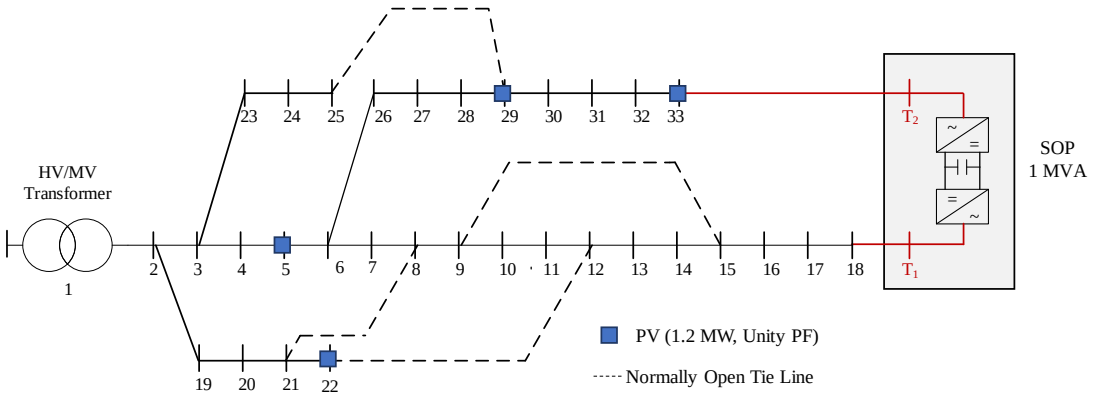

Fig. 5.5. Modified IEEE 33-node distribution network.

To fully demonstrate the thermal and voltage constraint management using the SOP, the thermal capacity of the transformer is assumed at 1 kA and the thermal

capacity of each line at 0.25 kA. The peak load in [198] is increased by 8%. The load profile and the PV generation profile in Fig. 5.2 are also used in this case. Without constraint management by using the SOP, the node voltages and line currents during a day are shown in Fig. 5.6. Note that except line 18-T_1 and line 33-T_2, the line number of line x-y (where node x is upstream of node y) is noted as y-1 for brevity.

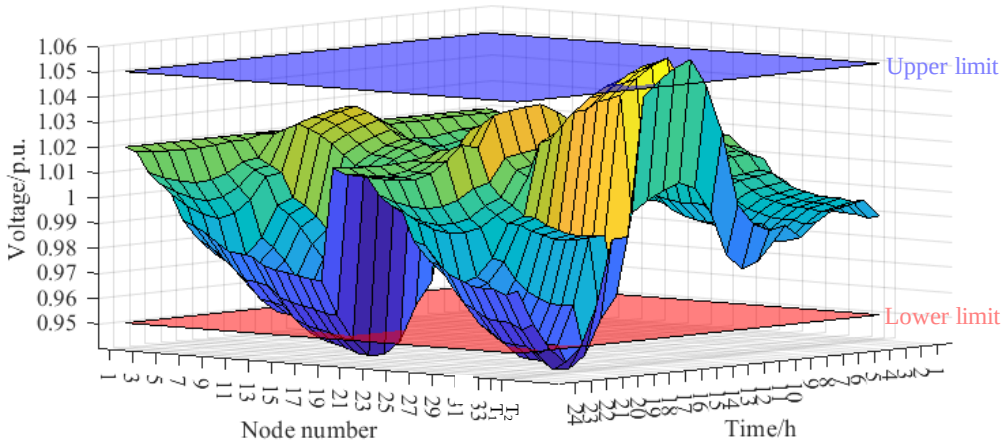

(a)

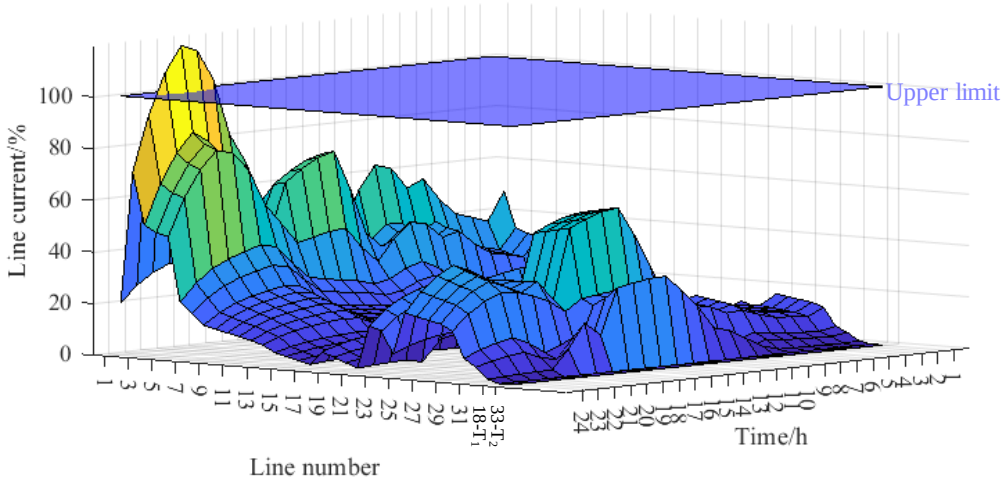

(b)

Fig. 5.6. Daily spatial-temporal distribution of (a) node voltages and (b) line currents of the modified IEEE 33-node distribution network without SOPs.

During 13:00-15:00, nodes on the top feeder (i.e., nodes 30-33 and node T_2) experience overvoltage problems. Nodes 13-18 and node T_1 on the bottom feeder and nodes 30-33 and node T_2 on the top feeder experience undervoltage problems during

different hours between 19:00-22:00. During 20:00-21:00, line 2-3 experiences the overloading problem.

The performance of the FOR-based constraint management method under three different measurement conditions is compared with local control [199] and OPF-based control [79] in this section. The three measurement conditions for the FOR-based method are as follows:

a) Local measurement (LM). Measurements at the SOP station are available, which include voltage measurements at node T_1 and node T_2 and line flow measurements on line 18-T_1 and line 33-T_2.

b) Moderate measurement (MM). Referring to [81], in addition to the local measurements at the SOP station, real-time measurements at the HV/MV substation and critical lines are also considered available for moderate measurement condition. The added measurements include line flow measurements at the feeder outlets of the HV/MV substation (i.e., line 2-3 and line 2-19) and the line segments (i.e., line 6-7 and line 6-26).

c) Global measurement (GM). All the lines are equipped with line flow measurements and all nodes are equipped with voltage measurements.

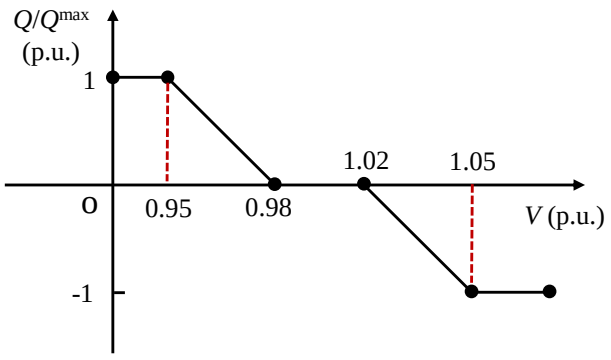

Fig. 5.7. Q-V curve for local control of the SOP in the modified IEEE 33-node distribution network.

The local control considered as a reference method can be achieved by using Q-V curve with the measurement of the voltages at the terminals of the SOP [199]. The parameters of the Q-V curves (which can be obtained by the method in [199]) for the two terminals of SOP in this study are selected as in Fig. 5.7.

Considering the SOP control objectives can be feeder load balancing, voltage profile improvement and power losses reduction (see Section 5.3.3), three corresponding indices are used in (5-29)-(5-31) respectively to evaluate the performance under different SOP control methods and measurement conditions. *B* and *N* are the set of lines and the set of nodes of the distribution network respectively.

$$LB_{index} = \sum_{t} \sum_{i \in B} \left(\frac{I_i}{I_{i\_rate}} \right)^2 \tag{5-29}$$

$$VP_{index} = \sum_{t} \sum_{i \in N} \left(V_{i,t} - V_{i,ref} \right)^2 \tag{5-30}$$

$$E_{loss} = \sum_{t} \sum_{i \in B} I_i^2 r_i \tag{5-31}$$

- **Results analysis**

(a) Constraints violation

The results of the node voltages and the line currents of the distribution network under local control, OPF-based control and FOR-based control are summarised in Table 5.1. The results with no SOP control are also listed for reference.

Table 5.1. Results of the voltage range and the maximum line current in the modified IEEE 33-node distribution network with SOPs during a day. (The voltages/ line currents marked in red indicate that they exceed the normal voltage range 0.95p.u.-1.05p.u./ the line capacity 100%.)

Control method	Measurement condition	Control objective	Minimum voltage-maximum voltage	Maximum line current
No control	—	—	0.94 p.u.-	117.8%

			1.06 p.u.	
Local control	LM	—	0.98 p.u.-1.04 p.u.	99.1%
FOR-based control	LM	FLB	0.95 p.u.-1.05 p.u.	113.3%
		VPI	0.98 p.u.-1.04 p.u.	99.3%
		PLR	0.95 p.u.-1.05 p.u.	113.3%
	MM	FLB	0.98 p.u.-1.05 p.u.	98.9%
		VPI	0.98 p.u.-1.04 p.u.	99.3%
		PLR	0.98 p.u.-1.05 p.u.	98.9%
	GM	FLB	0.97 p.u.-1.05 p.u.	98.9%
		VPI	0.98 p.u.-1.04 p.u.	99.1%
		PLR	0.97 p.u.-1.05 p.u.	98.9%
OPF-based control	GM	FLB	0.97 p.u.-1.05 p.u.	100.0%
		VPI	0.98 p.u.-1.04 p.u.	100.0%
		PLR	0.97 p.u.-1.05 p.u.	100.0%

From Table 5.1, the FOR-based control method with moderate/global measurement, local control and OPF-based control can solve the violation problems shown in Fig. 5.6, except the FOR-based control method with local measurement (termed as FOR-LM control for brevity). For clarity, the daily curves of node voltages and the line currents of the distribution network under FOR-LM control are presented in Fig. 5.8 and Fig. 5.9 respectively.

From Fig. 5.8 and Fig. 5.9, when using FLB/ PLR as the SOP control objective, FOR-LM control can only solve the overvoltage and undervoltage problems. The overloading problems (i.e., overloading on line 2-3) can be relieved but still remains. The reason is that the line flow on line 2-3 is unobservable under FOR-LM control. In addition, the observable lines are far away from line 2-3. Therefore, the optimisation of the observable line flows has little contribution to the reduction of line flow on line 2-

3. In contrast, using VPI as the SOP control objective, FOR-LM control can solve both the thermal and voltage violation problems. This indicates that improving the voltage profile (especially at the end nodes of the feeders) might benefit the distribution of line flows across the whole network, thus solving the overloading problem in this case.

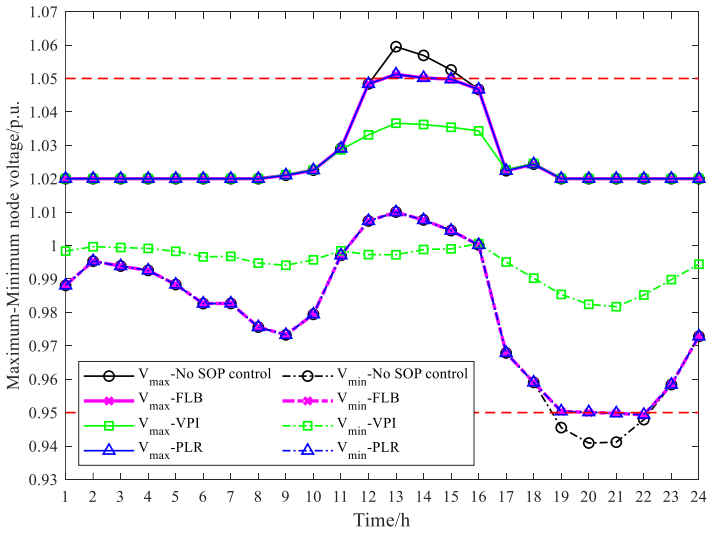

Fig. 5.8. Maximum and minimum voltages in the IEEE 33-node distribution network under FOR-LM control with different control objectives.

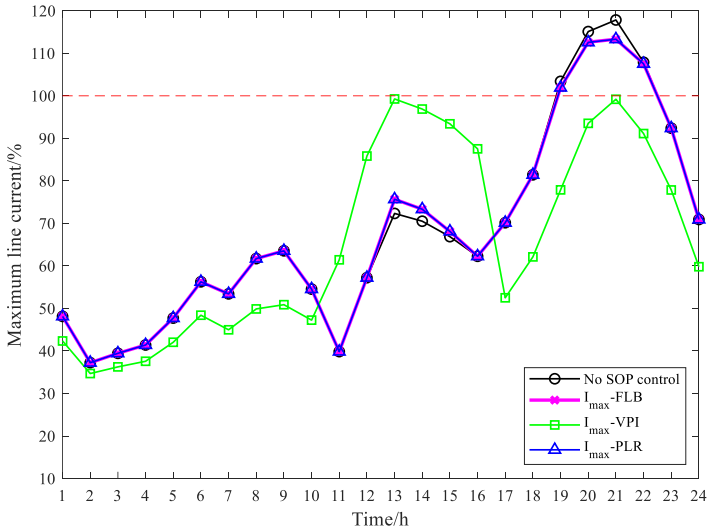

Fig. 5.9. Maximum line currents in the IEEE 33-node distribution network under FOR-LM control with different control objectives.

(b) Performance indices

The performance indices of different SOP control methods are obtained and shown in Fig. 5.10. Notably, the load balancing index (LB_{index}) is compared when feeder load

balancing is used as the objective function in both the FOR-based constraint management model and OPF-based model from [79]. Meanwhile, the voltage profile index (VP_{index}) and energy losses (E_{loss}) are compared when voltage profile improvement and power losses reduction are used as SOP control objectives.

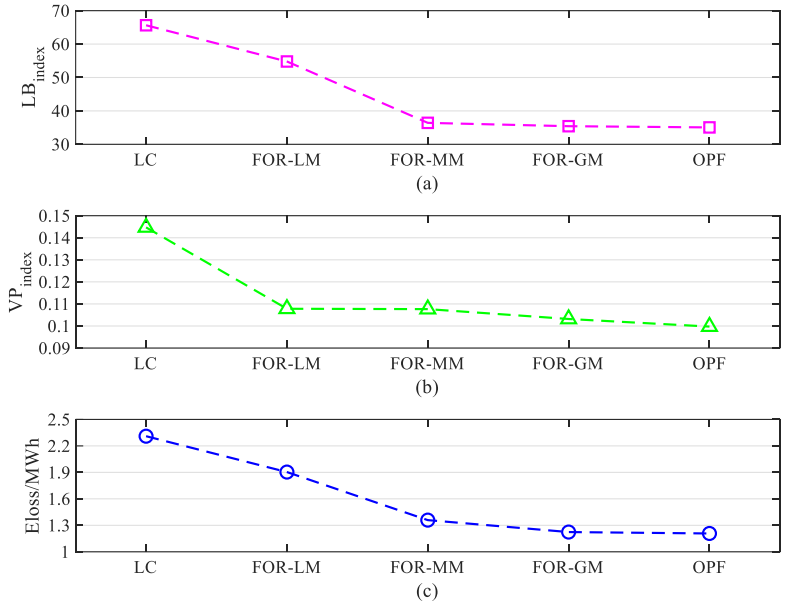

Fig. 5.10. Comparison of different SOP control methods in terms of: (a) feeder load balancing; (b) voltage profile improvement; (c) energy losses reduction.

In Fig. 5.10, the results for FOR-LM control are given for reference. Even with local measurement, the FOR-based method outperforms the local control method in all the three aspects. This is because the FOR-based method is formulated as an optimisation programme which strives for the optimal solution in terms of the three control objectives, rather than merely ensuring the observable node voltages/line flows be within the network constraints. In comparison with the OPF-based control, the performance of FOR-GM control is nearly the same as the OPF-based method. This validates that the FOR constraints in FOR-based method can be used to replace the power flow equations and network constraints in OPF-based method. Moreover, from the results in Fig. 5.10, the performance of the FOR-based method approaches to OPF-based method with increasing measurements. It is worth noting that if the SOP control

objective is voltage profile improvement, the performance of the FOR-based method can approach the optimum even with local measurement.

(c) Required computation time

The required computing time for different SOP control methods are also compared in Table 5.2. With the number of measurements increased, the network constraints to be considered by the FOR-based method rises, thus requiring more computation time for generating SOP set points. Under the "worst" case (i.e., global measurement), the computation time using the FOR-based method can be within 120 milliseconds (which is less than 1/18 of the time required by the OPF-based method on average).

Table 5.2. Computing time required by different SOP control methods.

SOP control method	Time for generating SOP set points	
	Average time/ms	Maximum time/ms
LC	0.05	0.94
FOR-LM	0.80	5.39
FOR-MM	2.70	6.90
FOR-GM	64.81	119.15
OPF	1184.65	2930.20

In summary, the FOR-based method can adapt to any measurement conditions. It can optimise the line flow distribution and voltage profiles while ensuring the observable line currents and node voltages within their limitations. The performance of the FOR-based control method relies on both the SOP control objectives and the measurement conditions. In this study, VPI is a best choice among the control objectives. With respect to the measurement conditions, global measurement ensures the optimal performance of the whole network, which is nearly the same with the OPF-based control. In contrast, moderate measurement (with only 8/70 measurement units

compared to the OPF-based control) can help the FOR-based method largely increases the computational efficiency, while achieving near-global optimisation compared with the results with global measurement. This indicates that the developed FOR-based method, if with measurements well planned, can achieve efficient SOP control. The costs of installing measurement units can also be largely reduced.

5.6. Summary

In this chapter, the FOR method is used for constraint management of distribution networks with SOPs. The FOR constraints are exploited in the formulation of the model for optimal SOP control, replacing power flow equations and network constraints normally used in the conventional OPF-based model. Due to the one-to-one correspondence between FOR boundaries and network constraints, the formulated model can adapt to various measurement conditions. Moreover, the FOR constraints can be converted into a format based on line flows and node voltages, allowing for the use of real-time measurements of these operating parameters rather than the measurements of nodal power load/generation that are normally not accessible online.

The quadratic constraints within the model are linearised to facilitate its transition to a quadratic programming framework. Additionally, auxiliary state variables for the SOP set points, line flows, and node voltages are introduced in the model. As a result, the FOR-based model is formulated in matrix form, where the matrices and coefficient vectors irrelevant to the measurements are segregated and can be prepared offline, thus further reducing the computational complexity.

By using the FOR-based method, near-global optimum results can be achieved even equipped with 8/70 measurement units as the OPF-based method in the modified IEEE 33-node case distribution network. Moreover, the FOR-based method can

generate SOP set points within milliseconds, which satisfies the requirement of real-time network constraint management.

Different SOP control objectives including feeder load balancing, voltage profile improvement and power losses reduction are used, and their performance is compared. Whatever the control objective is used, the observable line flows/node voltages can be managed within their limitations. However, the FOR-based constraint management method cannot ensure managing the unobservable nodes/lines of the network within their limitations. Under the circumstance where the network components with violation problems are not measured, voltage profile improvement is suggested to be used as the control objective. For the future work, appropriate planning of measurement units in different distribution networks is worthy of further investigation.

Chapter 6. Conclusions and future work

This chapter first concludes the work presented in the thesis and then discusses the aspects that can be further investigated in the future.

6.1. Conclusions

This thesis is set in the background of low carbon transition of electricity distribution networks. There are pressing challenges brought by rising uncertainties in renewable power generation and demand as well as inadequate real-time measurements in distribution networks. Nevertheless, at the same time, there are also promising opportunities featured by new power electronics solutions like SOPs. In this context, a feasible operation region methodology is proposed and developed, for accurately describing the network hosting capacity in an analytical way, supporting enhanced assessment and operation of low carbon distribution networks. Notably, the bottleneck of establishing the feasible operation region with SOPs is overcome by creatively introducing the concept of Minkowski Sum, which is a geometric method previously used in robot motion planning but seldom used in the power engineering domain.

The focus has been first placed on the development of the FOR formulas in distribution networks. Hyperplane expressions based on linear approximation have been commonly used in studies on FORs of transmission networks but cannot be directly applied in distribution networks since the R/X ration in distribution networks is high and its effect on FOR formulation cannot be neglected. To face the challenge, this thesis derives higher order analytical expressions (i.e., quadratic expressions) for more accurate description of FORs of distribution networks. A high-dimensional error analysis approach has also been provided for the validation. It has been demonstrated that the approximation of FORs by proposed quadratic expressions would maximally cause an overcurrent up to 116 % and an undervoltage down to 0.96p.u., which are able

to satisfy the requirements of engineering practice and are more accurate than the linear approximation using hyperplane expressions. Particularly for analytical thermal boundaries of the FOR, the errors of the quadratic expressions are significantly reduced compared to those of the existing hyperplane expressions.

Furthermore, there is increasing deployment of power electronics in distribution networks, but their impact on FORs of the networks has not been modelled so far. To bridge this research gap, this thesis innovatively modelled the impact of SOPs on FORs of distribution networks using a geometric model termed as Minkowski Sum. The model further enables the derivation of the FOR^{SOP} of a distribution network in an analytical way. The method can ensure that the errors in line currents and node voltages are confined to within 5% and 0.002 p.u. respectively in a test distribution network. The analytical expressions of FOR^{SOP} are also conservative due to the linearisation of the quadratic FOR formulas and the SOP constraints.

This thesis finally focused on an application of FORs by using the developed FOR formulas in constraint management of distribution networks. Compared to the conventional OPF constraints that include power flow equations and network thermal and voltage constraints, the FOR formulas are more applicable to incomplete measurement conditions in current distribution networks. This is because the FOR formulas establish the one-to-one correspondence between FOR boundaries and thermal/voltage constraints. In this regard, the optimisation model for network constraint management can adapt to various measurement conditions by using the FOR formulas rather than conventional OPF formulas. Another advantage is that the FOR-based method can achieve millisecond-level active management of the network with SOPs, which is 18 times faster than the OPF-based method on average. Moreover, the method allows for the use of real-time measurements of line flows and node voltages

rather than the measurements of nodal power load/generation that are normally not accessible online.

Besides the above contributions to the research field on FORs, the study presented in this thesis potentially holds significant industrial benefits. The FOR formulas provide DNOs with an effective tool for evaluating network hosting capacity, thus facilitating the fully utilisation of network capacity and reducing unnecessary reinforcement costs. Under the FOR scheme, the connection requests for low carbon technologies can be examined quickly by using the FOR formulas, thereby reducing the connection queues for customers or DG owners. Additionally, since the FOR-based constraint management method can adapt to various measurement conditions, DNOs can reduce the cost of measurement units by strategically installing them at critical buses or power lines. This benefit can be seen from the results of an IEEE 33-node test network, which show that even with only 8/70 measurement units, the FOR-based method can achieve near-global optimum results as the OPF-based method.

6.2. Future work

The following future work is identified to extend the work reported in this thesis:

6.2.1. Improvement of analytical expressions of feasible operation regions by data-driven methods

The key to deriving the analytical expressions of FOR boundaries is to obtain the explicit relationship between line currents (or node voltages) and power injections, which is very difficult without any assumptions. The errors from these assumptions can be quantified by the high-dimensional error-analysis approach proposed in this thesis.

In the future, data-driven methods can be further used to reduce the errors of the existing analytical expressions of FOR boundaries, as an extension of the analytical method and high-dimensional simulation approach presented in this thesis. By

acquiring a dataset of FOR boundary points that accurately represent the FOR boundaries through the high-dimensional simulation approach, it becomes possible to fine-tune the assumed parameters in the analytical expressions of FOR boundaries to reduce or potentially minimise the statistical errors associated with the analytical FOR boundaries.

6.2.2. Hosting capacity assessment

Quantitative indices related to FORs of distribution networks can be defined for the assessment of network hosting capacity. The results of network hosting capacity can be further compared to the results under conventional "worst-case" analysis. Additionally, the impact of different power electronics (e.g., SOPs and static synchronous compensator) is worthy of investigation and comparison in the future work.

6.2.3. Constraint management of distribution networks with different technologies

This thesis develops FOR-based constraint management method for optimally controlling SOPs in distribution networks. In particular, this method can adapt to various measurement conditions in distribution networks and generate SOP set points within milliseconds. These features can facilitate the implementation of the method to control other technologies in practical measurement conditions. An attractive topic is on the optimal control of different power electronic devices or flexible resources (e.g., energy storage systems), in the context of increasing uncertainties from renewable generation and customer behaviours.

6.2.4. Applications of the Minkowski Sum model

The Minkowski Sum model can be extended to analyse the impact of various equipment and technologies, such as capacitor banks, different power electronic devices like SVCs and STATCOMs and dynamic line rating, on the FORs of

distribution networks. Particularly, the technology of dynamic line rating, which considers real-time thermal rating, introduces a time-varying aspect to the FORs of distribution networks. Quantifying the impact of these equipment and technologies is worthy of further investigation.

Moreover, the Minkowski Sum model can be utilised in a similar way to analyse the effects of emerging technologies on the operation regions of multi-energy networks. The difference lies in considering the operational constraints of other energy networks, besides electricity networks, when formulating FORs of multi-energy networks. It is also noteworthy that while this thesis only considers steady-state thermal and voltage constraints of electricity distribution networks, dynamic constraints such as stability constraints in multi-energy networks can also be incorporated into the modelling.

The Minkowski Sum model also shows great potential in aggregating the flexibility regions of different resources such as controllable distributed generation, flexible load and energy storage in energy networks. In recent years, researchers have used the Minkowski Sum model to aggregate load-side resources such as flexible loads and electric vehicles [200], [201]. However, how to consider the great uncertainties in the generation and load resources and the time-dependent characteristics of energy storage in the developed Minkowski Sum-based flexibility region remains a great challenge.

References

[1] Met Office, "What is climate change?" [Online]. Available: https://www.metoffice.gov.uk/weather/climate-change/what-is-climate-change. [Accessed: 02-Nov-2023].

[2] BEIS, "United Kingdom of Great Britain and Northern Ireland's nationally determined contribution," 2022.

[3] International Energy Agency, "World energy outlook," 2022. [Online]. Available: https://www.iea.org/reports/world-energy-outlook-2022. [Accessed: 04-Dec-2023].

[4] United States Environmental Protection Agency, "Distributed generation of electricity and its environmental impacts," 2023. [Online]. Available: https://www.epa.gov/energy/distributed-generation-electricity-and-its-environmental-impacts.

[5] S. Ullah, A. M. A. Haidar, P. Hoole, H. Zen, and T. Ahfock, "The current state of distributed renewable generation, challenges of interconnection and opportunities for energy conversion based DC microgrids," *J. Clean. Prod.*, vol. 273, p. 122777, 2020.

[6] International Energy Agency, "Unlocking the potential of distributed energy resources power system opportunities and best practices," 2022.

[7] International Energy Agency, "Renewable energy market update-outlook for 2023 and 2024," 2023.

[8] National Grid ESO, "Future energy scenarios," 2023. [Online]. Available: https://www.nationalgrideso.com/future-energy/future-energy-scenarios/documents. [Accessed: 10-Oct-2023].

[9] National Grid, "How will our electricity supply change in the future?" 2022. [Online]. Available: https://www.nationalgrid.com/stories/energy-explained/how-will-our-electricity-supply-change-future. [Accessed: 10-Oct-2023].

[10] W. Cao, J. Wu, N. Jenkins, C. Wang, and T. Green, "Operating principle of soft open points for electrical distribution network operation," *Appl. Energy*, vol. 164, pp. 245–257, 2016.

[11] T. H. Chen, W. T. Huang, J. C. Gu, G. C. Pu, Y. F. Hsu, and T. Y. Guo, "Feasibility study of upgrading primary feeders from radial and open-loop to normally closed-loop arrangement," *IEEE Trans. Power Syst.*, vol. 19, no. 3, pp. 1308–1316, 2004.

[12] W. Cao, "Soft open points for the operation of medium voltage distribution networks," Cardiff University, 2015.

[13] Q. Qi, "Benefit analysis of using soft dc links in medium voltage distribution networks," Cardiff University, 2018.

[14] P. Li, G. Song, H. Ji, J. Zhao, C. Wang, and J. Wu, "A supply restoration method of distribution system based on soft open point," in *2016 IEEE Innovative Smart Grid Technologies - Asia (ISGT-ASIA)*, 2016, pp. 535–539.

[15] P. Li, J. Ji, H. Ji, G. Song, C. Wang, and J. Wu, "Self-healing oriented supply restoration method based on the coordination of multiple SOPs in active distribution networks," *Energy*, vol. 195, p. 116968, 2020.

[16] C. Heinrich and H. Schmitt, "Integration of new switching technologies in medium-voltage systems," *IEE Conf. Publ.*, vol. 5, no. 482, 2001.

[17] J. M. Bloemink and T. C. Green, "Increasing distributed generation penetration using soft normally-open points," *IEEE PES Gen. Meet. PES 2010*, pp. 1–8, 2010.

[18] J. M. Maza-Ortega, A. Gómez-Expósito, M. Barragán-Villarejo, E. Romero-Ramos, and A. Marano-Marcolini, "Voltage source converter-based topologies to further integrate renewable energy sources in distribution systems," *IET Renew. Power Gener.*, vol. 6, no. 6, pp. 435–445, 2012.

[19] S. K. Chaudhary, J. M. Guerrero, and R. Teodorescu, "Enhancing the capacity of the AC distribution system using DC interlinks - a step toward future DC grid," *IEEE Trans. Smart Grid*, vol. 6, no. 4, pp. 1722–1729, 2015.

[20] A. Aithal and J. Wu, "Operation and performance of a medium-voltage DC link," *CIRED - Open Access Proc. J.*, vol. 2017, no. 1, pp. 1355–1358, 2017.

[21] Q. Qi, C. Long, J. Wu, and J. Yu, "Impacts of a medium voltage direct current link on the performance of electrical distribution networks," *Appl. Energy*, vol. 230, no. February, pp. 175–188, 2018.

[22] Z. Gao, J. Ge, J. Wang, K. Xu, W. Li, C. Wang, and F. Xu, "Research on topology and control technology of soft multi-state open point based with fault isolation capability," *Power Syst. Prot. Control*, vol. 47, no. 15, pp. 48–54, 2019.

[23] N. Okada, M. Takasaki, H. Sakai, and S. Katoh, "Development of a 6.6 kV - 1 MVA transformerless loop balance controller," *PESC Rec. - IEEE Annu. Power Electron. Spec. Conf.*, pp. 1087–1091, 2007.

[24] S. Morozumi, "Micro-grid demonstration projects in Japan," *2007 Power Convers. Conf.*, pp. 635–642, 2003.

[25] C. Y. Tang, Y. F. Chen, Y. M. Chen, and Y. R. Chang, "Dc-link voltage control strategy for three-phase back-to-back active power conditioners," *IEEE Trans. Ind. Electron.*, vol. 62, no. 10, pp. 6306–6316, 2015.

[26] J. M. Bloemink and T. C. Green, "Benefits of distribution-level power electronics for supporting distributed generation growth," *IEEE Trans. Power Deliv.*, vol. 28, no. 2, pp. 911–919, 2013.

[27] H. Akagi and R. Kitada, "Control and design of a modular multilevel cascade BTB system using bidirectional isolated DC/DC converters," *IEEE Trans. Power Electron.*, vol. 26, no. 9, pp. 2457–2464, 2011.

[28] H. Wu, X. Lin, M. Ding, R. Bi, C. Luo, and B. Xu, "Adaptability evaluation and active power regulation of FID in active distribution network," *Int. J. Electr. Power Energy Syst.*, vol. 124, no. December 2019, p. 106351, 2021.

[29] X. Jiang, J. Xiao, B. She, and G. Zu, "Locating and sizing of partition flexible interconnection converter station in large urban power grids," *IET Gener. Transm. Distrib.*, vol. 13, no. 21, pp. 4830–4841, 2019.

[30] D. Diaz, A. Kumar, J. Deboever, S. Grijalva, J. Peppanen, M. Rylander, and J. Smith, "Scenario-selection for hosting capacity analysis of distribution feeders with voltage regulation equipment," *2019 IEEE Power Energy Soc. Innov. Smart Grid Technol. Conf. ISGT 2019*, pp. 2–6, 2019.

[31] R. Gupta, F. Sossan, and M. Paolone, "Countrywide PV hosting capacity and energy storage requirements for distribution networks: The case of Switzerland," *Appl. Energy*, vol. 281, no. June 2020, p. 116010, 2021.

[32] S. Wang, S. Chen, L. Ge, and L. Wu, "Distributed generation hosting capacity evaluation for distribution systems considering the robust optimal operation of OLTC and SVC," *IEEE Trans. Sustain. Energy*, vol. 7, no. 3, pp. 1111–1123, 2016.

[33] H. Ji, C. Wang, P. Li, J. Zhao, G. Song, and J. Wu, "Quantified flexibility evaluation of soft open points to improve distributed generator penetration in active distribution

networks based on difference-of-convex programming," *Appl. Energy*, vol. 218, no. December 2017, pp. 338–348, 2018.

[34] M. Alturki, A. Khodaei, A. Paaso, and S. Bahramirad, "Optimization-based distribution grid hosting capacity calculations," *Appl. Energy*, vol. 219, no. March 2017, pp. 350–360, 2018.

[35] F. Ding and B. Mather, "On distributed PV hosting capacity estimation, sensitivity study, and improvement," *IEEE Trans. Sustain. Energy*, vol. 8, no. 3, pp. 1010–1020, 2017.

[36] S. Mina Mirbagheri, D. Falabretti, V. Ilea, and M. Merlo, "Hosting capacity analysis: a review and a new evaluation method in case of parameters uncertainty and multi-generator," *Proc. - 2018 IEEE Int. Conf. Environ. Electr. Eng. 2018 IEEE Ind. Commer. Power Syst. Eur. EEEIC/I CPS Eur. 2018*, 2018.

[37] J. Le Baut, P. Zehetbauer, S. Kadam, B. Bletterie, N. Hatziargyriou, J. Smith, and M. Rylander, "Probabilistic evaluation of the hosting capacity in distribution networks," *IEEE PES Innov. Smart Grid Technol. Conf. Eur.*, 2017.

[38] F. F. Wu and S. Kumagai, "Steady-state security regions of power systems," *IEEE Trans. Circuits Syst.*, vol. 29, no. 11, pp. 703–711, 1982.

[39] F. F. Wu and Y. K. Tsai, "Probabalistic dynamic security assessment of power systems: part I—basic model," *IEEE Trans. Circuits Syst.*, vol. 30, no. 3, pp. 148–159, 1983.

[40] J. Xiao, G. Q. Zu, X. X. Gong, and C. S. Wang, "Model and topological characteristics of power distribution system security region," *J. Appl. Math.*, vol. 2014, 2014.

[41] T. Yang and Y. Yu, "Static voltage security region-based coordinated voltage control in smart distribution grids," *IEEE Trans. Smart Grid*, vol. 9, no. 6, pp. 5494–5502, 2018.

[42] T. Yang and Y. Yu, "Steady-state security region-based voltage/var optimization considering power injection uncertainties in distribution grids," *IEEE Trans. Smart Grid*, vol. 10, no. 3, pp. 2904–2911, 2019.

[43] J. Su, H. D. Chiang, and L. F. C. Alberto, "Two-time-scale approach to characterize the steady-state security region for the electricity-gas integrated energy system," *IEEE Trans. Power Syst.*, vol. 36, no. 6, pp. 5863–5873, 2021.

[44] J. Su, H. Chiang, Y. Zeng, and N. Zhou, "Toward complete characterization of the steady-state security region for the electricity-gas integrated energy system," *IEEE Trans. Smart Grid*, vol. 12, pp. 3004–3015, 2021.

[45] X. Li, G. Tian, Q. Shi, T. Jiang, F. Li, and H. Jia, "Security region of natural gas network in electricity-gas integrated energy system," *Int. J. Electr. Power Energy Syst.*, vol. 117, no. August 2019, p. 105601, 2020.

[46] T. Jiang, R. Zhang, X. Li, H. Chen, and G. Li, "Integrated energy system security region: Concepts, methods, and implementations," *Appl. Energy*, vol. 283, no. June 2020, p. 116124, 2021.

[47] X. Li, T. Jiang, L. Bai, X. Kou, F. Li, H. Chen, and G. Li, "Orbiting optimization model for tracking voltage security region boundary in bulk power grids," *CSEE J. Power Energy Syst.*, vol. PP, no. 99, pp. 476–487, 2022.

[48] E. Hnyilicza, S. T. Lee, and F. C. Schweppe, "Steady-state security regions:the set-theoretic approach," in *Proc. 1975 PICA Conf.*, 1975.

[49] C. C. Liu and F. F. Wu, "Analysis of small disturbance stability regions of power system models with real and reactive power flows.," *Proc. Am. Control Conf.*, vol. 2, no. 6, pp. 1162–1165, 1984.

[50] D. M. James, W. Shimo, Z. Qianglin, Z. Guozhong, T. T. Roger, and P. A. D, "Security boundary visualization for systems operation," *IEEE Trans. Power Syst.*, vol. 12, no. 2, pp. 940–947, 1997.

[51] Y. Yixin, S. Jifeng, J. Hongjie, and L. Peng, "Study on visualization of voltage stability feasible region of bulk power system," *Autom. Electr. Power Syst.*, vol. 25, no. 22, pp. 1-5 (in Chinese), 1999.

[52] J. Su, Y. Yu, H. Jia, P. Li, N. He, Z. Tang, and H. Fu, "Visualization of voltage stability region of bulk power system," *PowerCon 2002 - 2002 Int. Conf. Power Syst. Technol. Proc.*, vol. 3, no. 4, pp. 1665–1668, 2002.

[53] L. Qingchun, "Study on security region-based voltage security monitor in Liaoning power grid," 2009. [Online]. Available: https://wf.pub/thesis/article:Y1419199.

[54] J. Zhao, B. Zhang, and H. D. Chiang, "An optimal power flow model and approach with static voltage stability constraints," *Proc. IEEE Power Eng. Soc. Transm. Distrib. Conf.*, vol. 2005, pp. 1–6, 2005.

[55] D. Wang, Y. Yu, C. Fu, J. Zhang, J. Wu, H. Jia, and X. Uien, "Security region based probabilistic security assessment of power transmission system à basic concepts," *Proc. IEEE Power Eng. Soc. Transm. Distrib. Conf.*, vol. 2005, pp. 1–5, 2005.

[56] W. Gang and M. Shengwei, "A tangent plane analysis of the static voltage stability region boundary," *Autom. Electr. Power Syst.*, vol. 31, no. 11, pp. 6-11 (in Chinese), 2007.

[57] W. Gang, Z. Xuemin, and M. Shengwei, "Quadratic approximation analysis of static voltage stability region boundary," *Proc. CSEE*, vol. 28, no. 19, pp. 30-35 (in Chinese), 2008.

[58] J. Tao, J. Hongjie, J. Yilang, K. Xiangyu, and L. Ning, "Approximating method of wide area thermal security region boundary in bulk power system," *Trans. China Electrotech. Soc.*, vol. 31, no. 8, pp. 134-146 (in Chinese), 2016.

[59] X. Li, T. Jiang, G. Liu, L. Bai, H. Cui, and F. Li, "Bootstrap-based confidence interval estimation for thermal security region of bulk power grid," *Int. J. Electr. Power Energy Syst.*, vol. 115, no. July 2019, p. 105498, 2020.

[60] Y. Qiu, H. Wu, Y. Zhou, and Y. Song, "Global parametric polynomial approximation of static voltage stability region boundaries," *IEEE Trans. Power Syst.*, vol. 32, no. 3, pp. 2362–2371, 2017.

[61] Y. Yixin and L. Wenpeng, "Practical dynamic security regions of power systems," *Proc. CSEE*, vol. 10, no. Supplement, pp. 22–28, 1990.

[62] D. Cun and Y. Yixin, "Study of voltage stability region of power systems subject to serious load disturbance," *Autom. Electr. Power Syst.*, vol. 29, no. 2, pp. 13-19 (in Chinese), 2005.

[63] Electric Power Research Institue, "Program on technology innovation : probabilistic dynamic security region," 2007.

[64] B. Alhabib and Y. Yixin, "Security constrained distributed optimal power flow of interconnected power systems," *Trans. Tianjin Univ.*, vol. 14, no. 3, pp. 208–216, 2008.

[65] P. A. Dolloff, D. Adams, S. Anderson, M. Y. Vaiman, M. M. Vaiman, M. Povolotskiy, and D. T. Bradshaw, "Evaluate real-time system reliability using boundary-based concept for EKPC system," *IEEE Power Energy Soc. 2008 Gen. Meet. Convers. Deliv. Electr. Energy 21st Century, PES*, no. 3, pp. 2–9, 2008.

[66] Y. Makarov, S. Lu, X. Guo, J. Gronquist, P. Du, T. Nguyen, and J. Burns, "Wide area security region final report," 2010.

[67] E. A. Al-Ammar and M. A. El-Kady, "Application of operating security regions in power systems," *2010 IEEE PES Transm. Distrib. Conf. Expo. Smart Solut. a Chang. World*, no. May 2010, 2010.

[68] M. Chavez-Lugo, C. R. Fuerte-Esquivel, C. A. Canizares, and V. J. Gutierrez-Martinez, "Practical security boundary-constrained dc optimal power flow for electricity markets," *IEEE Trans. Power Syst.*, vol. 31, no. 5, pp. 3358–3368, 2016.

[69] Q. Hou, N. Zhang, D. S. Kirschen, E. Du, Y. Cheng, and C. Kang, "Sparse oblique decision tree for power system security rules extraction and embedding," *IEEE Trans. Power Syst.*, vol. 36, no. 2, pp. 1605–1615, 2021.

[70] J. Xiao, W. Gu, C. Wang, and F. Li, "Distribution system security region: Definition, model and security assessment," *IET Gener. Transm. Distrib.*, vol. 6, no. 10, pp. 1029–1035, 2012.

[71] J. Xiao, M. Zhang, L. Bai, B. She, and B. Zhang, "Boundary supply capability for distribution systems: Concept, indices and calculation," *IET Gener. Transm. Distrib.*, vol. 12, no. 2, pp. 499–506, 2018.

[72] H. Jiao, X. Lin, J. Xiao, G. Zu, C. Song, Z. Qiu, Z. Bao, and C. Zhou, "Concavity-convexity of distribution system security region. Part I: Observation results and mechanism," *Appl. Energy*, vol. 342, no. November 2022, p. 121169, 2023.

[73] S. Chen, Z. Wei, G. Sun, Y. Sun, and N. Lu, "Steady-state security regions of electricity-gas integrated energy systems," *IEEE Power Energy Soc. Gen. Meet.*, vol. 2016-Novem, pp. 1–5, 2016.

[74] J. Su, H. D. Chiang, and Y. Zeng, "Toward quantification of flexibility for an electricity-heat integrated energy system: Secure operation region approach," *IET Energy Syst. Integr.*, vol. 3, no. 2, pp. 142–157, 2021.

[75] T. Jiang, R. Zhang, X. Li, H. Chen, and G. Li, "Integrated energy system security region: Concepts, methods, and implementations," *Appl. Energy*, vol. 283, no. December 2020, p. 116124, 2021.

[76] S. Zhang, W. Gu, J. Wang, X. P. Zhang, X. Meng, S. Lu, G. Pan, and S. Ding, "Steady-state security region of integrated energy system considering thermal dynamics," *IEEE Trans. Power Syst.*, 2023.

[77] L. Liu, D. Wang, K. Hou, H. Jia, and S. Li, "Region model and application of regional integrated energy system security analysis," *Appl. Energy*, vol. 260, p. 114268, 2020.

[78] J. Xiao, B. Zhang, and F. Luo, "Distribution network security situation awareness method based on security distance," *IEEE Access*, vol. 7, pp. 37855–37864, 2019.

[79] C. Long, J. Wu, L. Thomas, and N. Jenkins, "Optimal operation of soft open points in medium voltage electrical distribution networks with distributed generation," *Appl. Energy*, vol. 184, pp. 427–437, 2016.

[80] S. Zhang, Y. Fang, H. Zhang, H. Cheng, and X. Wang, "Maximum hosting capacity of photovoltaic generation in sop-based power distribution network integrated with electric vehicles," *IEEE Trans. Ind. Informatics*, vol. 18, no. 11, pp. 8213–8224, 2022.

[81] I. Džafić, M. Gilles, R. A. Jabr, B. C. Pal, and S. Henselmeyer, "Real time estimation of loads in radial and unsymmetrical three-phase distribution networks," *IEEE Trans. Power Syst.*, vol. 28, no. 4, pp. 4839–4848, 2013.

[82] P. Li, H. Ji, C. Wang, J. Zhao, G. Song, F. Ding, and J. Wu, "Coordinated control method of voltage and reactive power for active distribution networks based on soft open point," *IEEE Trans. Sustain. ENERGY*, vol. 8, no. 4, pp. 1430–1442, 2017.

[83] M. A. Abdelrahman, C. Long, J. Wu, and N. Jenkins, “Optimal operation of multi-terminal soft open point to increase hosting capacity of distributed generation in medium voltage networks,” in *2018 53rd International Universities Power Engineering Conference (UPEC)*, 2018.

[84] M. A. Sayed and T. Takeshita, “All nodes voltage regulation and line loss minimization in loop distribution systems using UPFC,” *IEEE Trans. Power Electron.*, vol. 26, no. 6, pp. 1694–1703, 2011.

[85] P. Kumar, A. Rahul, and S. Subha, “Prospects of the applying of UPFC in modern distribution network,” *Middle - East J. Sci. Res.*, vol. 20, no. 8, pp. 929–933, 2014.

[86] J. Pereda and T. C. Green, “Direct modular multilevel converter with six branches for flexible distribution networks,” *IEEE Trans. Power Deliv.*, vol. 31, no. 4, pp. 1728–1737, 2016.

[87] J. M. Bloemink and T. C. Green, “Increasing photovoltaic penetration with local energy storage and soft normally-open points,” in *2011 IEEE Power And Energy Society General Meeting*, 2011.

[88] C. Yao, C. Zhou, J. Yu, K. Xu, P. Li, and G. Song, “A sequential optimization method for soft open point integrated with energy storage in active distribution networks,” in *Renewable Energy Integration with Mini/Microgrid*, 2018, vol. 145, pp. 528–533.

[89] H. Ji, C. Wang, P. Li, J. Zhao, G. Song, and J. Wu, “Quantified flexibility evaluation of soft open points to improve distributed generator penetration in active distribution networks based on difference-of-convex programming,” *Appl. Energy*, vol. 218, no. March, pp. 338–348, 2018.

[90] S. Baghban-Novin, A. Hamidi, S. Golshannavaz, and D. Nazarpour, “E-SOP’s contribution in a techno-economic and clean operation of distribution networks: A multi-objective optimization approach based on linear models,” *Int. Trans. Electr. ENERGY Syst.*, vol. 30, no. 2, 2020.

[91] P. Khamphakdi, M. Nitta, M. Hagiwara, and H. Akagi, “Zero-voltage ride-through capability of a transformerless back-to-back system using modular multilevel cascade converters for power distribution systems,” *IEEE Trans. Power Electron.*, vol. 31, no. 4, pp. 2730–2741, 2016.

[92] F. Z. Peng, Y. Liu, S. Yang, S. Zhang, D. Gunasekaran, and U. Karki, “Transformer-less unified power-flow controller using the cascade multilevel inverter,” *IEEE Trans. Power Electron.*, vol. 31, no. 8, pp. 5461–5472, 2016.

[93] S. Yang, Y. Liu, X. Wang, D. Gunasekaran, U. Karki, and F. Z. Peng, “Modulation and control of transformerless UPFC,” *IEEE Trans. Power Electron.*, vol. 31, no. 2, pp. 1050–1063, 2016.

[94] S. Debnath, J. Qin, B. Bahrani, M. Saeedifard, and P. Barbosa, “Operation, control, and applications of the modular multilevel converter: A review,” *IEEE Trans. Power Electron.*, vol. 30, no. 1, pp. 37–53, 2015.

[95] A. Nami, J. Liang, F. Dijkhuizen, and G. D. Demetriades, “Modular multilevel converters for HVDC applications: Review on converter cells and functionalities,” *IEEE Trans. Power Electron.*, vol. 30, no. 1, pp. 18–36, 2015.

[96] P. S. Georgilakis and N. D. Hatziargyriou, “Unified power flow controllers in smart power systems: Models, methods, and future research,” *IET Smart Grid*, vol. 2, no. 1, pp. 2–10, 2019.

[97] Q. Qi, J. Wu, and C. Long, “Multi-objective operation optimization of an electrical distribution network with soft open point,” *Appl. Energy*, vol. 208, pp. 734–744, 2017.

[98] H. Ji, C. Wang, P. Li, G. Song, and J. Wu, "SOP-based islanding partition method of active distribution networks considering the characteristics of DG, energy storage system and load," *Energy*, vol. 155, pp. 312–325, 2018.

[99] A. F. Ibrahim Diaaeldin, Shady Abdel Aleem, Ahmed El-Rafei, Almoataz Abdelaziz,Zobaa, "Optimal network reconfiguration in active distribution networks with soft open points and distributed generation," *Energies*, vol. 12, no. 21, p. 4172, 2019.

[100] M. B. Shafik, G. I. Rashed, and H. Chen, "Optimizing energy savings and operation of active distribution networks utilizing hybrid energy resources and soft open points: case study in Sohag, Egypt," *IEEE Access*, vol. 8, pp. 28704–28717, 2020.

[101] J. M. Bloemink and T. C. Green, "Required VSC efficiency for zero net-loss distribution network active compensation," in *2016 IEEE 7th International Symposium On Power Electronics For Distributed Generation Systems (PEDG)*, 2016.

[102] H. Ji, C. Wang, P. Li, F. Ding, and J. Wu, "Robust operation of soft open points in active distribution networks with high penetration of photovoltaic integration," *IEEE Trans. Sustain. Energy*, vol. 10, no. 1, pp. 280–289, 2019.

[103] L. Thomas, Y. Zhou, C. Long, J. Wu, and N. Jenkins, "A general form of smart contract for decentralized energy systems management," *Nat. ENERGY*, vol. 4, no. 2, pp. 140–149, 2019.

[104] W. Cao, J. Wu, N. Jenkins, C. Wang, and T. Green, "Benefits analysis of soft open points for electrical distribution network operation," *Appl. Energy*, vol. 165, pp. 36–47, 2016.

[105] V. B. Pamshetti, S. Singh, A. K. Thakur, S. P. Singh, and V. K. Bussa, "Integrated operation of conservation voltage reduction and network reconfiguration in PV-rich distribution network considering soft open point impact," in *2019 IEEE Industry Applications Society Annual Meeting*, 2019.

[106] L. Haishen, Z. Kai, L. Shengwei, G. Leijiao, W. Qingbiao, and H. Tao, "Allowable dg penetration capacity calculation of snop-based flexible distribution network," in *2018 China International Conference on Electricity Distribution (CICED)*, 2018, pp. 2148–2152.

[107] E. Luo, P. Cong, H. Lu, and Y. Li, "Two-stage hierarchical congestion management method for active distribution networks with multi-type distributed energy resources," *IEEE Access*, vol. 8, pp. 120309–120320, 2020.

[108] J. Zhao, Y. Wang, G. Song, P. Li, C. Wang, and J. Wu, "Congestion management method of low-voltage active distribution networks based on distribution locational marginal price," *IEEE Access*, vol. 7, pp. 32240–32255, 2019.

[109] P. Li, H. Ji, C. Wang, J. Zhao, G. Song, F. Ding, and J. Wu, "Optimal operation of soft open points in active distribution networks under three-phase unbalanced conditions," *IEEE Trans. Smart Grid*, vol. 10, no. 1, pp. 380–391, 2019.

[110] F. Sun, J. Ma, M. Yu, and W. Wei, "Optimized two-time scale robust dispatching method for the multi-terminal soft open point in unbalanced active distribution networks," *IEEE Trans. Sustain. Energy*, vol. 12, no. 1, pp. 587–598, 2021.

[111] P. Li, J. Ji, H. Ji, G. Song, C. Wang, and J. Wu, "Self-healing oriented supply restoration method based on the coordination of multiple SOPs in active distribution networks," *Energy*, vol. 195, 2020.

[112] Z. Li, Z. Tang, W. Chao, H. Zou, X. Wu, and C. Lin, "Multi-objective supply restoration in active distribution networks with soft open points," in *2018 2nd IEEE Conference On Energy Internet And Energy System Integration (EI2)*, 2018.

[113] J. Wang, N. Zhou, and Q. Wang, “Data-driven stochastic service restoration in unbalanced active distribution networks with multi-terminal soft open points,” *Int. J. Electr. Power Energy Syst.*, vol. 121, 2020.

[114] J. Zhao, M. Zhang, H. Yu, H. Ji, G. Song, P. Li, C. Wang, and J. Wu, “An islanding partition method of active distribution networks based on chance-constrained programming,” *Appl. Energy*, vol. 242, pp. 78–91, 2019.

[115] A. Escalera, M. Prodanovic, E. D. Castronuovo, and J. Roldan-Perez, “Contribution of active management technologies to the reliability of power distribution networks,” *Appl. Energy*, vol. 267, 2020.

[116] Q. Qi and J. Wu, “Increasing distributed generation penetration using network reconfiguration and soft open points,” in *8th International Conference on Applied Energy (ICAE2016)*, 2017, vol. 105, pp. 2169–2174.

[117] X. Xing, J. Lin, C. Wan, and Y. Song, “Model predictive control of lPC-looped active distribution network with high penetration of distributed generation,” *IEEE Trans. Sustain. Energy*, vol. 8, no. 3, pp. 1051–1063, 2017.

[118] P. Cong, W. Tang, C. Lou, B. Zhang, and X. Zhang, “Multi-stage coordination optimisation control in hybrid AC/DC distribution network with high-penetration renewables based on sop and VSC,” *J. Eng.*, vol. 2019, no. 16, pp. 2725–2731, 2019.

[119] J. Zhu, Y. Yuan, and W. Wang, “Multi-stage active management of renewable-rich power distribution network to promote the renewable energy consumption and mitigate the system uncertainty,” *Int. J. Electr. Power Energy Syst.*, vol. 111, pp. 436–446, 2019.

[120] H. Ji, H. Yu, G. Song, P. Li, C. Wang, and J. Wu, “A decentralized voltage control strategy of soft open points in active distribution networks,” *Energy Procedia*, vol. 159, pp. 412–417, 2019.

[121] J. Zhao, M. Yao, H. Yu, G. Song, H. Ji, and P. Li, “Decentralized voltage control strategy of soft open points in active distribution networks based on sensitivity analysis,” *Electron.*, vol. 9, no. 2, 2020.

[122] C. Xu, X. Yuan, Y. Xu, Z. Tan, C. Lin, and M. Chen, “Research on feeder power balancing technology based on snop droop control,” in *2019 IEEE 10th International Symposium On Power Electronics For Distributed Generation Systems (PEDG 2019)*, 2019, pp. 192–196.

[123] Y. Cai, Z. Qu, H. Yang, R. Zhao, Y. Lu, and Y. Yang, “Research on an improved droop control strategy for soft open point,” in *2018 21st International Conference on Electrical Machines And Systems (ICEMS)*, 2018, pp. 2000–2005.

[124] H. Hafezi and H. Laaksonen, “Autonomous soft open point control for active distribution network voltage level management,” in *2019 IEEE Milan Powertech*, 2019.

[125] G. Xinming, H. Qunhai, W. Tongzhen, and Y. Jingyuan, “A local control strategy for distributed energy fluctuation suppression based on soft open point,” *Energies*, vol. 13, no. 6, 2020.

[126] P. Li, H. Ji, H. Yu, J. Zhao, C. Wang, G. Song, and J. Wu, “Combined decentralized and local voltage control strategy of soft open points in active distribution networks,” *Appl. Energy*, vol. 241, no. November 2018, pp. 613–624, 2019.

[127] J. Alcalá, V. Cárdenas, A. R. Ramírez-López, and J. Gudiño-Lau, “Study of the bidirectional power flow in Back-to-Back converters by using linear and nonlinear control strategies,” *IEEE Energy Convers. Congr. Expo. Energy Convers. Innov. a Clean Energy Futur. ECCE 2011, Proc.*, pp. 806–813, 2011.

[128] Y. Hou, Y. Xu, Z. Wang, X. Chen, and H. Cui, “Research on application of three-port snop based on dual closed-loop control in distribution network,” in *2017 IEEE*

International Conference On Smart Technologies And Management For Computing, Communication, Controls, Energy And Materials (ICSTM), 2017, pp. 389–395.

[129] B. Li, Y. Liang, G. Wang, H. Li, and J. Ding, "A control strategy for soft open points based on adaptive voltage droop outer-loop control and sliding mode inner-loop control with feedback linearization," *Int. J. Electr. POWER ENERGY Syst.*, vol. 122, 2020.

[130] C. Wang, G. Song, P. Li, H. Ji, J. Zhao, and J. Wu, "Optimal siting and sizing of soft open points in active electrical distribution networks," *Appl. Energy*, vol. 189, pp. 301–309, 2017.

[131] Y. Yang, W. Pei, Q. Huo, J. Sun, and F. Xu, "Coordinated planning method of multiple micro-grids and distribution network with flexible interconnection," *Appl. Energy*, vol. 228, pp. 2361–2374, 2018.

[132] J. Wang, N. Zhou, C. Y. Chung, and Q. Wang, "Coordinated planning of converter-based dg units and soft open points incorporating active management in unbalanced distribution networks," *IEEE Trans. Sustain. Energy*, vol. PP, no. c, pp. 1–1, 2019.

[133] L. Zhang, C. Shen, Y. Chen, S. Huang, and W. Tang, "Coordinated allocation of distributed generation, capacitor banks and soft open points in active distribution networks considering dispatching results," *Appl. Energy*, vol. 231, pp. 1122–1131, 2018.

[134] I. Konstantelos, S. Giannelos, and G. Strbac, "Strategic valuation of smart grid technology options in distribution networks," *IEEE Trans. Power Syst.*, vol. 32, no. 2, pp. 1293–1303, 2017.

[135] S. Vavasis, "Convex Optimization," 1998.

[136] J. Flottemesch and M. Rother, "Optimized energy exchange in primary distribution networks with DC links," *Proc. 2004 IEEE Int. Conf. Electr. Util. Deregulation, Restruct. Power Technol.*, vol. 1, no. April, pp. 108–116, 2004.

[137] Siemens AG, "SIPLINK medium voltage direct-current transmission," 2011.

[138] T. Larsson, Å. Petersson, A. Edris, D. Kidd, R. Haley, and F. Aboytes, "Eagle pass back-to-back tie: A dual purpose application of voltage source converter technology," *Proc. IEEE Power Eng. Soc. Transm. Distrib. Conf.*, vol. 3, no. SUMMER, pp. 1686–1691, 2001.

[139] M. Marz, K. Copp, A. Manty, D. Dickmander, J. Danielsson, M. Bahrman, F. Johansson, P. Holmberg, H. Duchen, and P. Lundberg, "Mackinac HVDC converter automatic runback utilizing locally measured quantities," *CIGRE Conf. Innov. Evol. grid*, 2014.

[140] Ofgem, "Flexible urban networks – low voltage. project progress report," 2015.

[141] Ofgem, "Network equilibrium-closedown report," 2019.

[142] Ofgem, "Active response to distribution network constraints - submission report," 2017.

[143] "TPS & Northern Power Grid collaborate to help secure electricity supply in remote areas," *Turbo Power Systems*, 2018. [Online]. Available: https://www.turbopowersystems.com/tps-and-northern-powergrid-collaborate-to-secure-electricity/.

[144] J. Xiao, Y. Wang, F. Luo, L. Bai, F. Gang, R. Huang, X. Jiang, and X. Zhang, "Flexible distribution network: definition, configuration, operation, and pilot project," *IET Gener. Transm. Distrib.*, vol. 12, no. 20, SI, pp. 4492–4498, 2018.

[145] L. China Energy Engineering Group Co., "Active distribution network demonstration programme in Suzhou (China)," 2018. [Online]. Available: http://www.cgcpa.org.cn/bhyw/hydt/2018-10-16/8621.html.

[146] P. Qiu, “Smart VSC-HVDC based distribution network demonstration project in Hangzhou (China),” *Zhejiang Electric Power Corporation Research Institute*, 2020. [Online]. Available: https://www.sohu.com/a/367430173_742793.

[147] CIGRE, “B4 Newsletter-2020-December-20,” *CIGRE Newsletter*, 2020. [Online]. Available: https://b4.cigre.org/userfiles/files/B4 newsletters/B4Newsletter_2020-Dec-20.pdf.

[148] P. Roels, “Onshore power systems (OPS) SIHARBOR/SIPLINK,” 2009.

[149] T. Kamel, Z. Tian, and P. Tricoli, “Smart sop architectures and power control managements between light DC railway and LV distribution network,” in *The 10th International Conference on Power Electronics, Machines and Drives*, 2020.

[150] J. Xiao, G. Zu, X. Gong, and F. Li, “Observation of security region boundary for smart distribution grid,” *IEEE Trans. Smart Grid*, vol. 8, no. 4, pp. 1731–1738, 2017.

[151] R. J. Kaye and F. F. Wu, “Analysis of linearized decoupled power flow approximations for steady-state security assessment,” *IEEE Trans. Circuits Syst.*, vol. 31, no. 7, pp. 623–636, 1984.

[152] C. Liu, “A new method for the construction of maximal steady-state security regions of power systems,” *IEEE Trans. Power Syst.*, vol. PWRS-1, no. 4, 1986.

[153] Y. Yu, Y. Liu, C. Qin, and T. Yang, “Theory and method of power system integrated security region irrelevant to operation states: an introduction,” *Engineering*, vol. 6, no. 7, pp. 754–777, 2020.

[154] S. Chen, Z. Wei, G. Sun, W. Wei, and D. Wang, “Convex hull based robust security region for electricity-gas integrated energy systems,” *IEEE Trans. Power Syst.*, vol. 34, no. 3, pp. 1740–1748, 2019.

[155] Y. Liu and Y. Yu, “Probabilistic steady-state and dynamic security assessment of power transmission system,” *Sci. China Technol. Sci.*, vol. 56, no. 5, pp. 1198–1207, 2013.

[156] J. Xiao, C. Wang, B. She, F. Li, Z. Bao, and X. Zhang, “Total supply and accommodation capability curves for active distribution networks: Concept and model,” *Int. J. Electr. Power Energy Syst.*, vol. 133, no. August 2020, p. 107279, 2021.

[157] C. I. F. Agreira, S. M. F. De Jesus, S. L. De Figueiredo, C. M. Ferreira, J. A. D. Pinto, and F. P. M. Barbosa, “Probabilistic steady-state security assessment of an electric power system using a Monte Carlo approach,” *Proc. 41st Int. Univ. Power Eng. Conf.*, vol. 2, pp. 408–411, 2006.

[158] U. Shahzad and S. Asgarpoor, “Probabilistic risk assessment of an active distribution network using Monte Carlo simulation approach,” *51st North Am. Power Symp. NAPS 2019*, 2019.

[159] S. Kim and J. Hur, “A probabilistic modeling based on Monte Carlo simulation of wind powered EV charging stations for steady-states security analysis,” *Energies*, vol. 13, no. 20, 2020.

[160] E. Ciapessoni, D. Cirio, G. Kjølle, S. Massucco, A. Pitto, and M. Sforna, “Probabilistic risk-based security assessment of power systems considering incumbent threats and uncertainties,” *IEEE Trans. Smart Grid*, vol. 7, no. 6, pp. 2890–2903, 2016.

[161] Y. X. Yu and D. T. Wang, “Dynamic security risk assessment and optimization of power transmission system,” *Sci. China, Ser. E Technol. Sci.*, vol. 51, no. 6, pp. 713–723, 2008.

[162] M. B. Cain, R. P. ONeill, and A. Castillo, “History of optimal power flow and formulations,” *Fed. Energy Regul. Comm.*, no. December, pp. 1–36, 2012.

[163] B. P. Hayes and M. Prodanovic, "State forecasting and operational planning for distribution network energy management systems," *IEEE Trans. Smart Grid*, vol. 7, no. 2, pp. 1002–1011, 2016.

[164] A. Giannitrapani, S. Paoletti, A. Vicino, and D. Zarrilli, "Coordinated control of on-load tap changer and energy storage systems for voltage support in distribution networks," in *2017 IEEE 56th Annual Conference on Decision and Control (CDC)*, 2017.

[165] L. Zhou, F. Li, C. Gu, Z. Hu, and S. Le Blond, "Cost/benefit assessment of a smart distribution system with intelligent electric vehicle charging," *IEEE Trans. Smart Grid*, vol. 5, no. 2, pp. 839–847, 2014.

[166] S. K. Salman and I. M. Rida, "ANN-based AVC relay for voltage control of distribution network with and without embedded generation," *DRPT 2000 - Int. Conf. Electr. Util. Deregul. Restruct. Power Technol. Proc.*, no. April, pp. 263–267, 2000.

[167] X. Sun and J. Qiu, "Two-stage volt/var control in active distribution networks with multi-agent deep reinforcement learning method," *IEEE Trans. Smart Grid*, vol. 12, no. 4, pp. 2903–2912, 2021.

[168] M. E. Baran and F. Wu, "Network reconfiguration in distribution systems for loss reduction and load balancing," *IEEE Trans Power Deliv.*, vol. 4, no. 2, pp. 1401–1407, 1989.

[169] F. Capitanescu, L. F. Ochoa, H. Margossian, and N. D. Hatziargyriou, "Assessing the potential of network reconfiguration to improve distributed generation hosting capacity in active distribution systems," *IEEE Trans. Power Syst.*, vol. 30, no. 1, pp. 346–356, 2015.

[170] S. Lei, Y. Hou, F. Qiu, and J. Yan, "Identification of critical switches for integratingrenewable distributed generation by dynamic network reconfiguration," *IEEE Trans. Sustain. Energy*, vol. 9, no. 1, pp. 420–432, 2018.

[171] L. Bai, T. Jiang, F. Li, H. Chen, and X. Li, "Distributed energy storage planning in soft open point based active distribution networks incorporating network reconfiguration and DG reactive power capability," *Appl. Energy*, vol. 210, pp. 1082–1091, 2018.

[172] I. Diaaeldin, S. A. Aleem, A. El-Rafei, A. Abdelaziz, and A. F. Zobaa, "Optimal network reconfiguration in active distribution networks with soft open points and distributed generation," *Energies*, vol. 12, no. 21, 2019.

[173] L. Bird, J. Cochran, and X. Wang, "Wind and solar energy curtailment: experience and practices in the united states," *Natl. Renew. Energy Lab.*, no. March, p. 58, 2014.

[174] International Energy Agency, "Demand response," 2023. [Online]. Available: https://www.iea.org/energy-system/energy-efficiency-and-demand/demand-response. [Accessed: 04-Dec-2023].

[175] B. Hayes, I. Hernando-Gil, A. Collin, G. Harrison, and S. Djokić, "Optimal power flow for maximizing network benefits from demand-side management," *IEEE Trans. Power Syst.*, vol. 29, no. 4, pp. 1739–1747, 2014.

[176] J. Chen, W. Lee, M. Chen, "Using a static var compensator to balance a distribution system," *IEEE Trans. Ind. Applicat.*, vol. 35, no. 2, pp. 298-304, 1999.

[177] P. Rao, M. L. Crow, and Z. Yang, "STATCOM control for power system voltage control applications," *IEEE Trans. Power Deliv.*, vol. 15, no. 4, pp. 1311–1317, 2000.

[178] K. K. Sen, "SSSC - static synchronous series compensator: theory, modeling, and applications," *IEEE Trans. Power Deliv.*, vol. 13, no. 1, pp. 241–246, 1998.

[179] D. J. Hanson, M. L. Woodhouse, C. Howill, D. R. Monkhouse, and M. M. Osborne, "STATCOM : a new era of reactive compensation," no. June, pp. 151–160, 2002.

[180] ABB, "SVC and STATCOM: an overview," 2019.

[181] L. Xu, L Yao, C. Sasse, "Comparison of using SVC and STATCOM for wind farm integration," in 2006 International Conference on Power System Technology, 2006.

[182] Z. Zhang, L. F. Ochoa, and G. Valverde, "A novel voltage sensitivity approach for the decentralized control of DG plants," *IEEE Trans. Power Syst.*, vol. 33, no. 2, pp. 1566–1576, 2018.

[183] T. Sansawatt, L. F. Ochoa, and G. P. Harrison, "Smart decentralized control of DG for voltage and thermal constraint management," *IEEE Trans. Power Syst.*, vol. 27, no. 3, pp. 1637–1645, 2012.

[184] S. Song, C. Han, G. S. Lee, R. A. McCann, and G. Jang, "Voltage-sensitivity-approach-based adaptive droop control strategy of hybrid STATCOM," *IEEE Trans. Power Syst.*, vol. 36, no. 1, pp. 389–401, 2021.

[185] P. Li, H. Ji, H. Yu, J. Zhao, C. Wang, G. Song, and J. Wu, "Combined decentralized and local voltage control strategy of soft open points in active distribution networks," *Appl. Energy*, vol. 241, no. March, pp. 613–624, 2019.

[186] P. Li, J. Ji, H. Ji, J. Jian, F. Ding, J. Wu, and C. Wang, "MPC-based local voltage control strategy of DGs in active distribution networks," *IEEE Trans. Sustain. Energy*, vol. 11, no. 4, pp. 2911–2921, 2020.

[187] Z. Hu and F. Li, "Cost-benefit analyses of active distribution network management, part I: Annual benefit analysis," *IEEE Trans. Smart Grid*, vol. 3, no. 3, pp. 1067–1074, 2012.

[188] L. Kane and G. Ault, "A review and analysis of renewable energy curtailment schemes and Principles of Access: Transitioning towards business as usual," *Energy Policy*, vol. 72, no. 2014, pp. 67–77, 2014.

[189] UK Power Networks, "Flexible plug and play: communication trial report," 2014.

[190] X. Yang, Z. Zhou, Y. Zhang, J. Liu, J. Wen, Q. Wu, and S. jie Cheng, "Resilience-oriented co-deployment of remote-controlled switches and soft open points in distribution networks," *IEEE Trans. Power Syst.*, vol. 38, no. 2, pp. 1350–1365, 2022.

[191] R. Hu, W. Wang, Z. Chen, X. Wu, L. Jing, W. Ma, and G. Zeng, "Coordinated voltage regulation methods in active distribution networks with soft open points," *Sustainability*, vol. 12, no. 22, 2020.

[192] Y. Zheng, Y. Song, and D. J. Hill, "A general coordinated voltage regulation method in distribution networks with soft open points," *Int. J. Electr. Power Energy Syst.*, vol. 116, no. October 2019, p. 105571, 2020.

[193] L. Thomas, Y. Zhou, C. Long, J. Wu, and N. Jenkins, "A general form of smart contract for decentralized energy systems management," *Nat. Energy*, vol. 4, no. 2, pp. 140–149, 2019.

[194] National Grid ESO, "Transmission losses," 2019.

[195] Wikipedia, "N-sphere." [Online]. Available: https://en.wikipedia.org/wiki/N-sphere.

[196] "Centre for sustainable electricity and distributed generation." [Online]. Available: https://github.com/sedg/ukgds.

[197] H. Barki, F. Denis, and F. Dupont, "Contributing vertices-based Minkowski sum computation of convex polyhedra," *CAD Comput. Aided Des.*, vol. 41, no. 7, pp. 525–538, 2009.

[198] M. E. Baran and F. F. Wu, “Optimal capacitor placement on radial distribution systems,” *IEEE Trans. Power Deliv.*, vol. 4, no. 1, pp. 725–734, 1989.

[199] P. Li, H. Ji, H. Yu, J. Zhao, C. Wang, G. Song, and J. Wu, “Combined decentralized and local voltage control strategy of soft open points in active distribution networks,” *Appl. Energy*, vol. 241, pp. 613–624, 2019.

[200] F. Xiao, Y. Cui, J. Zhu, Y. Qiao, Z. Li, and Q. Ai, “A load-side resource aggregation method based on Minkowski Sum,” *Journal of Physics: Conference Series*, vol. 2728, no. 1, pp. 012073, 2024.

[201] J. Jian, M. Zhang, Y. Xu, W. Tang, and S. He, “An analytical polytope approximation aggregation of electric vehicles considering uncertainty for the day-ahead distribution network dispatching,” *IEEE Trans. Sustain. Energy*, vol. 15, no. 1, pp. 160-172, 2023.

Appendix

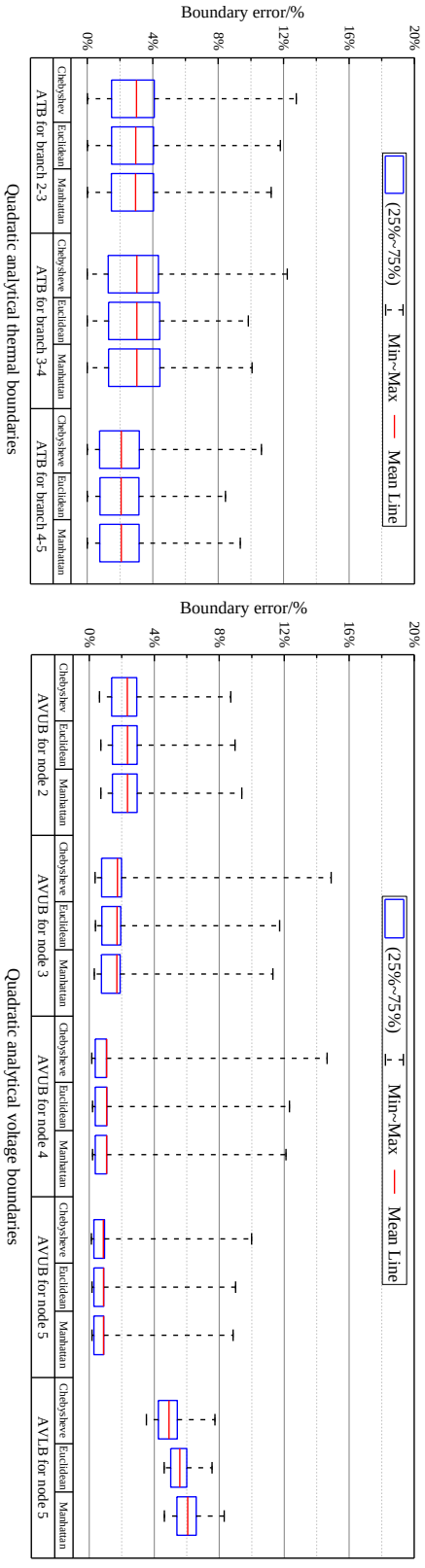
Boundary error/%
0%
4%
8%
12%
16%
20%
(25%~75%)
Min~Max
Mean Line
Chebyshev
Euclidean
Manhattan
ATB for branch 2-3
ATB for branch 3-4
ATB for branch 4-5
Quadratic analytical thermal boundaries
AVUB for node 2
AVUB for node 3
AVUB for node 4
AVUB for node 5
AVLB for node 5
Quadratic analytical voltage boundaries

(a)

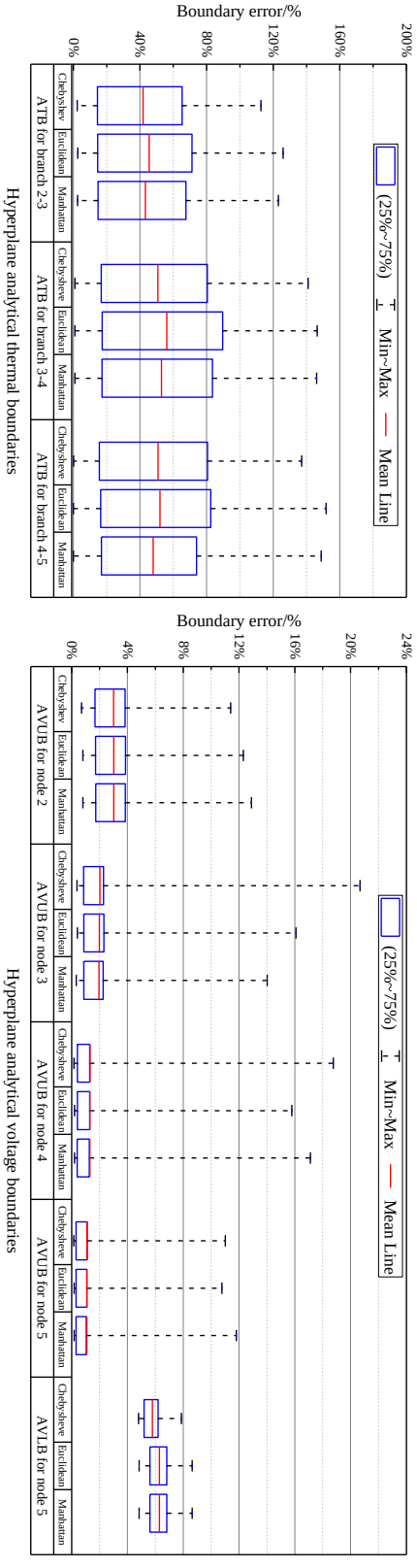

(b)

Fig. A.1. Boundary errors for (a) the quadratic expressions of each thermal/voltage boundary and (b) the hyperplane expressions of each thermal/voltage boundary in the 5-node feeder measured by multiple distance functions